The Journal of Antibiotics (2009) 62, 471–481

www.nature.com/ja

REVIEW ARTICLE

Biosynthetic genes for aminoglycoside antibiotics

Fumitaka Kudo[1] and Tadashi Eguchi[2]

Biosynthetic studies of aminoglycoside antibiotics have progressed remarkably during the last decade. Many biosynthetic gene clusters for aminoglycoside antibiotics including streptomycin, kanamycin, butirosin, neomycin and gentamicin have been identified to date. In addition, most butirosin and neomycin biosynthetic enzymes have been functionally characterized using recombinant proteins. Herein, we reanalyze biosynthetic genes for structurally related 2-deoxystreptamine (2DOS)-containing aminoglycosides, such as kanamycin, gentamicin and istamycin, based on genetic information including characterized biosynthetic enzymes in neomycin and butirosin biosynthetic pathways. These proposed enzymatic functions for uncharacterized enzymes are expected to support investigation of the complex biosynthetic pathways for this important class of antibiotics.
The Journal of Antibiotics (2009) **62,** 471–481; doi:10.1038/ja.2009.76; published online 31 July 2009

Keywords: aminoglycoside antibiotics; aminocyclitol; biosynthesis; biosynthetic enzyme; biosynthetic gene

INTRODUCTION

Aminoglycoside antibiotics are known as a classical but clinically important class of agents, especially against *Mycobacterium tuberculosis*.[1] In 1944, Selman Waksman found aminoglycoside antibiotic streptomycin from soil bacteria, which showed significant antibacterial activity, importantly anti-tuberculosis activity. This discovery led to the isolation of such bioactive compounds including kanamycin, found by Hamao Umezawa in Japan. These aminoglycoside antibiotics are structurally similar, possessing a core aminocyclitol moiety and various unusual sugars including aminosugars and deoxysugars (Figure 1). Combinations of sugar attachments and amino functionality are critical for antibacterial activity, which results from specific interaction with bacterial ribosomal RNAs to inhibit their protein synthesis. In fact, such specific interactions have been observed clearly through X-ray structural analysis.[2]

Emergence of bacteria that are resistant against such antibiotics remains a serious problem. Resistant enzymes in bacteria modify aminoglycosides through phosphorylation, adenylation and acetylation.[3,4] Modified aminoglycosides become unable to interact with bacterial rRNAs and therefore become ineffective. To prevent such modification reactions, deoxygenation and 4-amino-2*S*-hydroxybutyration of aminoglycoside have been developed as effective methods because resistant enzymes cannot reach or modify such antibiotics even though they can still interact with bacterial rRNAs.[5]

In spite of the ototoxic and nephrotoxic side effects of aminoglycosides, the highly specific RNA-binding ability has engendered the preparation of various analogous compounds to apply for human immunodeficiency virus inflectional disease[6] and antiplasmid approaches.[7,8] Consequently, aminoglycoside remains an important material in medicinal chemistry.

Biosynthetic studies of aminoglycosides have indeed been performed for many years. Initially, feeding experiments with radioisotope and stable isotope-labeled primary metabolites such as glucose and glucosamine elucidated the origin of carbon atoms.[9] Idiotrophic mutants were also constructed and used to postulate the biosynthetic pathway through the determination of structures of accumulated intermediates.[10] Cosynthesis with blocked mutants was also effective to determine the order of biosynthetic steps.[11] However, these experiments yielded no direct evidence for enzymatic reaction mechanisms.

Enzymatic analyses were performed extensively by Walker,[12] yielding important information to elucidate the complex biosynthetic pathway at the enzyme reaction level. However, only limited information about the enzymes was available at that time because the purification of quite small amounts of secondary metabolic enzymes from a natural source was usually a difficult task. In the 1980s, genetic analyses for natural product biosynthesis were initiated to identify the responsible biosynthetic genes. Initially, complementary gene fragments for idiotrophic mutants to restore antibiotic production were screened to identify the desired biosynthetic genes. In addition, resistant genes were used as a target to identify secondary metabolite biosynthetic gene clusters. A partial streptomycin biosynthetic gene cluster was then identified in 1987.[13] Subsequently, several biosynthetic genes for streptomycin were identified in association with the central gene cluster.[14] However, only a few biosynthetic genes were heterologously expressed and investigated to characterize the function to date.[15–18] Among those, the characterization of L-glutamine: *syllo*-inosamine aminotransferase StsC gave important information to elucidate the aminocyclitol-containing aminoglycosides biosynthetic pathway.[15] Using the hybridization method, Piepersberg and co-workers[15]

[1]Department of Chemistry, Tokyo Institute of Technology, Meguro-ku, Tokyo, Japan and [2]Department of Chemistry and Materials Science, Tokyo Institute of Technology, Meguro-ku, Tokyo, Japan
Correspondence: Professor T Eguchi, Department of Chemistry and Materials Science, Tokyo Institute of Technology, O-okayama, Meguro-ku, Tokyo 151-8551, Japan.
E-mail: eguchi@cms.titech.ac.jp
Received 4 June 2009; revised 9 July 2009; accepted 13 July 2009; published online 31 July 2009

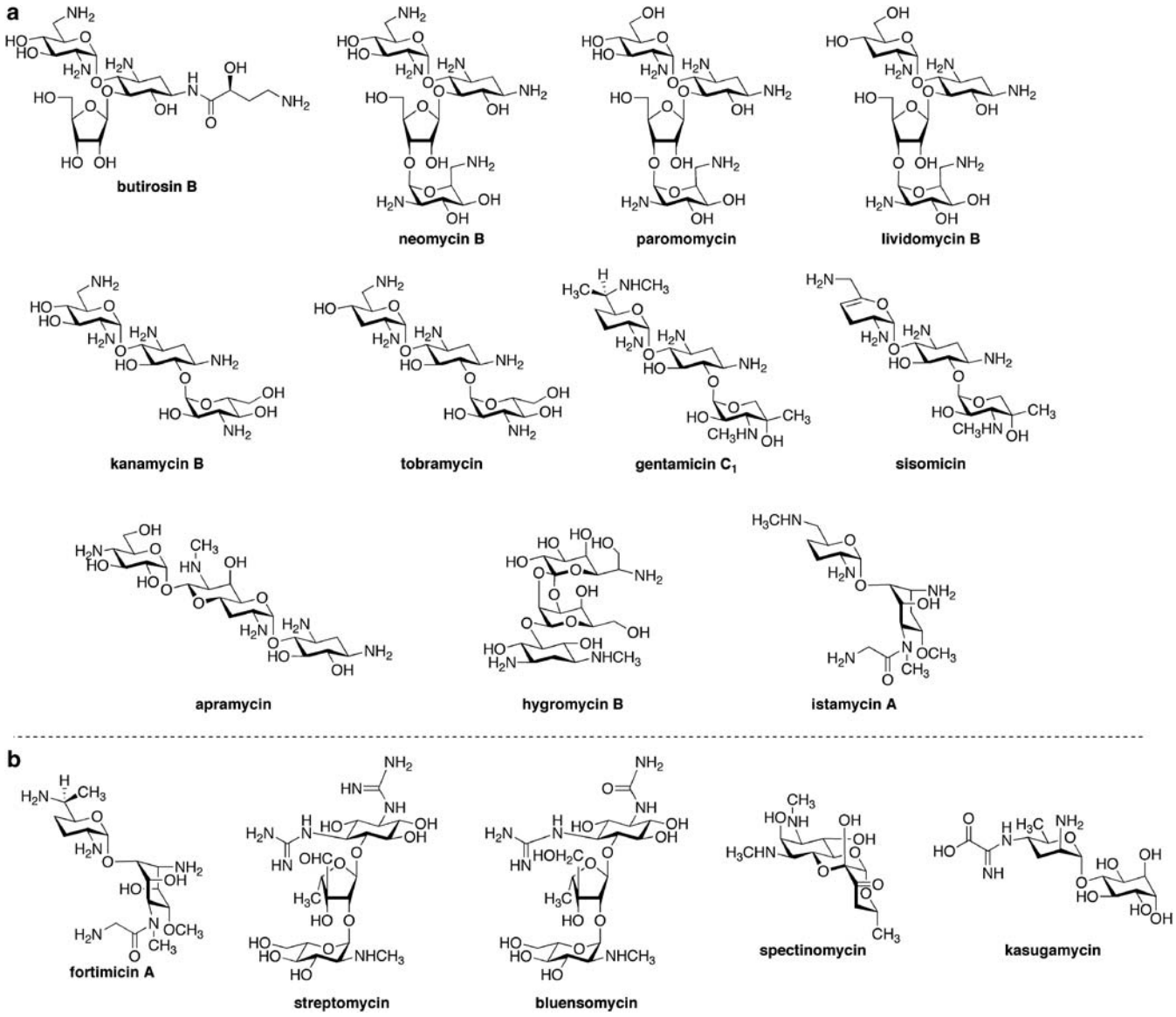

Figure 1 Aminoglycoside antibiotics whose biosynthetic genes are deposited in a public gene database such as DDBJ, EMBL and GenBank. (**a**) 2-deoxystreptamine-containing aminoglycoside antibiotics, (**b**) *myo*-inositol-derived aminocyclitol-containing aminoglycoside antibiotics.

showed that its homologous gene is conserved in the aminocyclitol antibiotic-producing microorganisms. In fact, StsC homologous aminotransferase genes are conserved completely in the genomes of aminocyclitol antibiotic-producing microorganisms as a specific feature.

In 1999, the 2-deoxy-*scyllo*-inosose (2DOI) synthase was isolated from butirosin-producing *Bacillus circulans* as a crucial enzyme at the first step in the 2-deoxystreptamine (2DOS) biosynthetic pathway.[19] Its corresponding gene, *btrC*, was then cloned and the recombinant enzyme was found to have 2DOI synthase activity.[20] In addition, a butirosin biosynthetic gene cluster (*btr*) was identified by chromosomal gene walking from the DOI synthase gene (Table 1).[21] The majority of aminoglycosides contain 2DOS as a core unique aminocyclitol aglycon. Therefore, the discovery of the *btr* gene boosted the identification of several other 2DOS-containing aminoglycoside biosynthetic gene clusters (Figures 1 and 2 and Table 1). To date, biosynthetic gene clusters for butirosin, neomycin, ribostamycin, paromomycin, lividomycin, kanamycin, tobramycin, gentamicin, sisomicin, istamycin, apramycin and hygromycin B have been identified, yielding important information to predict the biosynthetic pathway step by step, combined with previous mutant studies. It was readily speculated that conserved biosynthetic enzymes encoded in gene clusters could construct common structures of aminoglycosides. In accordance with that prediction, seven neamine-related biosynthetic genes and two unique ribostamycin-related biosynthetic genes were clearly classified. In addition, two neomycin-related enzymes and several butirosin-specific biosynthetic enzymes have been identified. Most enzymes in neomycin and butirosin biosynthesis have been functionally characterized with the recombinant proteins.[22] In this review, we first summarize the neomycin and butirosin biosynthetic enzymes characterized to date; then, we bioinformatically reanalyze the function of the biosynthetic genes for other 2DOS-containing aminoglycoside antibiotics including kanamycin, tobramycin, gentamicin and istamycin (also fortimicin).

Table 1 Biosynthetic enzymes of 2-deoxystreptamine-containing aminoglycoside antibiotics

	Characterized function or putative function	*Butirosin*	*Neomycin*	*Ribostamycin*	*Paromomycin*	*Lividomycin*	*Kanamycin*	*Tobramycin*	*Gentamicin*	*Istamycin*	*Fortimicin*	*Frankia sp. CcI3*	*Apramycin*	*Hygromycin B*
1a	2DOI synthase	BtrC	NeoC	RibC	ParC	LivC	KanC	TobC	GenC	IstC			AprC	HygC
2a	L-Gln:2DOI aminotransferase	BtrS	NeoS	RibS	ParS	LivS	KanS1, S2	TobS1, S2	GenS1, S2	IstS	ForS	3363	AprS	HygS
3a	2DOIA dehydrogenase (NAD^+ dependent)	BtrE	NeoE	RibE	ParE	LivE	KanE	TobE	GenE	IstE	ForE	3364	AprE	HygE
4a	UDP-GlcNAc:2DOS GlcNAc transferase	BtrM	NeoM	RibM	ParM	LivM	KanM1, M2	TobM1, M2	GenM1, M2	IstM	ForM	3362	AprM	
5a	2′-*N*-acetylparomamine deacetylase	BtrD	NeoD	RibD	ParD	LivD	KanN	TobN	GenD	IstD	ForD	3367	AprN	
6a	Paromamine 6′-dehydrogenase	BtrQ	NeoQ	RibQ	ParQ	LivQ	KanQ	TobQ	GenQ	IstQ	ForQ	3360	AprQ	
7a	L-Gln:6′-oxoparomamine aminotransferase	BtrB	NeoB	RibB	ParB	LivB	KanB	TobB	GenB1, B2, B3, B4	IstB	ForB	3369		
8b	PRPP:neamine 5′-phosphoribosyltransferase	BtrL	NeoL	RibL	ParL	LivL								
9b	5′-phosphoribostamycin phosphatase	BtrP	NeoP	RibP	ParP	LivP								
10c	UDP-GlcNAc:ribostamycin GlcNAc transferase		NeoF	RibF	ParF	LivF								
11c	Neomycin 5′″-epimerase? (radical SAM enzyme)		NeoN	RibN	ParN	LivN								
12	Acyl carrier protein (ACP)	BtrI												
13	γ-L-Glu-ACP ligase	BtrJ												
14	γ-L-Glu-ACP decarboxylase	BtrK												
15	γ-L-Glu-GABA-ACP monooxygenase	BtrO												
16	NAD(P)H:FMN oxidoreductase	BtrU												
17	γ-L-Glu-AHBA-ACP:ribostamycin γ-L-Glu-AHBA transferase	BtrH												
18	γ-L-Glu-butirosin γ-L-glutamyl cyclotransferase	BtrG												
19	Butirosin 3″-epimerase?	BtrF												
20	2DOIA dehydrogenase (radical SAM enzyme)	BtrN												
21	Unknown	BtrA	NeoA	RibA	ParA	LivA								
22	Hypothetical protein	BtrV	NeoX	RibX	ParX	LivX								
23	ABC transporter		NeoT	RibT	ParT	LivT							AprV	HygW
24	ABC transporter		NeoU	RibU	ParU	LivU							AprW	HygV
25	Aminoglycoside *N*-acetyltransferase (resistant)		AacC8	AacC8	AacC7									
26	ABC transporter	BtrW												
27	ABC transporter	BtrX												
28	Transcriptional regulator	BtrR1												
29	Transcriptional regulator	BtrR2												
30	Hypothetical protein	BtrT												
31	Putative regulator component		NeoI	RibI	ParI	LivI	KanI							HygI
32	Putative regulator component		NeoH	RibH	ParH	LivH	KanH							HygH
33	Putative regulator component		NeoG	RibG	ParG	LivG	KanG							HygG
34	Aminoglycoside *O*-phosphotransferase (resistant)		AphA	Rph	ParR(AphA)				GenP	IstP	ForP	3368		
35	Extracellular aminoglycoside phosphate phosphatase				ParK	LivK							AprZ	

Table 1 Continued

	Characterized function or putative function	*Butirosin*	*Neomycin*	*Ribostamycin*	*Paromomycin*	*Lividomycin*	*Kanamycin*	*Tobramycin*	*Gentamicin*	*Istamycin*	*Fortimicin*	*Frankia sp. Ccl3*	*Apramycin*	*Hygromycin B*
36	Unknown					LivO								
37	Hypothetical protein					LivV								
38d	Putative Fe-S oxidoreductase					LivW							AprD4	
39d	Putative dehydrogenase					LivY			GenD3				AprD3	
40	Aminoglycoside 6'-*N*-acetyltransferase						KanA							
41	Transcriptional regulator						KanR							
42	Putative transport protein						KanT	TobT						
43e	Putative dehydrogenase						KanD2	TobD2	GenD2					
44	Hypothetical protein						KanJ							
45	Hypothetical protein						KanK							
46	16S rRNA methylase						Kmr		GmrA, B		FmrB, O, P	3372, 3382		
47	Putative carbamoyltransferase							TobZ						
48	Putative carbamoyl-phosphate synthase							TobL						
49	Hypothetical protein							TobX						
50f	Putative tRNA-ribosyltransferase								GenO		FosA	3378		
51g	Radical SAM protein								GenD1					
52f	GTP cyclohydrolase								GenW		FosC	3383		
53h	Putative radical SAM methyltransferase								GenK		ForK (Fms7)	3370		
54g	Hypothetical protein								GenX					
55g	Hypothetical protein								GenU					
56g	Transmembrane efflux protein								GenV					
57f	Membrane antiporter								GenY		ForY			
58f	Hypothetical protein								GenA		FosE	3379		
59f	Radical SAM protein								GenF		FosF	3380		
60h	Hypothetical protein								GenG		FosG	3381		
61i	Hypothetical protein								GenH, I	IstH, I, J	ForH, I, J, V	3358, 3359		
62f	Putative methyltransferase								GenT		ForT	3377		
63g	Putative methyltransferase								GenN					
64j	Hypothetical protein									IstW	ForW	3361		
65j	Putative methyltransferase									IstO	ForO	3365		
66j	Radical SAM protein									IstL2	ForL2	3366		
67j	FAD-dependent oxidoreductase									IstZ	ForZ (Fms14)	3371		
68j	Carboxymuconolactone decarboxylase family protein									IstX	ForX	3376		
69k	Inositol 2-dehydrogenase										ForG	3374		
70j	Putative methyltransferase									IstN	ForN	3373		
71k	Inositol-phosphate phosphatase										For A			
72j	Radical SAM protein									IstL, L3	ForL	3357, 3375		
73	16S rRNA methylase									ImrA			KamB	

Table 1 Continued

	Characterized function or putative function	*Butirosin*	*Neomycin*	*Ribostamycin*	*Paromomycin*	*Lividomycin*	*Kanamycin*	*Tobramycin*	*Gentamicin*	*Istamycin*	*Fortimicin*	*Frankia sp. Ccl3*	*Apramycin*	*Hygromycin B*
74	Hypothetical protein									IstA			AprA	
75	Hypothetical protein									IstF				
76	Putative methyltransferase									IstU				
77	Putative kinase												AprU	
78	Sugar hydrolase												AprO	
79	UDP-glucose 4-epimerase												AprD1	
80	Hypothetical protein												AprF	
81	Hypothetical protein												AprG	
82	Glycosyltransferase family 28												AprH	
83	Putative methyltransferase												AprI	
84	Phosphosugar mutase												AprJ	
85	Putative ADP-heptose synthase												AprK	
86	Creatinine amidohydrolase												AprP	
87	UDP-GlcNAc C6 dehydratase												AprD2	
88	Aminotransferase												AprL	
89	UDP-glucose 4-epimerase												AprD5	
90	Hygromycin B kinase													HygA
91	Putative UDP-galactose 4-epimerase													HygK
92	Putative phosphatase													HygU
93	Glycosyl transferase group 1													HygD
94	Galactose-1-phosphate uridylyltransferase													HygO
95	Sugar isomerase													HygP
96	Hydroxylase													HygX
97	aminotransferase													HygL
98	NAD-dependent epimerase													HygJ
99	Radical SAM protein													HygY
100	Putative glycosyl transferase													HygF
101	D-glycero-D-manno-heptose 7-phosphate kinase													HygN
102	DNA methylase													HygM
103	Hypothetical protein													HygT

Butirosin biosynthetic enzymes (AB097196, *Bacillus circulans* SANK 72073), neomycin biosynthetic enzymes (AJ629247, *Streptomyces fradiae* DSM 40063), ribostamycin biosynthetic enzymes (AJ744850, *S. ribosidificus* NRRL B-11466), paromomycin biosynthetic enzymes (AJ628955, *S. rimosus* subsp. *paromomycinus* NRRL 2455), lividomycin biosynthetic enzymes (AJ748832, *S. lividus*), kanamycin biosynthetic enzymes (AJ628422, *S. kanamyceticus* DSM 40500), tobramycin biosynthetic enzymes (AJ810851, *Streptomyces* sp. DSM 40477), gentamicin biosynthetic enzymes (AJ628149, *Micromonospora echinospora* DSM 43036), istamycin biosynthetic enzymes (AJ845083, *S. tenjimariensis* ATCC 31603), fortimicin biosynthetic enzymes (AJ628421, *M. olivasterospora* DSM 43868), probable aminoglycoside-related biosynthetic enzymes in *Frankia* sp. Ccl3 (NC_007777, *Frankia* sp. Ccl3, complete genome), apramycin biosynthetic enzymes (AJ629123, *Streptomyces* sp. DSM 40477, AJ875019, *Streptoalloteichus hindustanus* DSM 44523), hygromycin B biosynthetic enzymes (AJ628642, *S. hygroscopicus* subsp. *hygroscopicus* DSM 40578). In the table, nos. 1–7 (a) are neamine-related biosynthetic enzymes; nos. 8, 9 (b) are ribosylation enzymes in ribostamycin-related compounds; nos. 10, 11 (c) are neomycin-related biosynthetic enzymes; nos. 12–20 are butirosin pathway-specific enzymes; nos. 38, 39 (d) are lividomycin- and apramycin-specific enzymes, which might be responsible for deoxygenation at C-3′; nos. 43, 2-2, 4-2 (e) are kanamycin-related biosynthetic enzymes; nos. 50, 52, 57–59, 62 (f) are gentamicin-, sisomicin- and fortimicin-specific enzymes; nos. 51, 54–56, 63 (g) are gentamicin- and sisomicin-specific enzymes; nos. 53, 60 (h) are gentamicin- and fortimicin-specific enzymes; no. 61 (i) is a gentamicin-, sisomicin-, fortimicin- and istamycin-specific enzyme; nos. 64–68, 70, 72 (j) are fortimicin- and istamycin-specific enzymes; nos. 69, 71 (k) are fortimicin-specific enzymes for *scyllo*-inosose biosynthesis from *myo*-inositol 1-phosphate; Others are pathway-specific enzymes, transcriptional regulators, transporters, resistant enzymes and unknown functional hypothetical proteins.

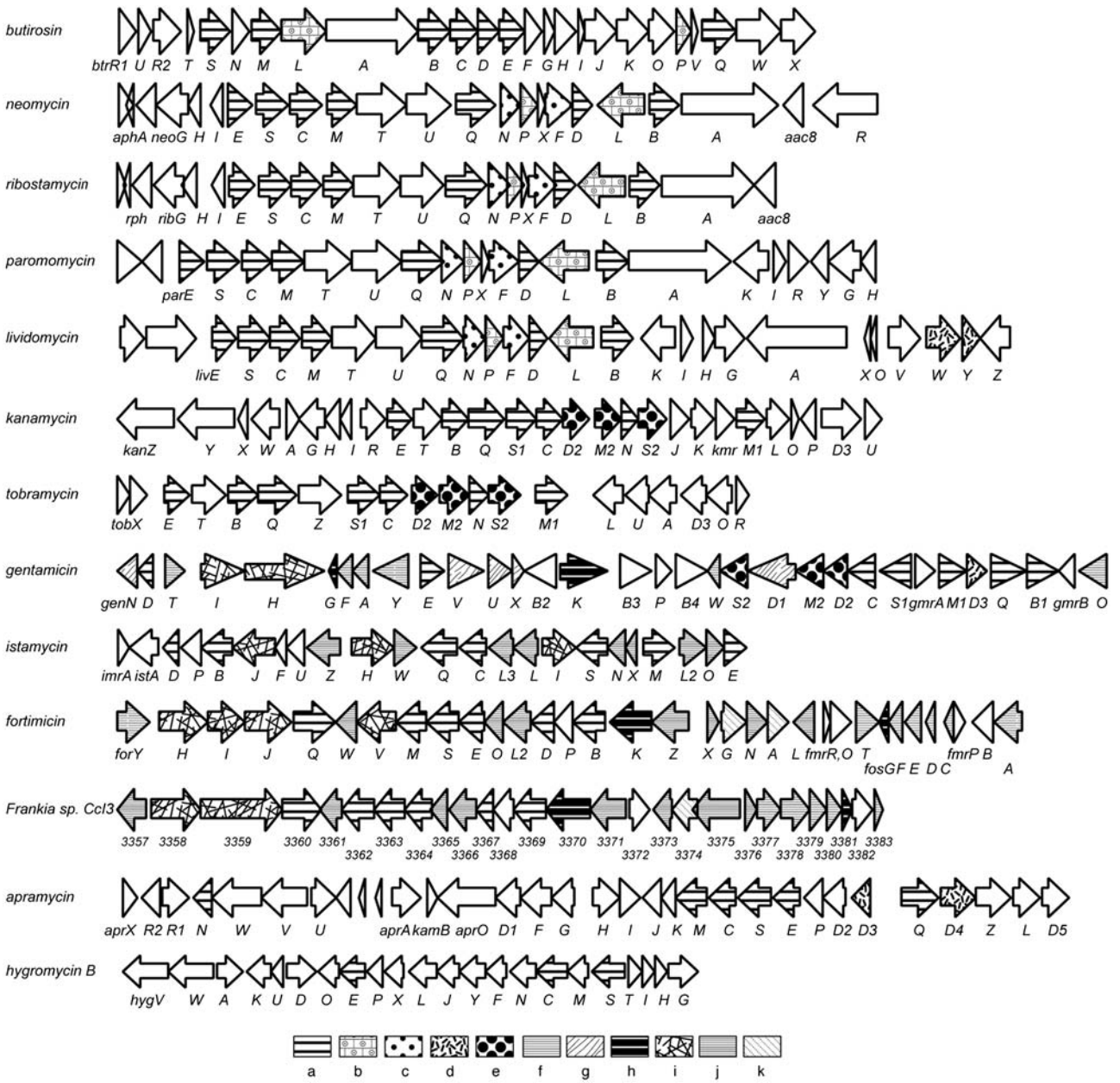

Figure 2 Biosynthetic gene clusters for aminoglycoside antibiotics. Characterized functions or putative functions of genes are showed in Table 1. Genes are classified according to the biosynthetic functions summarized in Table 1 (a)–(k).

NEOMYCIN-RELATED BIOSYNTHETIC GENES

We presented 2DOS biosynthetic genes in Table 1: many homologous proteins are conserved in the structurally related compounds (Figure 2). As many identical biosynthetic genes for aminoglycoside antibiotics are deposited as different symbols in the database, we use here the *btr* gene-based code names that are used systematically by Piepersberg *et al.*[23] Seven proteins (nos. 1–7 in Table 1), 2DOI synthase (BtrC, NeoC), L-glutamine:2DOI aminotransferase (BtrS, NeoS), NAD-dependent dehydrogenase (BtrE, NeoE), glycosyltransferase (BtrM, NeoM), deacetylase (BtrD, NeoD), flavin adenine dinucleotide (FAD)-dependent dehydrogenase (BtrQ, NeoQ) and another aminotransferase (BtrB, NeoB), are all conserved in butirosin, neomycin, ribostamycin, paromomycin, lividomycin, kanamycin, tobramycin, gentamicin and istamycin biosynthetic gene clusters, indicating that these are responsible for the construction of a common neamine-like structure. In fact, 2DOI formed from D-glucose-6-phosphate by 2DOI synthase is converted into 2-deoxy-*scyllo*-inosamine (2DOIA) by Gln:2DOI aminotransferase,[24,25] which is a homologous protein to StsC in streptomycin biosynthesis. Next, an NAD-dependent dehydrogenase catalyzes the dehydrogenation at C-1 of 2DOIA to give 3-amino-2,3-dideoxy-*scyllo*-inosose (amino-DOI).[26] Amino-DOI is then converted to 2DOS by dual functional Gln:2DOI aminotransferase to complete the 2DOS biosynthesis.[27]

Then, 2DOS is glycosylated using glycosyltransferase with UDP-*N*-acetyl-D-glucosamine (UDP-GlcNAc) as a glycosyl donor to give *N*-acetylparomamine, whose *N*-acetyl group is removed using a deacetylase to give paromamine.[28] Paromamine is believed to be a branching intermediate to neomycin-related aminoglycosides,

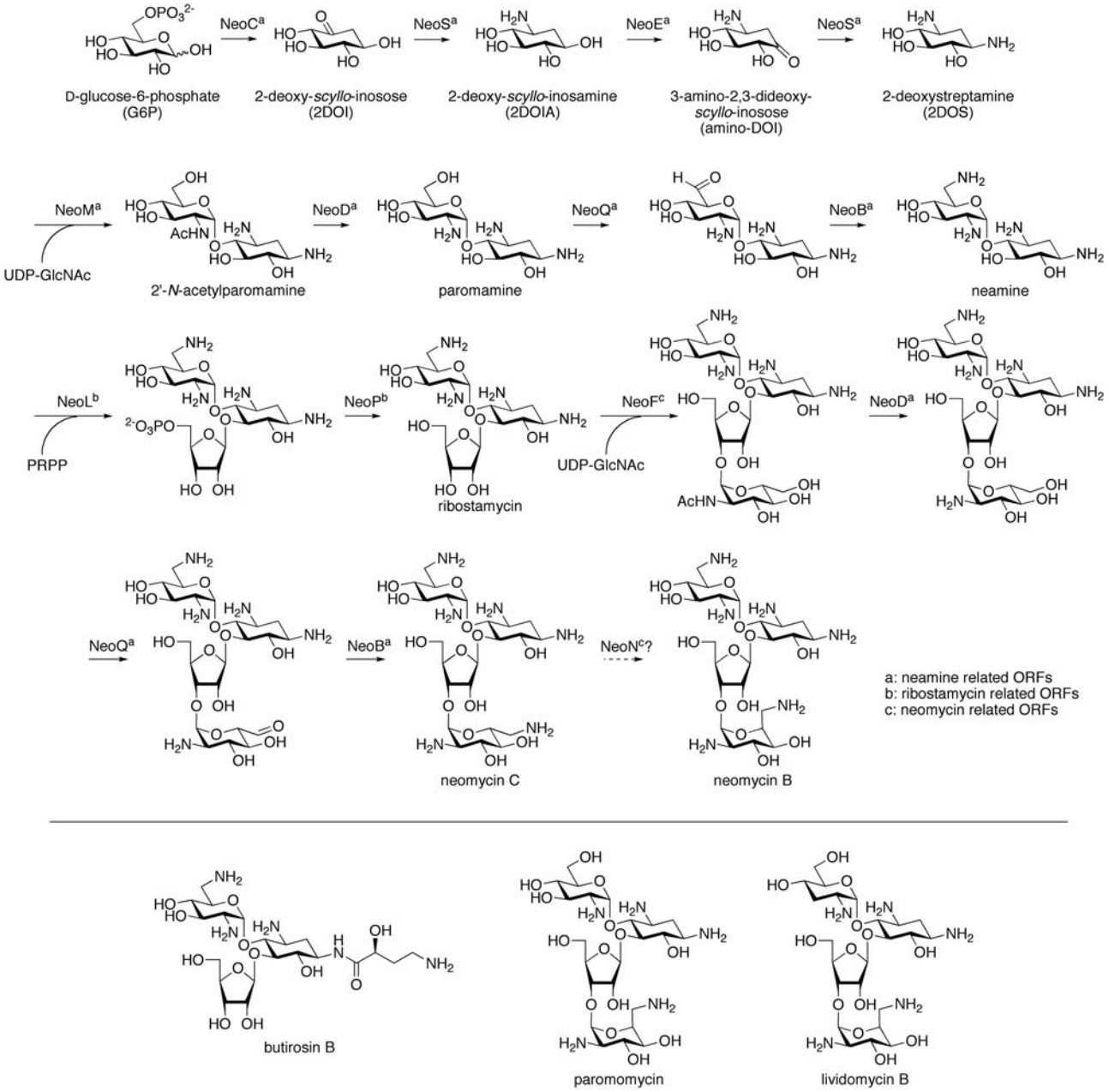

Figure 3 Neomycin biosynthetic pathway. Structurally related butirosin, paromomycin and lividomycin are shown.

kanamycin and gentamicin. In neomycin biosynthesis, C-6′ of paromamine is oxidized to 6′-oxoparomamine by an FAD-dependent dehydrogenase.[29] 6′-Oxoparomamine is then converted to neamine by another aminotransferase.[29] All these seven enzymes derived from the neomycin biosynthetic gene cluster were functionally characterized using its recombinant proteins (Figure 3).

Neamine is then ribosylated by two unique enzymes (nos. 8 and 9) for ribostamycin-related aminoglycoside biosynthesis. To date, BtrL and BtrP encoded in the butirosin biosynthetic gene cluster were used to verify the function.[30] Subsequently, BtrL was found to catalyze the phosphoribosylation with 5-phosphoribosyl-1-diphosphate as the ribosyl donor. Then, phosphatase BtrP catalyzes the dephosphorylation to give ribostamycin.

Among neomycin-related gene clusters, two unique proteins (nos. 10 and 11) are conserved except for transcriptional regulators, transporters and resistant enzymes. One (NeoF) was found to be responsible for the glycosylation with UDP-GlcNAc to give a pseudotetrasaccharide.[28] The *N*-acetyl moiety of the product is then deacetylated by a dual functional deacetylase (NeoD), which also catalyzes the deacetylation of *N*-acetylparomamine.[28] This product can be further converted to neomycin C by a dual functional FAD-dependent dehydrogenase (NeoQ) and an aminotransferase (NeoB) in the neamine biosynthesis.[29] Finally, a remaining radical SAM protein is apparently responsible for the epimerization at C-5‴ of neomycin C to give neomycin B, although its enzymatic activity has not been confirmed yet. Butirosin-specific enzymes (nos. 12–19) for the 4-amino-2*S*-hydroxybutyrate moiety were also characterized by the Cambridge group.[31,32] Details of the enzymatic functions of the butirosin biosynthetic enzymes were described in a recent review.[22]

Overall, most proteins encoded in the neomycin and butirosin biosynthetic gene cluster are apparently required for the construction

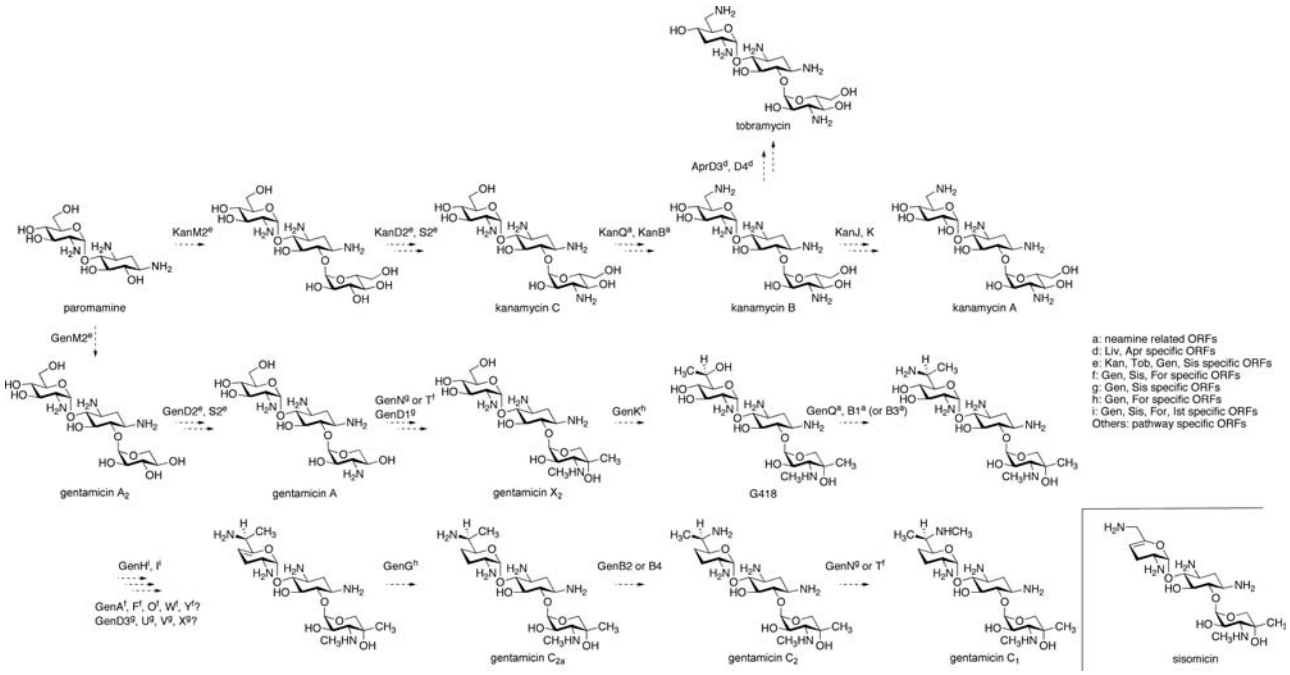

Figure 4 Kanamycin, tobramycin and gentamicin biosynthetic pathways. Structurally related sisomicin is also shown.

of aminoglycosides (Table 1). However, several proteins appear to be inactive and remain merely as evolutional relics. For example, BtrE encoded in the butirosin gene cluster was presumed to be responsible for the dehydrogenation of 2DOIA in the 2DOS pathway, although it showed no expected activity.[26] A butirosin-specific radical SAM enzyme, BtrN, was then found to be responsible for dehydrogenation instead of BtrE.[33] In addition, it is noteworthy that C-6′ of paromomycin and lividomycin remains in the hydroxy group, even though a set of dehydrogenase and aminotransferase responsible for the neamine biosynthesis is conserved. Therefore, the dehydrogenase should not recognize paromamine toward the neamine formation.

In lividomycin biosynthesis, the hydroxy group at C-3′ of paromomycin is expected to be removed by certain enzymes. This deoxy structure is also apparent in tobramycin and apramycin, which are produced by two independent biosynthetic gene clusters in the same microorganisms. Two unique enzymes, LivW and LivY (nos. 38 and 39), are conserved in both the lividomycin and apramycin biosynthetic gene clusters. Consequently, these putative radical SAM oxidoreductase and dehydrogenase appear to be responsible for deoxygenation at C-3′ of the paromamine moiety. The LivY homologous protein is also encoded in the gentamicin biosynthetic gene cluster and might be involved in the deoxygenation reaction at the corresponding position of gentamicin. It is unclear what enzyme is responsible for the mannosylation at C-5‴ of lividomycin B leading to lividomycin A. A certain glycosyltransferase outside of the gene cluster might be responsible for the reaction.

KANAMYCIN-RELATED BIOSYNTHETIC GENES

On the basis of the information described above for the characterized neomycin and butirosin biosynthetic enzymes, one can simply speculate about the functions of kanamycin biosynthetic enzymes (Figure 4). Paromamine biosynthesis is expected to be the same as the pathway in neomycin biosynthesis. Consequently, five conserved enzymes—(nos. 1–5) KanC, KanS1, KanE, KanM1 and KanN—might be responsible for paromamine formation. Recombinant KanM1 protein was reported to have only a weak glycosyltransferase activity with 2DOS and TDP-glucose and GDP-mannose.[34] In contrast, these five *kan* genes expressing *Streptomyces lividans* reportedly produce paromamine, indicating that our proposed enzymatic function is likely.[35] However, detailed enzymatic analysis is expected to be necessary to characterize the real function of KanM1.

One homologous glycosyltransferase, KanM2, is expected to attach glucose at the C-6 of paromamine with NDP-glucose. Then, oxidation and subsequent transamination can be catalyzed using a putative dehydrogenase, KanD2, and an aminotransferase, KanS2, respectively, to afford kanamycin C. These three proteins—KanM2, KanD2 and KanS2—are uniquely conserved in the kanamycin, tobramycin and gentamicin biosynthetic gene cluster (Table 1, nos. 4–2, 43, 2–2). The next oxidation and transamination can be catalyzed by an FAD-dependent oxidoreductase, KanQ, and a pyridoxal phosphate (PLP)-dependent aminotransferase, KanB, similar to neamine formation in the neomycin biosynthetic pathway.

Deamination and hydroxylation at C-2′ of kanamycin B to afford kanamycin A might be catalyzed by two unique unknown functional hypothetical proteins, KanJ and KanK, which are only unassigned open reading frames (ORFs), except for transcriptional regulators, transporters and resistance enzymes in the kanamycin biosynthetic gene cluster. Although a reverse scheme of oxidation and transamination in the conversion of a hydroxy to an amino group is simply inferred, KanJ and KanK show no homology to such enzymes. Alternatively, oxidation of the amino group to form an imine intermediate that is hydrolyzed non-enzymatically to be a ketone is the likely transformation. The presumed ketone intermediate might be reduced to be kanamycin A. Deoxygenation at C-3′ of kanamycin B leading to tobramycin can be catalyzed by a unique radical SAM oxidoreductase AprD4 and a dehydrogenase AprD3 in the apramycin gene cluster, as described above.

GENTAMICIN-RELATED BIOSYNTHETIC GENES

The gentamicin biosynthetic pathway shares several similar enzymatic reaction steps with the kanamycin biosynthetic pathway (Figure 4). GenC, GenS1, GenE, GenM1 and GenD seem to be responsible for the

paromamine formation, similar to the neomycin biosynthetic pathway. The Gen-specific and Sis-specific[36] enzymes, GenD1, GenD2, GenX, GenU, GenV, GenN, GenS2 and GenM2, could then be involved in the biosynthesis of the garosamine moiety. A putative glycosyltransferase, GenM2, is expected to be a xylose transferase, which could use NDP-xylose as a glycosyl donor. A putative dehydrogenase, GenD2, and a putative aminotransferase, GenS2, might be responsible for the oxidation and transamination at C-3″, similar to the kanamycin biosynthesis. A putative radical SAM *C*-methyltransferase, GenD1, can catalyze the *C*-methylation at C-6″ and a putative *N*-methyltransferase, GenN, can catalyze *N*-methylation either of N-6′ or N-3″. The other proteins—GenX, GenU and GenV—might be involved in the other chemistry in the garosamine formation or unexpected reaction steps.

Gentamicin-specific genes compared with sisomicin biosynthetic genes are GenK, GenB2, GenB4 and GenG. GenK and GenG are also conserved in the fortimicin biosynthetic gene cluster. Consequently, a putative radical SAM *C*-methyltransferase, GenK, might catalyze the *C*-methylation of the purpurosamine moiety. Another hypothetical protein, GenG, might be involved in the reduction of C-4′ and C-5′. In contrast, the putative PLP-dependent enzymes GenB2 and GenB4 might be responsible for the PLP-dependent epimerization at C-6′ in the late stage of the biosynthesis.

In the gentamicin, sisomicin, fortimicin and istamycin biosynthetic gene clusters, GenH, GenI, GenQ and GenB1 (and/or B3 also) are conserved. They are apparently responsible for the biosynthesis of the common feature of the purpurosamine moiety. A putative FAD-dependent dehydrogenase, GenQ, and a putative aminotransferase, GenB1, are expected to be responsible for the oxidation and transamination at C-6′, as is apparent in neamine biosynthesis. Moreover, other hypothetical proteins, GenH and GenI, are apparently responsible for the dideoxygenation of C-3′ and C-4′. This enzymatic transformation can contain dehydration and subsequent reduction. Consequently, certain redox enzymes are apparently involved in this sequential reaction. GenO, GenW, GenY, GenA, GenF and GenT are conserved in fortimicin biosynthetic genes and might be involved in the dideoxygenation reaction, although, in that case, istamycin biosynthesis requires extra ORFs outside of the gene cluster for the dideoxygenation. Among these, GenF is presumed to be a radical SAM oxidoreductase. It might therefore be involved in the reduction step in deoxygenation. The istamycin biosynthetic gene cluster contains an extra radical SAM enzyme, IstL3, which might be involved in the reduction chemistry. A putative methyltransferase, GenT, might catalyze *N*-methylation either of N-6′ or N-3″, and the other hypothetical proteins GenO, GenW, GenY and GenA might assist dehydration reactions in dideoxygenation as an acid/base catalyst or attach good leaving groups such as phosphate. Alternatively, these might be inactive for biosynthetic enzymatic reactions. A putative dehydrogenase, GenD3, might be involved in reduction during deoxygenation, as described in the section describing lividomycin/apramycin deoxygenation.

Heterologous expression of *genC*, *genS1*, *genE*, *genM1*, *genD* and *genM2* genes in *S. venezuelae* was attempted, resulting in gentamicin A2 formation.[37] This result clearly supports the above-proposed function of Gen enzymes. In addition, *genD1* gene disruption yielded accumulation of gentamicin A2, indicating that this putative radical SAM *C*-methyltransferase works after gentamicin A2 formation.[38] Detailed enzymatic analysis of GenD1 is necessary to determine the true substrate.

FORTIMICIN–ISTAMYCIN BIOSYNTHETIC GENES

In istamycin biosynthesis, 2DOI synthase IstC and 2DOI aminotransferase IstS are expected to be used to synthesize the aminocyclitol skeleton (Figure 5). In contrast, in fortimicin biosynthesis, *myo*-inositol 1-phosphate can be used as the precursor, and a putative inositol phosphate phosphatase, ForA, and a putative inositol, 2-dehydrogenase ForG, catalyze dephosphorylation and oxidation to give *scyllo*-inosose, which is converted to *scyllo*-inosamine by a putative aminotransferase, ForS. The following pathway is expected to be similar to the paromamine–neamine pathway, except for the regiospecificity of a putative NAD-dependent dehydrogenase, ForE, which must oxidize C-6 of the cyclitol moiety instead of C-1 after pseudosaccharide formation catalyzed using a putative glycosyltransferase ForM and a putative deacetylase ForD. A putative

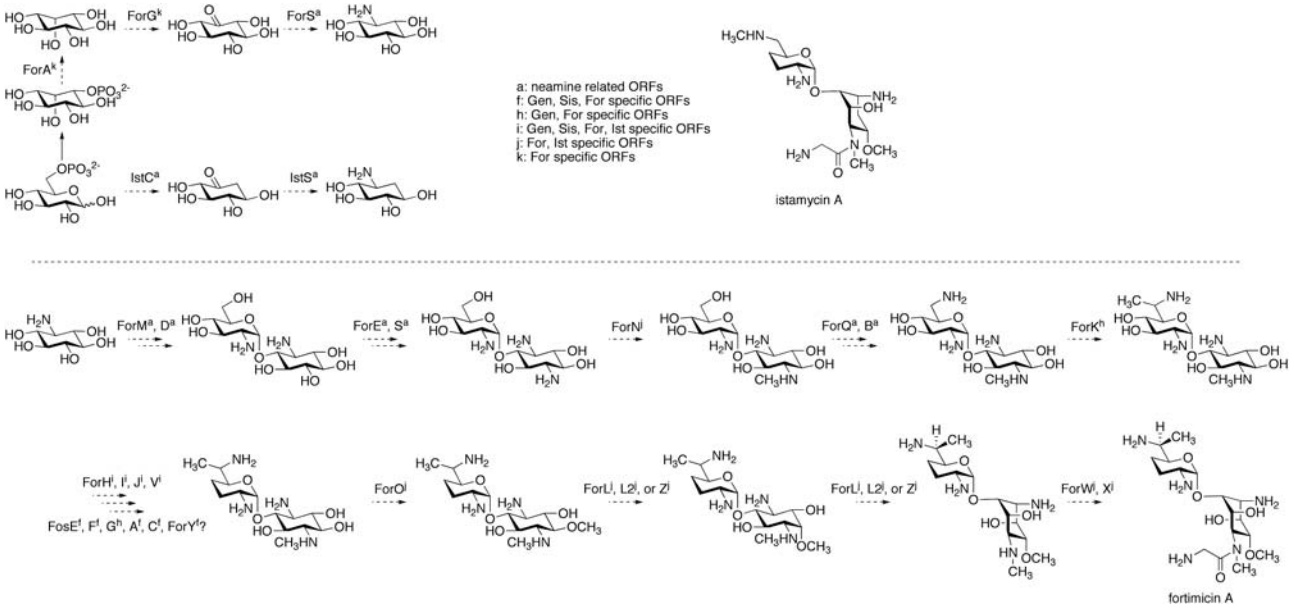

Figure 5 Fortimicin biosynthetic pathway. Structurally related istamycin is also shown.

dual functional aminotransferase, ForS, is then presumed to catalyze transamination at C-6 of the cyclitol moiety.

In fortimicin and istamycin biosynthesis, dideoxygenation of a sugar moiety is also interesting to determine which enzymes are responsible. Although several homological hypothetical proteins, ForH, ForI, ForJ and ForV, are conserved in the For, Ist, Gen and Sis gene clusters, the numbers of proteins differ. Moreover, these proteins would not be sufficient for the presumed two sets of dehydration and reduction to construct the dideoxy moiety, as discussed above. Consequently, several redox enzymes conserved in the For, Gen and Sis gene clusters might be involved in such dehydration and reduction. In istamycin biosynthesis, some extra radical SAM enzymes, IstL, IstL2 or IstL3, might be involved in the reduction. During fortimicin biosynthesis, two unique enzymes conserved in For and Gen might be responsible for the *C*-methylation and deoxygenation. A putative radical SAM enzyme, ForK, was in fact verified to be the *C*-methyltransferase by a gene complementation study.[39] Another hypothetical enzyme, ForG, might be involved in dideoxygenation, as described in the section of the gentamicin biosynthetic pathway.

Finally, the For-specific and Ist-specific enzymes are ForW, ForO, ForL, ForL2, ForZ, ForX and ForN, which are apparently involved in the fortamine moiety. The putative methyltransferases, ForO and ForN, can catalyze either *O*-methylation or *N*-methylation of the cyclitol moiety. Two putative radical SAM enzymes, ForL and ForL2, and/or an FAD-dependent oxidoreductase, ForZ, can be involved in redox reactions such as epimerization reactions at C-3 and C-4. The remaining two hypothetical proteins, ForW and ForX, might be involved in the glycyltransfer reaction. The istamycin-specific methyltransferase, IstU, might be involved in *N*-methylation of the amino group at C-6′.

OTHER 2DOS-CONTAINING AMINOGLYCOSIDE BIOSYNTHETIC GENES

The apramycin and hygromycin B biosynthetic enzymes are unique, even though several 2DOS and neamine-related biosynthetic enzymes are conserved. The apramycin biosynthetic gene cluster lacks one aminotransferase gene for amination at C-6′ of paromamine (Table 1). Therefore, a possible aldehyde intermediate might be formed using a putative FAD-dependent dehydrogenase, AprQ, and then converted to the octose moiety, although the timing of the enzymatic reaction is unclear. Two putative dehydrogenase AprD3 and oxidoreductase AprD4 conserved in the Apr and Liv clusters are apparently involved in the deoxygenation, as described above. The remaining Apr-specific enzymes are expected to be involved in the construction of the octose moiety and attachment of the additional sugar moiety.

Hygromycin B biosynthetic gene cluster contains three 2DOS biosynthetic enzymes; the other ORFs appear to be unique for hygromycin B biosynthesis, as presented in Table 1. Several Hyg enzymes are conserved in the spectinomycin biosynthetic gene cluster[40] and are apparently responsible for a similar acetal structure.

OTHER AMINOGLYCOSIDE BIOSYNTHETIC GENES

The streptomycin, bluensomycin, spectinomycin and kasugamycin biosynthetic genes are also known. Actually, the streptomycin biosynthetic system has historically been well studied at the genetic and enzymatic levels. In fact, its complex regulation system has been mostly established.[41] However, not so many biosynthetic enzymes have been characterized even now because, probably, the biosynthetic pathway for streptomycin is too unique to predict appropriate functions compared with other aminoglycoside biosynthetic genes. Among the streptomycin biosynthetic enzymes, Gln:*scyllo*-inosose aminotransferase StsC[15] and Arg:inosamine-phosphate amidinotransferase StrB1[16] are characterized biochemically. Characterization of StsC was important, as described in the Introduction section, and thus led to the characterization of Gln:2DOI aminotransferase BtrS in the 2DOS biosynthesis.[24] This characteristic inosose aminotransferase is conserved completely in the aminocyclitol-containing aminoglycoside antibiotic biosynthetic gene clusters (Table 1). Kasugamycin lacks the amino functionality in the cyclitol moiety and therefore does not possess the aminotransferase gene in the gene cluster.[42]

Several biosynthetic enzymes for bluensomycin[43] and spectinomycin[44] have also been characterized, but those studies have not been performed systematically yet. Biochemical characterization of many other enzymes is necessary to understand complex biosynthetic pathways for these aminoglycosides on the enzymatic reaction level.

CONCLUDING REMARKS

A tremendous amount of genetic information is made available through genome projects of living systems, including those of microorganisms. Consequently, on the basis of its genomic information, one can predict that *Frankia* sp. CcI3 would produce fortimicin/istamycin-like aminoglycoside antibiotics (Figure 2 and Table 1). In addition, recombinant proteins expressed in heterologous host strains are now easily obtained for functional characterization. However, as we described above, so many uncharacterized proteins are encoded in small secondary metabolic biosynthetic gene clusters even now. Our classification of 2DOS aminoglycoside antibiotic biosynthetic enzymes would help to investigate the function, leading to the elucidation of whole biosynthetic pathways. Fundamentally, aminoglycoside biosynthesis contains several sets of oxidation/transamination for conversion of a hydroxy group to an amino group, glycosylation/deacetylation to attach a glucosamine, phosphoribosylation/dephosphorylation to attach a ribose group, glucosylation, probable dehydration/reduction to make a deoxysugar moiety, methylation and epimerization. Combinations of these enzymatic reactions and substrate specificity of the enzymes determine the final structure of aminoglycosides. Once we assimilate the insights of enzymatic reactions, including substrate specificities, and handle such enzymes through protein engineering, a rational combinatorially fashioned biosynthetic approach to create various structural aminoglycosides can be undertaken. It is therefore now important to verify the proposed function of the enzymes, including hypothetical proteins. Our proposed biosynthetic pathways suggest that many unknown functional hypothetical proteins might be involved in the biosynthesis of aminoglycosides. Characterization of such proteins would expand the number of functional enzymes and contribute greatly to the development of bioscience. We are therefore now struggling to characterize such aminoglycoside biosynthetic enzymes.

ACKNOWLEDGEMENTS

Our biosynthetic study has been supported by many grants from MEXT and nongovernment foundations. We gratefully acknowledge our numerous colleagues, especially the late Professor Katsumi Kainuma, who initiated our 2DOS-containing aminoglycoside biosynthetic studies 20 years ago. His contribution to this field is continuously and greatly appreciated.

1 Davies, J. in Aminoglycoside Antibiotics. In the beginning there was streptomycin (ed Arya, D.P.) 1–13 (John Wiley & Sons Inc., Hoboken, NJ, 2007).
2 Carter, A. P. *et al.* Functional insights from the structure of the 30S ribosomal subunit and its interactions with antibiotics. *Nature* **407,** 340–348 (2000).

3 Wright, G. D. Aminoglycoside-modifying enzymes. *Curr. Opin. Microbiol.* **2,** 499–503 (1999).
4 Shakya, T. & Wright, G. D. Mechanisms of aminoglycoside antibiotic resistance. in *Aminoglycoside Antibiotics* (ed. Arya, D. P.) 119–140 (John Wiley & Sons Inc., Hoboken, NJ, 2007).
5 Kondo, S. & Hotta, K. Semisynthetic aminoglycoside antibiotics: development and enzymatic modifications. *J. Infect. Chemother.* **5,** 1–9 (1999).
6 Elson-Schwab, L. & Tor, Y. Targeting HIV-1 RNA with Aminoglycoside antibiotics and their derivatives. in *Aminoglycoside Antibiotics* (ed. Arya, D. P.) 267–287 (John Wiley & Sons Inc., Hoboken, NJ, 2007).
7 Denap, J. C., Thomas, J. R., Musk, D. J. & Hergenrother, P. J. Combating drug-resistant bacteria: small molecule mimics of plasmid incompatibility as antiplasmid compounds. *J. Am. Chem. Soc.* **126,** 15402–15404 (2004).
8 Thomas, J. R. & Hergenrother, P. J. Targeting RNA with small molecules. *Chem. Rev.* **108,** 1171–1224 (2008).
9 Rinehart, Jr. K. L. & Stroshane, R. M. Biosynthesis of aminocyclitol antibiotics. *J. Antibiot.* **29,** 319–353 (1976).
10 Rinehart, Jr. K. L. Biosynthesis and mutasynthesis of aminocyclitol antibiotics. *J. Antibiot.* **32,** S32–S46 (1979).
11 Furumai, T., Takeda, K., Kinumaki, A., Ito, Y. & Okuda, T. Biosynthesis of butirosins. II. Biosynthetic pathway of butirosins elucidated from cosynthesis and feeding experiments. *J. Antibiot.* **32,** 891–899 (1979).
12 Walker, J. B. Enzymic synthesis of aminocyclitol moieties of aminoglycoside antibiotics from inositol by *Streptomyces* spp.: detection of glutamine-aminocyclitol aminotransferase and diaminocyclitol aminotransferase activities in a spectinomycin producer. *J. Bacteriol.* **177,** 818–822 (1995).
13 Distler, J., Braun, C., Ebert, A. & Piepersberg, W. Gene cluster for streptomycin biosynthesis in *Streptomyces griseus*: analysis of a central region including the major resistance gene. *Mol. Gen. Genet.* **208,** 204–210 (1987).
14 Distler, J., Mansouri, K., Mayer, G., Stockmann, M. & Piepersberg, W. Streptomycin biosynthesis and its regulation in Streptomycetes. *Gene* **115,** 105–111 (1992).
15 Ahlert, J., Distler, J., Mansouri, K. & Piepersberg, W. Identification of *stsC*, the gene encoding the L-glutamine:*scyllo*-inosose aminotransferase from streptomycin-producing Streptomycetes. *Arch. Microbiol.* **168,** 102–113 (1997).
16 Fritsche, E., Bergner, A., Humm, A., Piepersberg, W. & Huber, R. Crystal structure of L-arginine:inosamine-phosphate amidinotransferase StrB1 from *Streptomyces griseus*: an enzyme involved in streptomycin biosynthesis. *Biochemistry* **37,** 17664–17672 (1998).
17 Beyer, S., Mayer, G. & Piepersberg, W. The StrQ protein encoded in the gene cluster for 5′-hydroxystreptomycin of *Streptomyces glaucescens* GLA.0 is a alpha-D-glucose-1-phosphate cytidylyltransferase (CDP-D-glucose synthase). *Eur. J. Biochem.* **258,** 1059–1067 (1998).
18 Yamase, H., Zhao, L. & Liu, H.-w. Engineering a hybrid sugar biosynthetic pathway: production of L-rhamnose and its implication on dihydrostreptose biosynthesis. *J. Am. Chem. Soc.* **122,** 12397–12398 (2000).
19 Kudo, F., Hosomi, Y., Tamegai, H. & Kakinuma, K. Purification and characterization of 2-deoxy-*scyllo*-inosose synthase derived from *Bacillus circulans*. A crucial carbocyclization enzyme in the biosynthesis of 2-deoxystreptamine-containing aminoglycoside antibiotics. *J. Antibiot.* **52,** 81–88 (1999).
20 Kudo, F. *et al*. Molecular cloning of the gene for the key carbocycle-forming enzyme in the biosynthesis of 2-deoxystreptamine-containing aminocyclitol antibiotics and its comparison with dehydroquinate synthase. *J. Antibiot.* **52,** 559–571 (1999).
21 Ota, Y. *et al.* Butirosin-biosynthetic gene cluster from *Bacillus circulans*. *J. Antibiot.* **53,** 1158–1167 (2000).
22 Kudo, F. & Eguchi, T. Biosynthetic enzymes for the aminoglycosides butirosin and neomycin. *Methods Enzymol.* **459,** 493–519 (2009).
23 Piepersberg, W., Aboshanab, K. M., Schmidt-Beissner, H. & Wehmeier, U. F. The biochemistry and genetics of aminoglycoside producers. in *Aminoglycoside Antibiotics* (ed. Arya, D. P.) 15–118 (John Wiley & Sons Inc., Hoboken, NJ, 2007).
24 Tamegai, H. *et al.* Identification of L-glutamine: 2-deoxy-*scyllo*-inosose aminotransferase required for the biosynthesis of butirosin in *Bacillus circulans*. *J. Antibiot.* **55,** 707–714 (2002).
25 Huang, F., Li, Y., Yu, J. & Spencer, J. B. Biosynthesis of aminoglycoside antibiotics: cloning, expression and characterization of an aminotransferase involved in the pathway to 2-deoxystreptamine. *Chem. Commun.* 2860–2861 (2002).
26 Kudo, F., Yamamoto, Y., Yokoyama, K., Eguchi, T. & Kakinuma, K. Biosynthesis of 2-deoxystreptamine by three crucial enzymes in *Streptomyces fradiae* NBRC 12773. *J. Antibiot.* **58,** 766–774 (2005).
27 Yokoyama, K. *et al.* Stereochemical recognition of doubly functional aminotransferase in 2-deoxystreptamine biosynthesis. *J. Am. Chem. Soc.* **127,** 5869–5874 (2005).
28 Yokoyama, K., Yamamoto, Y., Kudo, F. & Eguchi, T. Involvement of two distinct *N*-acetylglucosaminyltransferases and a dual-function deacetylase in neomycin biosynthesis. *Chembiochem.* **9,** 865–869 (2008).
29 Huang, F. *et al.* Elaboration of neosamine rings in the biosynthesis of neomycin and butirosin. *Chembiochem.* **8,** 283–288 (2007).
30 Kudo, F., Fujii, T., Kinoshita, S. & Eguchi, T. Unique *O*-ribosylation in the biosynthesis of butirosin. *Bioorg. Med. Chem.* **15,** 4360–4368 (2007).
31 Li, Y., Llewellyn, N. M., Giri, R., Huang, F. & Spencer, J. B. Biosynthesis of the unique amino acid side chain of butirosin: possible protective-group chemistry in an acyl carrier protein-mediated pathway. *Chem. Biol.* **12,** 665–675 (2005).
32 Llewellyn, N. M., Li, Y. & Spencer, J. B. Biosynthesis of butirosin: transfer and deprotection of the unique amino acid side chain. *Chem. Biol.* **14,** 379–386 (2007).
33 Yokoyama, K., Numakura, M., Kudo, F., Ohmori, D. & Eguchi, T. Characterization and mechanistic study of a radical SAM dehydrogenase in the biosynthesis of butirosin. *J. Am. Chem. Soc.* **129,** 15147–15155 (2007).
34 Park, S. H. *et al.* Expanding substrate specificity of GT-B fold glycosyltransferase via domain swapping and high-throughput screening. *Biotechnol. Bioeng.* **102,** 988–994 (2009).
35 Nepal, K. K., Oh, T. J. & Sohng, J. K. Heterologous production of paromamine in *Streptomyces lividans* TK24 using kanamycin biosynthetic genes from *Streptomyces kanamyceticus* ATCC12853. *Mol. Cells* **27,** 601–608 (2009).
36 Hong, W. R. *et al.* Molecular cloning and sequence analysis of the sisomicin biosynthetic gene cluster from *Micromonospora inyoensis*. *Biotechnol. Lett.* **31,** 449–455 (2009).
37 Park, J. W. *et al.* Genetic dissection of the biosynthetic route to gentamicin A2 by heterologous expression of its minimal gene set. *Proc. Natl Acad. Sci. USA* **105,** 8399–8404 (2008).
38 Kim, J. Y. *et al.* Gene inactivation study of *gntE* reveals its role in the first step of pseudotrisaccharide modifications in gentamicin biosynthesis. *Biochem. Biophys. Res. Commun.* **372,** 730–734 (2008).
39 Kuzuyama, T., Seki, T., Dairi, T., Hidaka, T. & Seto, H. Nucleotide sequence of fortimicin KL1 methyltransferase gene isolated from *Micromonospora olivasterospora*, and comparison of its deduced amino acid sequence with those of methyltransferases involved in the biosynthesis of bialaphos and fosfomycin. *J. Antibiot.* **48,** 1191–1193 (1995).
40 Kim, K. R., Kim, T. J. & Suh, J. W. The gene cluster for spectinomycin biosynthesis and the aminoglycoside-resistance function of *spcM* in *Streptomyces spectabilis*. *Curr. Microbiol.* **57,** 371–374 (2008).
41 Hara, H., Ohnishi, Y. & Horinouchi, S. DNA microarray analysis of global gene regulation by A-factor in *Streptomyces griseus*. *Microbiology* **155,** 2197–2210 (2009).
42 Ikeno, S., Aoki, D., Hamada, M., Hori, M. & Tsuchiya, K. S. DNA sequencing and transcriptional analysis of the kasugamycin biosynthetic gene cluster from *Streptomyces kasugaensis* M338–M1. *J. Antibiot.* **59,** 18–28 (2006).
43 Walker, J. B. Pathways of biosynthesis of the guanidinated inositol moieties of streptomycin and bluensomycin. *Methods Enzymol.* **43,** 429–433 (1975).
44 Thapa, L. P., Oh, T. J., Liou, K. & Sohng, J. K. Biosynthesis of spectinomycin: heterologous production of spectinomycin and spectinamine in an aminoglycoside-deficient host, *Streptomyces venezuelae* YJ003. *J. Appl. Microbiol.* **105,** 300–308 (2008).

The Journal of Antibiotics (2009) 62, 483–487

www.nature.com/ja

ORIGINAL ARTICLE

Five new epothilone metabolites from *Sorangium cellulosum* strain So0157-2

Jidong Wang, Hui Zhang, Linping Ying, Chuanxi Wang, Nan Jiang, Yue Zhou, Haibin Wang and Hua Bai

With the aim of identifying more novel natural epothilone derivatives produced by the epothilones A and B producing strain *Sorangium cellulosum* strain So0157-2, a large-scale fermentation (5000 l) of the strain was carried out. As a result, five new epothilone variants (1–5) were isolated from the fermentation broth. Their structures were established as 3-α-D-arabinofuranosides of epothilones A (1), B (2), D (3), C_9 (4) and 8-demethyl epothilone A (5) by extensive NMR analysis and chemical methods. Bioassay results showed that compounds 1 and 2 had a weaker cytotoxic activity than did epothilone B.
The Journal of Antibiotics (2009) **62,** 483–487; doi:10.1038/ja.2009.55; published online 3 July 2009

Keywords: cytotoxic activity; epothilone derivatives; *Sorangium cellulosum*

INTRODUCTION

Epothilones are naturally occurring 16-membered ring macrolides that constitute a novel class of antimicrotubule-targeting agents. As the major products, epothilones A and B, were originally isolated from fermentations of the soil-derived myxobacterium *Sorangium cellulosum* So ce90,[1–3] many natural epothilone analogs and related structures have been described.[4–6] Moreover, synthetic and semisynthetic methods were important alternatives for obtaining epothilone analogs. At present, more epothilone variants are prepared in a synthetic manner.[7,8] Of all the epothilones and other variants coming from natural resources and synthesis, ixabepilones have been approved by FDA in 2007 for clinical use for the treatment of certain forms of breast cancer, in addition to a number of them being in preclinical and clinical trials.[9] The attractive potential of epothilones led us to search for more potent and selective epothilone derivatives to satisfy the needs of chemotherapy for tumors. Presumably, when fermentation was scaled up, there were some minor and new analogs that were not isolated in small-scale fermentation. Hence, we investigated the chemical compositions of large-scale fermentation (5000 l) of epothilones A and B producing strain *S. cellulosum* strain So0157-2,[10] and five new epothilone variants (**1–5**, Figures 1 and 2) were obtained. Their structures were established as 3-α-D-arabinofuranosides of epothilones A (**1**), B (**2**), D (**3**), C_9 (**4**) and 8-demethyl epothilone A (**5**) by extensive NMR analysis and chemical methods. This paper describes the isolation and structure determination of the five new compounds and the cytotoxic activity of compounds **1** and **2**.

RESULTS AND DISCUSSION

Structure elucidation

In the large-scale production and isolation of epothilones A and B from the strain *S. cellulosum* strain So0157-2, the byproducts, including other epothilones, were pooled and a crude extract was obtained. The pooling crude extract was isolated by silica gel column chromatography and semi-preparative HPLC to afford five new epothilone derivatives (**1–5**).

Compound **1** was isolated as a colorless oil. Its molecular formula of $C_{31}H_{47}NO_{10}S$ was deduced from high-resolution electrospray ionization mass spectrometry (HRESIMS) *m/z* 648.2840 ($[M+Na]^+$, calcd 648.2818). The IR spectrum showed the hydroxyl absorption band at 3444 cm^{-1}. The ^1H NMR spectrum of **1** showed two characteristic downfield singlet signals and one singlet methyl signal of epopthilones A and B at δ 7.26, 6.55 and 2.69, respectively. In addition to one vinyllic methyl at δ 2.07, two aliphatic methyl doublets at δ 1.16 and 1.03 and two aliphatic methyl singlets at δ 1.20 and 1.32 were observed in the upfield. These data agreed well with those of epothilone A, except for a singlet proton signal at δ 5.12 and five proton signals between δ 4.04 and δ 3.60. The ^{13}C NMR and distortionless enhancement by polarization transfer 135 (DEPT 135) spectra of **1** exhibited 32 carbons. Except for five oxygenated carbons (one acetal carbon, three oxygenated methines and one oxygenated methylene), the chemical shifts of the remaining carbons were almost identical to that of epothilone A. By a detailed analysis of ^1H and ^{13}C NMR data and ^1H-^1H correlation spectroscopy (^1H-^1H COSY) and heteronuclear multiple bond correlation (HMBC) spectra, a furanose was connected to the anomeric carbon at δ 109.0. These data showed that compound **1** included two moieties, aglycone was epothilone A and sugar was a furanose. The connection position of sugar to aglycone epothilone A was confirmed by HMBC experiments. The crossing peak between δ 5.12 (anomeric proton) and the δ 80.7 (C-3) indicated that sugar connected to epothilone A by an ether bond between C-3 and C-1′. Thus, the gross planar structure of **1** was established. The attempt to perform acid hydrolysis of compound **1** to

Zhejiang Hisun Pharmaceutical Co. Ltd, Taizhou, Zhejiang, China
Correspondence: Professor H Wang, Zhejiang Hisun Pharmaceutical Co. Ltd, Taizhou, Zhejiang 318000, China.
E-mail: hbwang@hisunpharm.com
Received 29 April 2009; revised 12 June 2009; accepted 15 June 2009; published online 3 July 2009

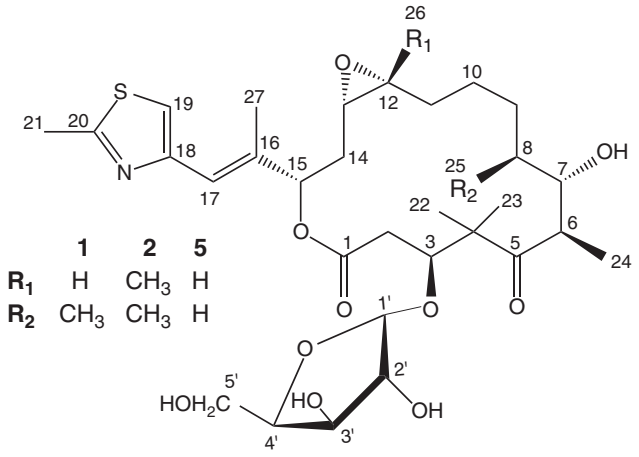

Figure 1 The structures of compounds **1**, **2** and **5**.

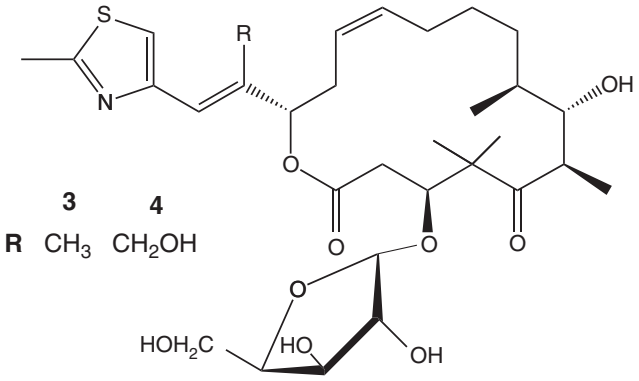

Figure 2 The structures of compounds **3** and **4**.

obtain epothilone A was unsuccessful because of the instability of the three-membered ring between C-11 and C-12. By a detailed comparison of the ^{1}H and ^{13}C NMR data of **1** with those of epothilone A in conjunction with concurring with epothilone A, the relative and absolute configuration of the aglycone of **1** was assigned as that of epothilone A.

Acid hydrolysis of **1** afforded an aglycone and a sugar, and the sugar component identified by co-chromatography with authentic samples of arabinose, ribose and xylose on TLC analysis, and the identical R_F values of the sugar moiety with those of arabinose indicated that the sugar moiety of **1** was arabinose. Absolute configuration for the arabinose was determined to be the D form according to the procedure developed by Tanaka *et al.*[11] Comparison of the ^{13}C NMR data of the furanose moiety of **1** with that of methyl α-D-arabinofuranoside and methyl β-D-arabinofuranoside reported in the literature,[12] along with the small coupling constant (J=1.2 Hz) of the anomeric proton, assigned the configuration of the anomeric center (C-1′) to be α.

Compound **2** was obtained as a colorless oil. HRESIMS gave its molecular formula as $C_{32}H_{49}NO_{10}S$. The ^{1}H and ^{13}C NMR data of **2** were similar to those of compound **1,** except for the fact that a singlet methyl was present at δ 1.29 in the ^{1}H NMR spectrum and an oxygenated quarternary carbon was present at δ 62.0 in the ^{13}C NMR spectrum. Comparing the NMR data of the aglycone of **2** with those of epothilone B, the aglycone of **2** was very similar to epothilone B. Hence the aglycone of **2** was elucidated as epothilone B. The NMR data of sugar moiety were the same as those of **1** and were identified as α-D-arabinofuranose. The linkage of the sugar moiety to epothilone B was confirmed by the HMBC correlations of δ 5.09 (H-1′) and δ 78.6 (C-3).

Compound **3** was isolated as a colorless oil. The molecular formula of **3** was determined to be $C_{31}H_{47}NO_9S$ on the basis of HRESIMS analysis [*m/z* 632.2895 $(M+Na)^+$] and was supported by ^{1}H and ^{13}C NMR data (Tables 1 and 2). The numbers of carbon of **3** were the same as that of **1**. The only difference in NMR spectra between **3** and **1** was that the three-membered ring of C12-C13 in **1** was replaced by a double bond in **3**. Comparing the NMR data of the aglycone of **3** with those of epothilone D, the aglycone of **3** was very similar to epothilone D and the aglycone of **3** was assigned to be epothilone D. The sugar moiety of **3** was established as α-D-arabinofuranose, similar to that of **1**. The connection of the aglycone and sugar moiety was also supported by the HMBC correlation of δ 5.19 (H-1′) and δ 79.4 (C-3).

Compound **4** was assigned the molecular formula of $C_{31}H_{47}NO_{10}S$, similar to that of **1**, on the basis of HRESIMS analysis [*m/z* 648.2800 $(M+Na)^+$] and NMR data (Tables 1 and 2). Analysis of the ^{1}H and ^{13}C NMR data for **4** revealed the presence of nearly identical structural features as those found in **3**, except that the C-27 methyl in **3** was replaced by a hydroxylmethyl in **4**. This result was supported by the ^{1}H-^{13}C long-range correlations between δ_H 6.61 (H-17) and δ_C 58.3 (C-27), 119.3 (C-19) and 79.6 (C-15), and between δ_H 4.35 (H-27) and δ_C 123.4 (C-17), 140.5 (C-16) and 79.6 (C-15). A comparison of the NMR data of the aglycone of **4** with those of epothilone C_9 revealed the aglycone of **4** to be very similar to epothilone C_9 and hence the aglycone of **4** was assigned to be epothilone C_9. The sugar moiety of **4** was established as α-D-arabinofuranose, similar to that of **1**. The connection of aglycone and sugar moiety was confirmed by the HMBC correlation of δ 5.18 (H-1′) and δ 78.8 (C-3).

Compound **5** has a molecular formula of $C_{30}H_{45}NO_{10}S$, consistent with a structure having one less methyl group than does **1**. Comparing the ^{1}H NMR data of **5** with that of **1**, only a doublet methyl was found to be absent in **5**. The present HMBC correlation between δ_H 1.03 (H_3-25) and δ_C 78.7 (C-7) in **1** was not observed in **5,** and the ^{1}H-^{1}H COSY correlation of δ 3.85 (H-7) and a methylene signal at δ 1.46 and 1.60 (H_2-8) suggested that the C-25 methyl in **1** was replaced by a hydrogen atom in **5**. As a result, the aglycone of **5** was elucidated as 8-demethylepothilone A and the sugar moiety of **5** was established as α-D-arabinofuranose, similar to that of **1**. The connection of aglycone of **5** and sugar moiety was supported by the HMBC correlation of δ 5.15 (H-1′) and δ 78.5 (C-3). Thus, the structure of **5** was established.

Biological activity

Compounds **1** and **2** were evaluated for cytotoxic activity against two tumor cell lines by CCK-8 methods,[13] and the results showed that compounds **1** and **2** had a weaker cytotoxic activity than did epothilone B (Table 3).

Previous studies with regard to the structure–activity–relationship of various epothilone analogs had established that, in general, changes in the 16-membered macrolide framework led to a loss of tubulin affinity. For instance, sterechemical inversion[14] and ring contraction/expansion[15] reduced tubulin-binding affinity. Specifically, the C-3 diastereomer (3R) of epothilone A had been reported to be inactive in both tubulin polymerization and cytotoxicity assays.[16] A recent study showed that the 3-hydroxyl group may not be directly involved in the fundamental network of interactions between epothilones and b-tubulin.[17] This suggested that the less potent of **1** and **2,** than epothilone B, may be attributed to the change of conformation of the

Table 1 ^{1}H NMR data for compounds 1–5 (1 in CD_3OD, 2–5 in $CDCl_3$, *J* in Hz)

Proton	***1***	***2***	***3***	***4***	***5***
2	2.92 (m)	2.60 (dd, 16.9, 10.0)	2.58 (dd, 15.8, 10.8)	2.60 (dd, 15.6, 10.6)	2.62 (dd, 15.4, 9.3)
	2.74 (m)	2.42 (dd, 16.9, 2.4)	2.43 (dd, 15.8, 2.1)	2.48 (dd, 15.6, 2.4)	2.48 (dd, 15.4, 2.6)
3	4.11 (dd, 9.8, 2.2)	4.25 (m)	4.24 (m)	4.24 (m)	4.31 (dd, 9.3, 3.0)
6	3.20 (m)	3.17 (m)	3.06 (m)	3.08 (m)	2.96 (m)
7	3.71 (m)	3.71 (m)	3.71 (m)	3.72 (m)	3.85 (m)
8	1.56 (m)	1.74 (m)	1.70 (m)	1.74 (m)	1.60 (m)
					1.46 (m)
9	1.56 (m)	1.63 (m)	1.31 (m)	1.34 (m)	1.60 (m)
	1.29 (m)	1.39 (m)			
10	1.56 (m)	1.53 (m)	1.65 (m)	1.68 (m)	1.60 (m)
			1.27 (m)	1.26 (m)	1.46 (m)
11	1.78 (m)	1.74 (m)	2.25 (m)	2.27 (m)	1.66 (m)
	1.50 (m)	1.41 (m)	2.01 (m)	2.00 (m)	1.60 (m)
12	2.96 (m)		5.47 (m)	5.49 (m)	2.93 (m)
13	3.12 (m)	2.81 (dd, 9.0, 3.0)	5.41 (m)	5.36 (m)	3.02 (m)
14	2.23 (m)	2.13 (m)	2.81 (m)	2.85 (m)	2.12 (m)
	1.84 (m)	1.99 (m)	2.16 (m)	2.11 (m)	1.94 (m)
15	5.38 (br d, 9.8)	5.51 (dd, 9.6, 2.5)	5.37 (br d, 10.1)	5.38 (br d, 10.6)	5.49 (dd, 9.0, 3.8)
17	6.55 (br s)	6.61 (br s)	6.59 (br s)	6.61 (br s)	6.65 (br s)
19	7.26 (s)	6.99 (s)	6.98 (s)	7.13 (s)	7.01 (s)
21	2.69 (s)	2.69 (s)	2.70 (s)	2.74 (s)	2.70 (s)
22	1.20 (s)	1.09 (s)	1.09 (s)	1.09 (s)	1.11 (s)
23	1.32 (s)	1.34 (s)	1.36 (s)	1.33 (s)	1.33 (s)
24	1.16 (d, 6.7)	1.15 (d, 6.8)	1.19 (d, 6.7)	1.18 (d, 6.8)	1.15 (d, 6.9)
25	1.03 (d, 6.8)	1.02 (d, 7.0)	1.02 (d, 6.8)	1.03 (d, 7.1)	
26		1.29 (s)			
27	2.07 (br s)	2.06 (d, 1.0)	2.07 (d, 0.8)	4.45 (br d, 14.0)	2.07 (d, 0.9)
				4.35 (br d, 14.0)	
1′	5.12 (d, 1.2)	5.09 (br s)	5.19 (br s)	5.18 (br s)	5.15 (br s)
2′	3.82 (dd, 3.3, 1.2)	3.95 (s)	3.92 (br s)	3.86 (m)	3.94 (br s)
3′	3.77 (dd, 5.2, 3.3)	3.95 (s)	3.95 (br d, 8.6)	3.95 (br d, 9.9)	3.98 (m)
4′	4.04 (m)	4.25 (m)	4.26 (m)	4.25 (m)	4.24 (m)
5′	3.68 (m)	3.81 (dd, 11.9, 2.8)	3.85 (dd, 11.9, 2.9)	3.84 (br d, 11.5)	3.82 (dd, 11.9, 2.6)
	3.60 (dd, 11.8, 5.0)	3.72 dd, 11.9, 3.0)	3.76 (dd, 11.9, 1.7)	3.73 (br d, 11.5)	3.73 (dd, 11.9, 2.1)

16-membered macrolide framework influenced by the 3-α-D-arabinofuranoside moiety. Further work should be carried out to clarify the conformation of **1** and **2** and the structure–activity–relationship of C-3-substituted epothilones. Moreover, compounds **1–5** demonstrate the possibility of structure–activity–relationship being involved in the development of the second generation of epothilone.

EXPERIMENTAL SECTION

General experimental procedures

The UV spectra were obtained on a Varian CARY 300 BIO spectrophotometer (Varian Inc., Cary, NC, USA); IR spectra were recorded on a Nicolet Magna FT-IR 750 spectrometer (ν_{max} in cm^{-1}; Nicolet, Tokyo, Japan); ^{1}H and ^{13}C NMR spectra were measured with a Bruker DRX-400 (400 MHz for ^{1}H and 100 MHz for ^{13}C; Bruker, Rheinstetten, Germany) spectrometer. Chemical shifts are reported in parts per million (p.p.m.) (δ), using residual $CHCl_3$ (δ_H 7.26 p.p.m.; δ_C 77.0) or CD_3OD (δ_H 3.30 p.p.m.; δ_C 49.0) as an internal standard, with coupling constants (*J*) in Hz. ^{1}H and ^{13}C NMR assignments were supported by ^{1}H-^{1}H COSY, heteronuclear multiple quantum correlation and HMBC experiments. Electrospray ionization mass spectrometry (ESIMS) and HRESIMS spectra were taken on a Q-TOF Micro LC-MS-MS mass spectrometer (Agilent Technologies UK Ltd., Manchester, UK). The analytic (Zorbax SB-C18, 5 μm, 250×4.6 mm i.d.) and semi-preparative (Zorbax SB-C18, 5 μm, 250×9.4 mm i.d.) RP-HPLC was conducted on an Agilent 1100 series (Agilent Technologies Inc., Palo Alto, CA, USA). Commercial silica gel (Qing Dao Hai Yang Chemical Group Co., Qingdao, Shandong, China; 100–200 and 200–300 mesh) was used for column chromatography.

Myxobacterium material

The producing organism *S. cellulosum* strain So0157-2 was provided by Professor Yuezhong Li at the Shandong University, China and was deposited in the China Center of Typical Culture Collection (CCTCC) with accession no: CCTCC M 208078. Stock cultures were placed on a starch-yeast agar plate (0.8% soluble starch, 0.2% glucose, 0.2% peptone, 0.2% yeast extract, 0.2% $MgSO_4$, 0.1% $CaCl_2$, pH 7.8 autoclave at 121 °C for 30 min). Flask cultures were incubated at 30 °C on a rotary shaker at 250 r.p.m. for 4 days. Fermentation was carried out in a 50 l first seed fermentor (containing 30 l fermentation broth), in a 500 l second seed fermentor (containing 300 l fermentation broth), and finally in a 5000 l fermentor (containing 3000 l fermentation broth) successively. The following production medium was used: 1.0% soluble starch, 0.4% glucose, 0.2% peptone, 0.2% yeast extract, 0.2% $MgSO_4$, 0.1% $CaCl_2$, pH 7.8, autoclave. For the continuous adsorption of epothilones, 2.0% (v/v) of XAD-1600 (Rohm and Haas, Paris, France) was added. Fermentation was carried out at 28 °C for 12 days, stirring at 40 r.p.m. with an aeration rate of 120 m^3 of air per hour.

Extraction and isolation

Adsorber resin (60 l) was separated from the 3000 l fermentation broth with a process filter. After washing the resin with water, the resin was eluted with four

Table 2 ^{13}C NMR and HMBC data for compounds 1–5 (1 in CD_3OD, 2–5 in $CDCl_3$)

Carbon	***1***	***2***	***3***	***4***	***5***	*HMBC (C→H#)*
1	172.6 s	170.1 s	169.9 s	170.3 s	169.9 s	2, 3, 15
2	39.2 t	39.0 t	39.0 t	38.8 t	38.8 t	
3	80.7 d	78.6 d	79.4 d	78.8 d	78.5 d	1′, 22, 23
4	53.6 s	53.5 s	53.3 s	53.1 s	53.2 s	
5	218.9 s	218.9 s	219.7 s	219.7 s	220.5 s	3, 22, 23, 24
6	47.7 d	42.8 d	42.2 d	42.4 d	44.4 d	24
7	78.7 d	73.3 d	73.9 d	73.9 d	69.1 d	24
8	37.3 d	35.7 d	37.9 d	37.9 d	31.9 t	
9	31.7 t	31.0 t	32.2 t	32.3 t	24.8 t	
10	25.7 t	21.9 t	27.2 t	27.3 t	23.8 t	
11	28.3 t	32.8 t	27.5 t	27.6 t	26.4 t	
12	58.9 d	62.0 s	133.7 d	134.0 s	57.1 d	
13	56.5 d	61.8 d	124.6 d	124.4 d	54.4 d	
14	33.8 t	32.9 t	31.6 t	32.1 t	32.2 t	
15	78.3 d	78.2 d	79.5 d	79.6 d	77.9 d	17, 27
16	139.6 s	137.7 s	138.6 s	140.5 s	137.5 s	27
17	120.9 d	121.7 d	120.9 d	123.4 d	121.4 d	27
18	153.0 s	151.3 s	151.6 s	150.9 s	151.4 s	
19	118.0 d	117.0 d	116.6 d	119.3 d	116.9 d	17
20	167.1 s	166.3 s	166.2 s	167.3 s	166.2 s	21
21	18.7 q	17.0 q	18.8 q	19.1 q	18.8 q	
22	24.8 q	19.8 q	20.1 q	20.8 q	20.0 q	
23	23.7 q	23.4 q	23.9 q	23.6 q	23.2 q	
24	16.6 q	12.7 q	13.3 q	13.3 q	11.3 q	
25	19.0 q	17.0 q	15.8 q	15.8 q		
26		22.3 q				
27	15.2 q	14.7 q	15.1 q	58.3 t	15.3 q	17
1′	109.0 d	108.7 d	109.2 d	108.8 d	108.4 d	
2′	83.0 d	79.2 d	78.8 d	79.6 d	79.4 d	
3′	78.7 d	78.3 d	78.2 d	77.9 d	78.3 d	
4′	86.6 d	87.9 d	88.1 d	87.9 d	88.0 d	
5′	63.1 t	62.2 t	62.3 t	62.4 t	62.1 t	

Table 3 Cytotoxicity of compounds 1 and 2 against tumor cell lines (IC_{50}, μg ml^{-1})

	Compounds		
Cell lines	***1***	***2***	*Epothilone B*
A549	1.57	0.846	0.00249
LOVO	9.22	0.801	0.0393
SKOV-3	27.06	15.47	0.00129

bed volumes of 95% ethanol to obtain the ethanol eluent. The ethanol eluent was diluted to about 30% ethanol and subjected to a XAD-1600 resin column, eluting with 30, 40, 50, 60 and 70% ethanol (each concentration eluted with two bed volumes). The eluents eluting with 60 and 70% ethanol were pooled and concentrated in vacuo at 50 °C to give a mixture. The mixture was dissolved in $CHCl_3$ and chromatographed on a silica gel column eluting with petroleum ether/acetone from 70:30–40:60, and fractions 1–4 were obtained on the basis of the TLC profiles. Analysis of fraction 1 by HPLC showed that it mainly contained epothilones A and B. Fractions 2–4 were subjected to a Sephadex LH-20 column (Pharmacia, Uppsala, sweden) and eluted with ethanol and detected by TLC to give subfraction 2, subfraction 3 and subfraction 4, respectively. Subfraction 2 was further separated by semi-preparative HPLC eluting with MeOH/H_2O (80:20) to give compound **3** (t_R16.2 min, 21 mg). Subfraction 3 was also isolated by semi-preparative HPLC eluting with MeOH/CH_3CN/H_2O (35:10:55) to afford compounds **4** (t_R 22.8 min, 11 mg) and **5** (t_R 26.6 min, 8 mg). Subfraction 4 was further purified by semi-preparative HPLC eluting with CH_3CN/H_2O (45:55) to obtain compound **1** (t_R 15.0 min, 55 mg) and one collection (t_R 17.0 min). The collection was further separated by semi-preparative HPLC eluting with MeOH/CH_3CN/H_2O (35:10:55) to give compound **2** (t_R 28.1 min, 10 mg).

Epothilone A 3-α-D-arabinofuranoside (1). Colorless oil; [α]25 D-13.3 (*c* 0.3, EtOH); UV (EtOH) λ_{max} 249 (ε 12083), 206 (ε 20416) nm; IR (KBr): ν_{max} 3444, 1738, 1689 cm^{-1}; ^1H and ^{13}C NMR data, see Tables 1 and 2; ESIMS *m/z* 626 $[M+H]^+$, 648 $[M+Na]^+$; HRESIMS *m/z* 648.2840 $[M+Na]^+$ (calcd for $C_{31}H_{47}NO_{10}SNa$, 648.2818).

Epothilone B 3-α-D-arabinofuranoside (2). Colorless oil; [α]25 D-3.57 (*c* 0.28, EtOH); UV (EtOH) λ_{max} 249 (ε 10437), 212 (ε 13845) nm; IR (KBr): ν_{max} 3455, 1739, 1689 cm^{-1}; ^1H and ^{13}C NMR data, see Tables 1 and 2; ESIMS *m/z* 640 $[M+H]^+$, 662 $[M+Na]^+$; HRESIMS *m/z* 662.2982 $[M+Na]^+$ (calcd for $C_{32}H_{49}NO_{10}SNa$, 662.2975).

Epothilone D 3-α-D-arabinofuranoside (3). Colorless oil; [α]25 D-27.4 (*c* 0.84, EtOH); UV (EtOH) λ_{max} 251 (ε 16443), 213 (ε 20503) nm; IR (KBr): ν_{max} 3457, 1738, 1687 cm^{-1}; ^1H and ^{13}C NMR data, see Tables 1 and 2; ESIMS *m/z* 610 $[M+H]^+$, 632 $[M+Na]^+$; HRESIMS *m/z* 632.2895 $[M+Na]^+$ (calcd for $C_{31}H_{47}NO_9SNa$, 632.2869).

Epothilone C_9 3-α-D-arabinofuranoside (4). Colorless oil; [α]25 D-26.2 (*c* 0.42, EtOH); UV (EtOH) λ_{max} 254 (ε 10714), 209 (ε 9970) nm; IR (KBr): ν_{max} 3446, 1737, 1688 cm^{-1}; ^1H and ^{13}C NMR data, see Tables 1 and 2; ESIMS *m/z* 626 $[M+H]^+$, 648 $[M+Na]^+$; HRESIMS *m/z* 648.2800 $[M+Na]^+$ (calcd for $C_{31}H_{47}NO_{10}SNa$, 648.2818).

8-Demethyl epothilone A 3-α-D-arabinofuranoside (5). Colorless oil; [α]25 D+7.9 (*c* 1.13, EtOH); UV (EtOH) λ_{max} 250 (ε 7087), 214 (ε 8798) nm; IR (KBr): ν_{max} 3438, 1736, 1690 cm^{-1}; ^1H and ^{13}C NMR data, see Tables 1 and 2; ESIMS *m/z* 612 $[M+H]^+$, 634 $[M+Na]^+$; HRESIMS *m/z* 634.2681 $[M+Na]^+$ (calcd for $C_{30}H_{45}NO_{10}SNa$, 634.2662).

Acid hydrolysis of 1

Compound **1** (4.4 mg). was dissolved in 1 M HCl (1 ml) and then heated at 80 °C for 4 h. Aglycone was extracted with $CHCl_3$ thrice, and the aqueous residue was evaporated under reduced pressure. The residue was compared with standard sugars of arabinose, ribose and xylose (Sigma, St Louis, MO, USA) using TLC [*n*-butanol: CH_3COOH: H_2O=4:1:1] analysis, which showed the sugar (R_F=0.4) to be arabinose.

Determination of the absolute configuration of arabinose

The above drying aqueous residue was dissolved in pyridine (0.1 ml) containing L-cysteine methyl ester hydrochloride (1 mg) and heated at 60 °C for 1 h. Arylisothiocyanate (1.2 µl) was added to the mixture, which was heated at 60 °C for 1 h. The reaction mixture was directly analyzed by reversed-phase HPLC on an ODS column (4.6×250 mm) at 35 °C with an isocratic elution of 25% CH_3CN in 50 mM H_3PO_4 for 30 min and a subsequent washing of the column with 90% CH_3CN at a flow rate of 0.8 ml min^{-1}. Peaks were detected with an ultraviolet detector at 250 nm. The peak of the reaction mixture was detected at 15.72 min (D-arabinose). Treated in the same manner, standard D-arabinose (Sigma) gave a peak at 15.76 min and L-arabinose (Sigma) gave a peak at 14.60 min.

Antitumor bioassays

For cytotoxicity measurements, stock epothilonoside solutions were prepared at 100 µg/ml in dimethyl sulfoxide and stored at −20 °C. Human lung carcinoma A549, large intestine cancer cells LOVO and Human Ovarian Cancer Cell Line SKOV-3 were obtained from the Institute of Biochemistry and Cell Biology, Shanghai, Chinese Academy of Sciences. All cell lines were routinely cultured in Dulbecco's modified Eagle's medium containing 10% calf serum at 37 °C for 4 h, in a humidified atmosphere of 5% CO_2 incubator. The adherent cells at their logarithmic growth stage were digested, and were inoculated onto a 96-well culture plate at a density of 1.0×10^4/well for the determination of proliferation. Test samples ranging from 0.1–100 µg ml^{-1} in 100 µl were added to cells in triplicate wells, and incubation was continued for 72 h. Coloration substrate, cell counting kit-8 (CCK-8, Dojindo, Kumamoto, Japan), was added to the medium, followed by further incubation for 3 h. Absorbance at 450 nm with a 600 nm reference was measured thereafter. Media and dimethyl sulfoxide control wells, in which compound was absent, were included in all the experiments in order to eliminate the influence of dimethyl sulfoxide. The inhibitory rate of cell proliferation was calculated by the following formula:

Growth inhibition (%)=$[OD_{control}-OD_{treated}]/OD_{control}\times100\%$.

The cytotoxicity of compound on tumor cells was expressed as IC_{50} values (the drug concentration reducing the absorbance in treated cells by 50%, with respect to untreated cells) and was calculated by the LOGIT method.

^1H and ^{13}C NMR spectra of five new epothilone variants (**1–5**) are detailed in Supplementary information.

1 Höfle, G., Bedorf, N., Gerth, K. & Reichenbach, H. (GBF). Epothilones, process for preparing the same and their use as medicaments and as plant protecting agents. D.E. 4,138,042, May 27 (1993).
2 Gerth, K., Bedorf, N., Höfle, G., Irschik, H. & Reichenbach, H. Epothilons A and B: antifungal and cytotoxic compounds from *Sorangium cellulosum* (Myxobacteria). production, physico-chemical and biological properties. *J. Antibiot.* **49,** 560–563 (1996).
3 Höfle, G. *et al.* Epothilone A and B-novel 16-membered macrolides with cytotoxic activity: isolation, crystal structures, and conformation in solution. *Angew. Chem. Int. Ed. Engl.* **35,** 1567–1569 (1996).
4 Hardt, I. H. *et al.* New natural epothilones from *Sorangium cellulosum*, strains So ce90/B2 and So ce90/D13: isolation, structure elucidation, and SAR studies. *J. Nat. Prod.* **64,** 847–856 (2001).
5 Arslanian, R. L. *et al.* A new cytotoxic epothilone from modified polyketide synthases heterologously expressed in *Myxococcus xanthus*. *J. Nat. Prod.* **65,** 1061–1064 (2002).
6 Starks, C. M., Zhou, Y., Liu, F. & Licari, P. J. Isolation and characterization of new epothilone analogues from recombinant *Myxococcus xanthus* fermentations. *J. Nat. Prod.* **66,** 1313–1317 (2003).
7 Nicolaou, K. C., Roschangar, F. & Vourloumis, D. Chemical biology of epothilones. *Angew. Chem. Int. Ed. Engl.* **37,** 2014–2045 (1998).
8 Dong, S. D. *et al.* Rapid access to epothilone analogs via semisynthetic degradation and reconstruction of epothilone D. *Tetrahedron Lett.* **45,** 1945–1947 (2004).
9 Lee, J. J. & Swain, S. M. The epothilones: translating from the laboratory to the clinic. *Clin. Cancer Res.* **14,** 1618–1624 (2008).
10 Gong, G. L. *et al.* Mutation and a high-throughput screening method for improving the production of epothilones of *Sorangium*. *J. Ind. Microbiol. Biotechnol.* **34,** 615–623 (2007).
11 Tanaka, T., Nakashima, T., Ueda, T., Tomii, K. & Kouno, I. Facile discrimination of aldose enantiomers by reversed-phase HPLC. *Chem. Pharm. Bull.* **55,** 899–901 (2007).
12 Gorin, P. A. J. & Mazurek, M. Further studies on the assignment of signals in ^{13}C magnetic resonance spectra of aldoses and derived methyl glycosides. *Can. J. Chem.* **53,** 1212–1223 (1975).
13 Wang, J. D. *et al.* HS071, A new furan-type cytotoxic metabolite from *Streptomyces* sp. HS-HY-071. *J. Antibiot.* **61,** 623–626 (2008).
14 Nicolaou, K. C. *et al.* Designed epothilones: solid phase synthesis on microtubes, tubulin assembly properties and cytotoxic action against taxol-resistant tumor cells. *Angew. Chem. Int. Ed. Engl.* **36,** 2097–2103 (1997).
15 Nicolaou, K. C. *et al.* Probing the ring size of epothilones: total synthesis of [14]-, [15]-, [17]-, and [18]-epothilones A. *Angew. Chem. Int. Ed. Engl.* **37,** 81–84 (1998).
16 Meng, D. *et al.* Remote effects in macrolide formation through ring-forming olefin metathesis: an application to the synthesis of fully active epothilone congeners. *J. Am. Chem. Soc.* **119,** 2733–2734 (1997).
17 Erdélyi, M. *et al.* Conformational preferences of natural and C3-modified epothilones in aqueous solution. *J. Med. Chem.* **51,** 1469–1473 (2008).

Supplementary Information accompanies the paper on The Journal of Antibiotics website (http://www.nature.com/ja)

The Journal of Antibiotics (2009) 62, 489–493

www.nature.com/ja

ORIGINAL ARTICLE

In vitro evaluation of the antimicrobial activity of HM-242, a novel antiseptic compound

Junji Okunishi[1], Yutaka Nishihara[1], Shirou Maeda[2] and Masahiro Ikeda[1]

The antimicrobial activities of N^4-octyl-6,6-dimethyl-N^2-(4-methylbenzyl)-1,6-dihydro-1,3,5-triazine-2,4-diamine (HM-242), a novel synthetic compound, were compared with those of chlorhexidine gluconate (CHG). HM-242 was a more potent microbicide than CHG *in vitro*; however, its minimal inhibitory concentrations were similar. In particular, HM-242 killed various Gram-positive bacteria, including methicillin-resistant *Staphylococcus aureus* and vancomycin-resistant *Enterococcus faecalis*, both efficiently and rapidly. HM-242 also showed potent virucidal activity against enveloped viruses such as influenza virus and herpes simplex virus. These characteristics suggest that HM-242 may well be useful as an antiseptic.
The Journal of Antibiotics (2009) **62,** 489–493; doi:10.1038/ja.2009.56; published online 3 July 2009

Keywords: bactericidal; chlorhexidine gluconate; disinfection; microbicidal; virucidal

INTRODUCTION

Antiseptics have a number of important roles in infection control in clinical settings, including hand hygiene and skin surface disinfection of surgical fields and catheter insertion sites. Antiseptics prevent infection by decreasing the number of microbes and thereby decreasing the transmission of pathogens.[1–6]

Currently, healthcare-associated infections caused by multidrug-resistant organisms (including methicillin-resistant *Staphylococcus aureus* (MRSA), vancomycin-resistant *Enterococcus faecalis* (VRE) and certain Gram-negative bacilli[4,7–10]) are a significant problem. The presence of MRSA and VRE in US hospitals has been steadily increasing since the 1990s. As multidrug-resistant organisms become more prevalent, it becomes more important to prevent infection by using antiseptics besides administration of antibiotics to cure infectious diseases.[8,11] Several investigations have found that various antibiotic-resistant pathogenic microorganisms were as susceptible to disinfectants as antibiotic-sensitive strains, and the Center for Disease Control and Prevention (CDC) does not recommend any special strategies or germicides with higher potencies against multidrug-resistant organisms.[4,5,8,12]

Chlorhexidine gluconate (CHG) has been widely used for many years. CHG is one of the best antiseptics because it has not only broad-spectrum antibacterial activity, persistent efficacy and residual activity, but is also compatible with most materials, and is safe for humans.[1,3,7,13–18] Therefore, the CDC specifically recommends CHG as the preferred agent for cutaneous antisepsis and surgical hand antisepsis in its 'Guideline for the Prevention of Intravascular Catheter-Related Infections' and its 'Guideline for Hand Hygiene in Health-Care Settings.'[17,19]

Methodologies such as time-kill studies, minimal bactericidal concentration (MBC) studies, minimal inhibitory concentration (MIC) studies, carrier tests and phenol coefficient tests are ordinarily used to evaluate the efficacy of antiseptics *in vitro*. One of the most important characteristics of an antiseptic is that it has microbicidal activity rather than just microbistatic activity because an antiseptic agent needs to kill microorganisms quickly.[1,3] According to some *in vitro* time-kill studies, chlorhexidine does not kill Gram-positive cocci any faster than it kills Gram-negative bacilli.[3,20] It is important to develop a new antiseptic agent that is fast-acting, persistent, safe and has broad-spectrum virucidal efficacy because Gram-positive cocci such as MRSA and VRE cause healthcare-associated infections. HM-242 is a novel candidate antiseptic that was synthesized recently.[21] We show here the results of *in vitro* efficacy studies that compare HM-242 with CHG. We found that HM-242 is a fast-acting, broad-spectrum microbicide with characteristics that make it suitable for use as an antiseptic.

MATERIALS AND METHODS

Test substance and antiseptic

HM-242 was synthesized by Hamari Chemicals Ltd, Osaka, Japan (Figure 1). Maskin Solution (20% (w/v) CHG aqueous solution) was provided by Maruishi Pharmaceutical Co. Ltd, Osaka, Japan.

Test organisms

The following microorganisms except for clinical isolate were obtained from American Type Culture Collection (Manassas, VA, USA) and used in this study:

Test bacteria and fungi for *in vitro* evaluations

Acinetobacter calcoaceticus (ATCC no. 23055), *Acinetobacter baumannii* (ATCC no. 15308), *Bacteroides fragilis* (ATCC no. 25285), *Candida albicans* (ATCC no. 10231), *C. tropicalis* (ATCC no. 750), *Citrobacter koseri* (ATCC no. 27028), *Enterobacter aerogenes* (ATCC no. 13048), *E. faecalis* VSE (ATCC no. 29212),

[1]Department of Preclinical Development, Central Research Laboratories, Maruishi Pharmaceutical Co. Ltd, Osaka, Japan and [2]CT Laboratory, Hamari Chemicals Ltd, Osaka, Japan
Correspondence: J Okunishi, Central Research Laboratories, Maruishi Pharmaceutical Co. Ltd, 2-2-18, Imazu-Naka, Tsurumi-Ku, Osaka 538-0042, Japan.
E-mail: junji_okunishi@maruishi-pharm.co.jp
Received 8 May 2009; revised 29 May 2009; accepted 5 June 2009; published online 3 July 2009

E. faecalis MDR (ATCC no. 51299), *E faecalis* VRE (ATCC no. 51575), *E. faecium* VSE (ATCC no. 6569), *E. faecium* VRE (ATCC no. 51559), *Escherichia coli* (ATCC nos. 25922 and 11229), *E. coli* O157:H7 (ATCC no. 43895), *Haemophilus influenzae* (ATCC no. 19418), *Klebsiella pneumoniae pneumoniae* (ATCC no. 29995), *Micrococcus luteus* (ATCC no. 7468), *Proteus mirabilis* (ATCC no. 7002), *Proteus vulgaris* (ATCC no. 13315), *Providencia rettgeri* (ATCC no. 35565), *Pseudomonas aeruginosa* (ATCC nos. 27853, 15442, BAA-47; PAO1), *P. aeruginosa* MDR (no. 112905Pa16 Clinical isolate), *Salmonella enterica enterica* serovar Typhimurium (ATCC no. 14028), *Serratia marcescens* (ATCC no. 14756), *S. aureus aureus* MSSA (ATCC no. 29213, ATCC no. 6538), *S. aureus aureus* MRSA (ATCC no. 33591), *S. epidermidis* MSSE (ATCC no. 12228), *S. epidermidis* MRSE (ATCC no. 51625), *S. haemolyticus* (ATCC no. 29970), *S. hominis hominis* (ATCC no. 27844), *S. saprophyticus* (ATCC no. 15305), *S. pneumoniae* PSSP (ATCC no. 6303), *S. pneumoniae* PRSP (ATCC no. 700904), *S. pyogenes* (ATCC no. 19615), *Stenotrophomonas maltophilia* (ATCC no. 13637).

Viruses and cells used for *in vitro* evaluations

Herpes simplex virus (HSV) type 1 was passaged and cultured in Vero cells (African green monkey kidney cells). Human influenza virus A H3N2 (FluV) was passaged and cultured in MDCK cells (Madin–Darby canine kidney epithelial cells).

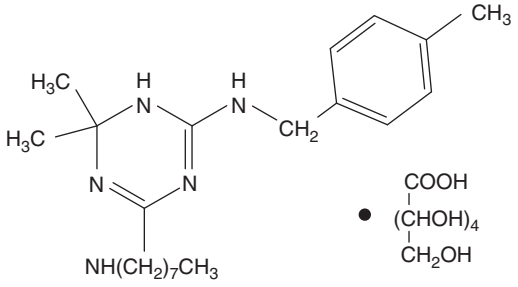

Figure 1 Chemical structure of HM-242.

In vitro evaluation of antimicrobial activity

In vitro antimicrobial activity against 37 bacterial strains and 2 yeast strains was evaluated by microdilution in accordance with the CLSI method of MIC evaluation.[22] The drug was serially diluted to obtain concentrations ranging from 256 to 0.12 μg ml^{-1}. Next, the challenge strain was added to the assay solution. Finally, the reaction mixture was incubated under ordinary culture conditions, and MICs were determined visually.

In vitro bactericidal activity

The MBCs were determined for 37 bacterial strains and 2 yeast strains. Test solutions were prepared containing 12 different concentrations (0.25–512 μg ml^{-1}) of each drug in water. A 10 μl aliquot of each challenge strain containing approximately 5×10^6 CFU ml^{-1} was exposed to 190 μl of each concentration of each drug for 15, 30 and 60 s. After the exposure, 30 μl of the reaction mixture was transferred to 30 μl of neutralizer (3% lecithin, 10% Tween-80). Next, 20 μl of the neutralization mixture was transferred to 180 μl of the growth medium and incubated at 37 °C for 24 h. After the incubations were complete, the MBC of each product at each time of exposure was determined visually on the basis of the turbidity of the growth media.

In vitro time-kill evaluation using bacteria and yeast

A time-kill study was performed using the same bacteria and yeast strains that were used in the MIC and MBC evaluations. Test solutions containing three concentrations (0.005, 0.05 and 0.5%) of each drug in water were prepared. Challenge strain solutions containing approximately 1×10^9 CFU ml^{-1} of each organism in sterile peptone-saline solution were exposed to 9.5 ml of each test solution at room temperature for 15, 30 and 60 s. After the exposure, a 500 μl aliquot of each test mixture was transferred to 9.5 ml of neutralizer (3% lecithin, 10% Tween-80). The neutralization mixture was serially diluted and inoculated onto appropriate agar plates. The plates were incubated under

Table 1 Minimal inhibitory concentrations of HM-242 and CHG

	MIC (mg ml^{-1})			MIC (mg ml^{-1})	
Organism	*HM-242*	*CHG*	*Organism*	*HM-242*	*CHG*
Gram-positive bacteria			*Bacteroides fragilis* ATCC no. 25285	16.0	8.0
Enterococcus faecalis VSE ATCC no. 29212	4.0	2.0	*Citrobacterkoseri* ATCC no. 27028	32.0	16.0
E. faecalis MDR ATCC no. 51299	4.0	4.0	*Enterobacteraerogenes* ATCC no. 13048	16.0	8.0
E. faecalis VRE ATCC no. 51575	4.0	4.0	*Escherichia coli* ATCC no. 25922	16.0	1.0
E. faecium VSE ATCC no. 6569	2.0	1.0	*E. coli* ATCC no. 11229	32.0	1.0
E. faecium VRE ATCC no. 51559	2.0	4.0	*E. coli O157: H7*ATCC no. 43895	16.0	1.0
Micrococcus luteus ATCC no. 7468	64.0	32.0	*Haemophilus influenzae* ATCC no. 19418	8.0	1.0
S. aureus MSSA ATCC no. 29213	2.0	1.0	*Klebsiella pneumoniae* ATCC no. 29995	32.0	8.0
S. aureus MSSA ATCC no. 6538	4.0	1.0	*Proteus mirabilis* ATCC no. 7002	32.0	32.0
S. aureus MRSA ATCC no. 33591	4.0	1.0	*P. vulgaris* ATCC no. 13315	8.0	4.0
S. epidermidis MSSE ATCC no. 12228	1.0	0.5	*Providencia rettgeri* ATCC no. 35565	16.0	16.0
S. epidermidis MRSE ATCC no. 51625	2.0	0.5	*Pseudomonas aeruginosa* ATCC no. 27853	32.0	8.0
S. haemolyticus ATCC no. 29970	1.0	1.0	*P. aeruginosa* ATCC no. 15442	32.0	32.0
S. hominis ATCC no. 27844	1.0	<0.125	*P. aeruginosa* ATCCno. BAA-47PAO1	32.0	16.0
S. saprophyticus ATCC no. 15305	1.0	<0.125	*P. aeruginosa* MDRBSLI no. 112905Pa16	64.0	16.0
Streptococcus pneumoniae PSSP ATCC no. 6303	4.0	8.0	*Salmonella entericaserovar* Typhimurium ATCC no. 14028	64.0	16.0
S. pneumoniae PRSP ATCC no. 700904	4.0	8.0	*Serratia marcescens* ATCC no. 14756	64.0	128.0
S. pyogenes ATCC no. 19615	<0.125	<0.125	*Stenotrophomonas maltophilia* ATCC no. 13637	16.0	4.0
Gram-negative bacteria			*Yeast*		
Acinetobacter calcoaceticus ATCC no. 23055	8.0	4.0	*Candida albicans* ATCC no. 10231	8.0	16.0
A. baumannii ATCC no. 15308	16.0	8.0	*C. tropicalis* ATCC no. 750	4.0	8.0

Abbreviations: CHG, chlorhexidine gluconate; MIC, minimal inhibitory concentration.

conditions appropriate for each species. After incubation, the number of colonies was counted, and the logarithm decrement (log_{10} reduction) was calculated.

In vitro virucidal activity

In vitro virucidal evaluations were conducted similar to the time-kill studies, except that viruses were used instead of bacteria and yeasts. Exposure times, neutralization solutions and drug concentrations also varied. In detail, viral titers were determined by calculating 50% tissue culture infectious doses ($TCID_{50}$) from titration end points in 96-well microtiter plates with preformed cell culture monolayers. The virucidal reaction was carried out with drug concentrations of 0.1 and 0.5% for 0.5, 1, 5 and 10 min. After each exposure, a portion of the mixture was diluted more than 500-fold with the appropriate neutralization solution. Log_{10} reduction values were calculated as ($log_{10}TCID_{50}$ of control−$log_{10}TCID_{50}$ of test sample).

RESULTS

In vitro antimicrobistatic effects of HM-242 on bacteria and yeasts

The susceptibility of 37 bacterial strains and 2 yeast strains to HM-242 was evaluated with the microdilution method (Table 1). HM-242's

Table 2 Minimum bactericidal concentrations of HM-242 and CHG

	MBC ($mg\,ml^{-1}$)					
	HM-242			CHG		
Organism	*15 s*	*30 s*	*60 s*	*15 s*	*30 s*	*60 s*
Gram-positive bacteria						
Enterococcus faecalis VSE ATCC no. 29212	64	32	32	>512	>512	>512
E. faecalis MDR ATCC no. 51299	64	32	16	>512	>512	>512
E. faecalis VRE ATCC no. 51575	64	64	16	>512	>512	>512
E. faecium VSE ATCC no. 6569	128	64	16	>512	>512	>512
E. faecium VRE ATCC no. 51559	32	16	16	>512	>512	>512
Micrococcus luteus ATCC no. 7468	64	32	16	>512	512	16
Staphylococcus aureus MSSA ATCC no. 29213	16	32	16	>512	>512	>512
S. aureus MSSA ATCC no. 6538	64	32	32	>512	>512	>512
S. aureus MRSA ATCC no. 33591	32	32	32	>512	>512	>512
S. epidermidis MSSE ATCC no. 12228	16	8	8	>512	64	64
S. epidermidis MRSE ATCC no. 51625	16	8	8	8	4	4
S. haemolyticus ATCC no. 29970	8	4	8	512	128	8
S. hominis ATCC no. 27844	32	8	16	128	16	16
S. saprophyticus ATCC no. 15305	8	4	4	64	32	8
Streptococcus pneumoniae PSSP ATCC no. 6303	32	16	16	>512	>512	>512
S. pneumoniae PRSP ATCC no. 700904	32	16	8	>512	>512	>512
S. pyogenes ATCC no. 19615	32	8	8	>512	>512	>512
Gram-negative bacteria						
Acinetobacter calcoaceticus ATCC no. 23055	8	8	8	>512	512	16
A. baumannii ATCC no. 15308	128	128	16	>512	>512	>512
Bacteroides fragilis ATCC no. 25285	32	16	8	>512	>512	>512
Citrobacter koseri ATCC no. 27028	32	32	16	>512	>512	>512
Enterobacter aerogenes ATCC no. 13048	128	64	64	>512	>512	>512
Escherichia coli ATCC no. 25922	16	16	16	>512	512	256
E. coli ATCC no. 11229	32	32	32	>512	>512	>512
E. coli O157:H7 ATCC no. 43895	64	32	32	>512	>512	>512
Haemophilus influenzae ATCC no. 19418	256	32	32	256	128	64
Klebsiella pneumoniae ATCC no. 29995	64	16	16	512	128	32
Proteus mirabilis ATCC no. 7002	256	128	128	>512	>512	>512
P. vulgaris ATCC no. 13315	64	32	64	>512	>512	>512
Providencia rettgeri ATCC no. 35565	256	64	64	>512	>512	>512
Pseudomonas aeruginosa ATCC no. 27853	32	16	32	>512	>512	512
P. aeruginosa ATCC no. 15442	64	64	16	>512	>512	512
P. aeruginosa ATCC no. BAA-47 PAO1	64	32	32	>512	>512	>512
P. aeruginosa MDR BSLI no. 112905Pa16	>512	256	64	>512	>512	512
Salmonella enterica serovar Typhimurium ATCC no. 14028	32	32	16	>512	>512	>512
Serratia marcescens ATCC no. 14756	256	64	64	>512	>512	>512
Stenotrophomonas maltophilia ATCC no. 13637	512	64	32	>512	>512	>512
Yeasts						
Candida albicans ATCC no. 10231	512	128	64	>512	>512	>512
C. tropicalis ATCC no. 750	256	256	256	>512	>512	>512

Abbreviations: CHG, chlorhexidine gluconate; MBC, minimal bactericidal concentration; MDR, multidrug-resistant organism.

MIC values were similar to those of CHG. The MIC values of HM-242 ranged from <0.125 to 64 $\mu g\,ml^{-1}$, and those of CHG ranged from <0.125 to 128 $\mu g\,ml^{-1}$. The MIC_{90} values of HM-242 and CHG were 64 and 32 $\mu g\,ml^{-1}$, respectively.

In vitro antimicrobicidal activity

The MBC of HM-242 in the 60-s exposure protocol was less than 8 $\mu g\,ml^{-1}$ for eight of the strains, and it ranged from 16 to 128 $\mu g\,ml^{-1}$ for the other 30 strains (Table 2). The most resistant test organism, *C. tropicalis*, was killed by 256 $\mu g\,ml^{-1}$ of HM-242. By contrast, the 60-s MBC of CHG for 26 strains was higher than the highest concentration used in this assay (512 $\mu g\,ml^{-1}$), and was therefore not determined. The 60-s MBC of CHG for three strains was less than 8 $\mu g\,ml^{-1}$, and it ranged from 256 to 16 $\mu g\,ml^{-1}$ for seven strains. The other three strains were killed by 512 $\mu g\,ml^{-1}$ of CHG. The 60-s MBC_{90} of HM-242 was 64 $\mu g\,ml^{-1}$, and that of CHG was not determined ($>512\,\mu g\,ml^{-1}$).

The results of the time-kill studies using bacteria and fungi are shown in Table 3. Exposure for 15 s to 0.5, 0.05 or 0.005% HM-242 reduced the populations of 38, 32 and 8 challenge strains, respectively, by more than 5.0 log_{10} (Table 3). Exposure for 15 s to 0.5 and 0.05% CHG reduced the populations of eight and one challenge strains, respectively, by more than 5.0 log_{10}. Exposure for 60 s to 0.05% CHG failed to reduce the population of any of the strains by 5.0 log_{10}.

Table 3 Distribution of test strains in the time-kill study of the bactericidal activities HM-242 and CHG

		HM-242				*CHG*			
		Log_{10} reduction				*Log_{10} reduction*			
Test concentration	*Exposure time (s)*	*−1*	*>1–3*	*>3–5*	*>5*	*−1*	*>1–3*	*>3–5*	*>5*
0.50%	15	0	1	0	38	11	11	9	8
	30	0	1	0	38	7	9	10	13
	60	0	0	1	38	6	3	10	20
0.05%	15	0	3	4	32	17	13	8	1
	30	0	3	1	35	12	12	14	1
	60	0	1	1	37	9	10	10	10
0.005%	15	12	9	10	8	22	15	2	0
	30	6	10	8	15	17	20	2	0
	60	5	3	12	19	15	17	7	0

Abbreviation: CHG, chlorhexidine gluconate.

The results of the time-kill studies using HSV and FluV are shown in Figure 2. Within 0.5 min, 0.5 and 0.1% HM-242 reduced the viability titer of the test viruses below the detection limit of the assay. CHG at concentrations of 0.5 and 0.1% failed to detectably kill FluV at any exposure time less than 5 min. CHG killed only 45.1% of FluV after 10 min of exposure. Against HSV, 0.5% CHG reduced the viability titer to below the detection limit after just 1 min. The cytotoxicities of HM-242 and CHG to Vero cells and MDCK cells were assayed by the same procedure. A 1:256 dilution of a 0.5% solution of either drug was toxic to Vero cells, and a 1:512 dilution of either drug was toxic to MDCK cells.

DISCUSSION

Antiseptic hand washing has been used by medical personnel to control infections ever since Semmelweis discovered that it reduces patient mortality from hand-borne pathogens.[1,16,23,24] Today, antiseptic hand washing has moved beyond the medical professions and is now common practice in food preparation, public facilities and domestic life. CHG has long been used in clinical settings and is an excellent antiseptic. Various reports and guidelines recommend CHG because of its broad activity spectrum, persistence, consistent efficacy and safety.[1,3,7,12–17] However, some problems with CHG have been noted, including its suboptimal bactericidal kinetics (CHG was slower than another antiseptic) and rare anaphylactic reactions to it in humans.[25–30] Recently, a new compound, HM-242, was synthesized as a novel disinfectant. We found that HM-242 has broad-spectrum and fast-acting microbicidal activity *in vitro*. All of the bacterial and yeast strains tested, including the antibiotic-resistant strains MRSA, VRE, MDRP and PRSP, were sensitive to HM-242, and were significantly inhibited by the presence of HM-242 ($\leqslant 64\,\mu g\,ml^{-1}$). Although HM-242's antimicrobial activity is similar to that of CHG, the MBC study revealed that HM-242 is a more effective microbicide for a wide variety of microorganisms. In the time-kill study, HM-242 showed excellent bactericidal and fungicidal efficiency at lower concentrations and shorter exposure times than did CHG. The viability counts of all the microorganisms tested were reduced by exposure to 0.05% HM-242 for 15 s. By contrast, nearly half of the test strains treated with 0.05% CHG were unaffected. In general, MIC data are used to estimate the susceptibility patterns of test strains. A compound that has shown effectiveness in MIC studies and with good time-kill

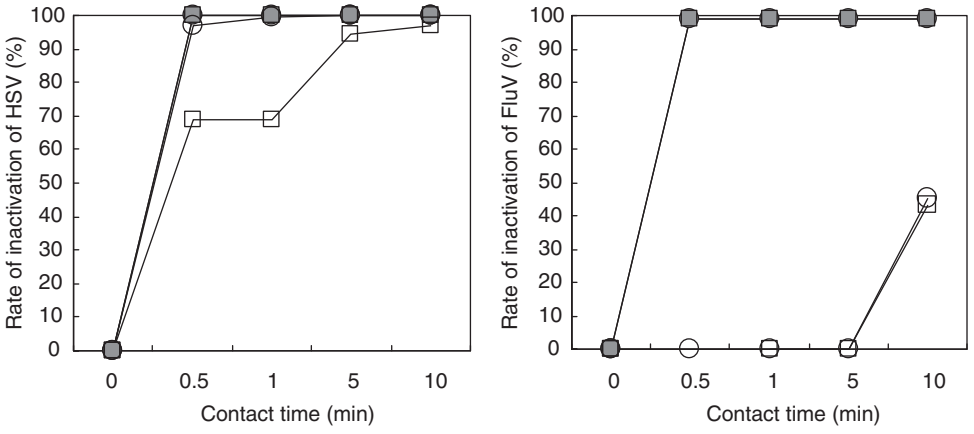

Figure 2 Time-kill study of activity against herpes simplex virus (HSV) and FluV. Symbols: closed circles, 0.5% HM-242; closed squares, 0.1% HM-242; open circles, 0.5% chlorhexidine gluconate (CHG); open squares, 0.1% CHG.

kinetics against both nosocomial flora and resident flora would be effective in the health-care settings where these pathogens are encountered. One important characteristic of antiseptics used by health-care professionals is that they act as microbiologically lethal agents. Time-kill kinetic studies allow the rate of kill of an antiseptic to be assessed provided certain variables are controlled.[1,5] The results of the time-kill studies with HM-242 revealed that it possesses fast-acting and potent bactericidal activity against all of the tested strains, including the multidrug-resistant organisms.

Furthermore, HM-242 had potent virucidal activity that reduced HSV and FluV titers to a level below the detection limit of our assay within 30 s. By contrast, CHG was ineffective against FluV even after 300 s. To be appropriate for use in health-care settings, an antiseptic must have a broad microbial spectrum that includes the nosocomial pathogens. In this respect, HM-242's virucidal activity makes it superior to CHG.

To be an effective antiseptic agent, a drug cannot be merely bacteriostatic; it must be a fast-acting bactericide. The results of the MBC and time-kill studies indicate that HM-242 kills pathogenic bacteria, yeasts and viruses both efficiently and rapidly. Antiseptics with broad-spectrum activity that includes virucidal activity are vital to preventing the spread of infections. The cytotoxicity data indicate that HM-242 is as safe as CHG, which is well known for its low irritability to human skin. Thus, HM-242 has many of the properties required of an antiseptic substance, and it may be as suitable as CHG for controlling the spread of infections.

1 Paulson, D. S. (ed.) *Handbook of Topical Antimicrobials. Industrial Applications in Consumer Products and Pharmaceuticals* (Marcel Dekker, New York, USA, 2003).
2 Rutala, W. A. & Weber, D. J. Registration of disinfectants based on relative microbicidal activity. *Infect. Control Hosp. Epidemiol.* **25,** 333–341 (2004).
3 Block, S. S. (ed.) *Disinfection, Sterilization, and Preservation*, 5th ed. (Williams & Wilkins, Philadelphia, PA, 2000).
4 Rutala, W. A. & Weber, D. J. *Guideline for Disinfection and Sterilization in Healthcare Facilities, 2008* 1–158 (Centers for Disease Control and Prevention (CDC), Atlanta, 2008).
5 Rutala, W. A. APIC guideline for selection and use of disinfectants. *Am. J. Infect. Control* **24,** 313–342 (1996).
6 Lister, J. On the topical antimicrobial drug product principle in the practice of surgery. *Lancet* **2,** 353–356 (1867).
7 McDonnell, G. & Russell, A. D. Antiseptics and disinfectants: activity, action, and resistance. *Clin. Microbiol. Rev.* **12,** 147–179 (1999).
8 Siegel, J. D., Rhinehart, E., Jackson, M. & Chiarello, L. Management of multidrug-resistant organisms in health care settings, 2006. *Am. J. Infect. Control* **35,** S165–S193 (2007).
9 Tambe, S. M., Sampath, L. & Modak, S. M. *In vitro* evaluation of the risk of developing bacterial resistance to antiseptics and antibiotics used in medical devices. *J. Antimicrob. Chemotherapy* **47,** 589–598 (2001).
10 Sakagami, Y., Yokoyama, H., Nishimura, H., Ose, Y. & Tashima, T. The mechanism of resistance of *Pseudomonas aeruginosa* to chlorhexidine digluconate. *J. Antibact. Antifung. Agents* **17,** 153–160 (1989).
11 NNIS. National Nosocomial Infections Surveillance (NNIS) System Report, data summary from January 1992 through June 2004, issued October 2004. *Am. J. Infect. Control* **32,** 470–485 (2004).
12 Siegel, J. D., Rhinehart, E., Jackson, M. & Chiarello, L. 2007 guideline for isolation precautions: preventing transmission of infectious agents in health care settings. *Am. J. Infect. Control* **35,** S65–S164 (2007).
13 Gilbert, P. & Moore, L. E. Cationic antiseptics: diversity of action under a common epithet. *J. Appl. Microbiol.* **99,** 703–715 (2005).
14 Kampf, G. & Kramer, A Epidemiologic background of hand hygiene and evaluation of the most important agents for scrubs and rubs. *Clin. Microbiol. Rev.* **17,** 863–893 (2004).
15 Hidalgo, E. & Dominguez, C. Mechanisms underlying chlorhexidine-induced cytotoxicity. *Toxicol. In Vitro* **15,** 271–276 (2001).
16 Mangram, A. J., Horan, T. C., Pearson, M. I., Silver, L. C. & Javis, W. R. Guideline for prevention of surgical site infection, 1999. *Infect. Control Hosp. Epdemiol.* **20,** 247–278 (1999).
17 Boyce, J. M. & Pittet, D. Guideline for hand hygiene in health-care settings. *Am. J. Infect. Control* **30,** S1–S46 (2002).
18 Rosenberg, A., Alatary, S. D. & Peterson, A. F. Safety and efficacy of the antiseptic chlorhexidine gluconate. *Surg. Gynecol. Obstet.* **143,** 789–792 (1976).
19 O'Grady, N. P., Alexander, M., Dellinger, E. P. & Weinstein, R. A. Guidelines for the prevention of intravascular catheter-related infections. *MMWR Recomm. Rep.* **51** (RR-10), 1–29 (2002).
20 Food and Drug Administration. Tentative final monograph for healthcare antiseptic drug products: proposed rule. *Fed. Reg.* **59,** 31402–31452 (1994).
21 Maeda, S., Kita, T. & Meguro, K. Synthesis of Novel 4,6-Di(substituted)amino-1, 2-dihydro-1,3,5-triazine derivatives as topical antiseptic agents. *J. Med. Chem.* **52,** 597–600 (2009).
22 Clinical and Laboratory Standards Institute. *Methods for Dilution Antimicrobial Susceptibility Tests for Bacteria That Grow Anaerobically*; Approved Standard—6th edn, (CLSI Document M7-A6, Pennsylvania, USA, 2003).
23 Semmelweis, I. P. The etiology, concept, prevention of childbed fever. *Am. J. Obstet. Gynecol.* **172,** 236–237 (1995).
24 Larson, E. L., Early, E., Cloonan, P., Sugrue, S. & Parides, M. An organizational climate intervention associated with increased handwashing and decreased nosocomial infections. *Behav. Med.* **26,** 14–22 (2000).
25 Shimizu, M., Okuzumi, K. & Kimura, S. *In vitro* antiseptic susceptibility of clinical isolates from nosocomial infections. *Dermatology* **204,** S21–S27 (2002).
26 Garvey, L. H., Kroigaard, M. & Husum, B. IgE-mediated allergy to chlorhexidine. *J. Allergy Clin. Immunol.* **120,** 409–415 (2007).
27 Okano, M., Nomura, M. & Aoki, T. Anaphylactic symptoms due to chlorhrxidine gluconate. *Arch. Dermatol.* **125,** 50–52 (1989).
28 Beaudouin, E., Kanny, G. & Moneret-Vautrin, D. A. Immediate hypersensitivity to chlorhexidine: literature review. *Eur Ann Allergy Clin Immunol* **36,** 123–126 (2004).
29 Krautheim, A. B., Jermann, T. H. & Bircher, A. J. Chlorhexidine anaphylaxis: case report and review of the literature. *Contact Dermat* **50,** 113–116 (2004).
30 Knight, B. A., Puy, R., Douglass, J., O'Hehir, R. E. & Thien, F. Chlorhexidine anaphylaxis: a case report and review of the literature. *Intern. Med. J.* **31,** 436–437 (2001).

The Journal of Antibiotics (2009) 62, 495–500

www.nature.com/ja

ORIGINAL ARTICLE

Solid-phase total synthesis of the chitinase inhibitor Argadin using a supported acetal resin

Tomoyasu Hirose[1], Toshiaki Sunazuka[1], Akihiro Sugawara[1], Yoshihiko Noguchi[1], Toshiaki Tanaka[1], Kanami Iguchi[1], Tsuyoshi Yamamoto[1], Hiroaki Gouda[2], Kazuro Shiomi[1] and Satoshi Ōmura[1]

A versatile solid-phase total synthesis was applied to the rapid preparation of Argadin, a natural product isolated and characterized as a cyclopentapeptide by our group, which possesses superior inhibitory activity against family-18 chitinases. The synthetic strategy includes peptide synthesis by using an Fmoc (9-fluorenylmethoxycarbonyl) protective group, macrolactamization, acetylguanylation and formation of hemiaminal accompanied by total deprotection, including cleavage from resin.

The Journal of Antibiotics (2009) **62,** 495–500; doi:10.1038/ja.2009.57; published online 3 July 2009

Keywords: Argadin; chitinase; solid phase; total synthesis

INTRODUCTION

Chitinases hydrolyze chitin, a linear homopolymer of *N*-acetyl-D-glucosamine, that is present in a wide range of organisms, including bacteria, fungi, insects, viruses, higher plants and animals, and have a variety of roles in the biological world.[1–3] Chitinases are currently classified into two different families of glycosyl hydrolases, namely family-18 and family-19, on the basis of amino acid sequence similarities.[4] Family-18 contains chitinases from various organisms, whereas family-19 chitinases are only found in plants and *Streptomyces* species. As chitin is a major component of fungal cell walls, the exoskeletons of crustaceans and insects, as well as the microfilarial sheaths of parasitic nematodes, family-18 chitinases have important physiological roles in these organisms.[1–3] Family-18 chitinase inhibitors have thus become a subject of interest owing to their potential as anti-fungal agents,[5] pesticides for controlling pests[6] and promise as insecticides to control disease vectors, such as malaria.[7] They also offer significant potential for the treatment of asthma and other diseases in humans.[8]

During the screening for chitinase inhibitors, two new cyclic pentapeptides, Argadin (**1**)[9] and Argifin (**2**),[10–12] were isolated from the cultured broths of *Clonostachys* sp. FO-7314 and *Gliocladium* sp. FTD-0668, respectively, by our research group, and found to be potent chitinase inhibitors of blowfly (*Lucilia cuprina*)[10] and *Serratia marcescens* chitinases (*Sm*Chi),[13–16] both of which are family-18 chitinases (Figure 1). Developments of practical and efficient total syntheses of **1** and **2** are important objectives, as the original sources do not produce these cyclic peptides with sufficient quantities. In fact, the total syntheses of **1** and **2**, involving hybrid approaches of solid- and liquid-phase reaction sequences, have been reported by Dixon *et al.*[17,18] They developed an improved synthetic route for **2** and analogs on the basis of an all-solid-phase approach.[19] More recently, we have independently reported the total synthesis of **2** accomplished by solid-phase synthetic protocols for the entire reaction sequence, except for the final cleavage step from resin. We have also evaluated acyclic peptide analogs of **2**[20] and have investigated the application of *in situ* click chemistry with *Sm*Chi to swiftly generate more potent chitinase inhibitors using the simplified structure of natural **2**.[21]

In this study, we describe our efficient solid-phase total synthesis of **1** using glycerol polystyrene resin along with only one-time HPLC separation at the final step.

RESULTS AND DISCUSSION

Our retrosynthetic analysis for Argadin (**1**) is outlined in Scheme 1. The cyclic peptide structure of **1** allowed us to adopt a solid-phase synthetic strategy on the basis of an application of an 9-fluorenylmethoxycarbonyl (Fmoc) protective group for the amine of amino acid fragments with allyl protection on the carboxylic acid of the L-aspartic-β-semialdehyde[22] unit. This strategy enables cyclization of the linear precursor that is still attached to a solid support by the side chain of an L-aspartic-β-semialdehyde residue. Our synthetic strategy of **1** offers many advantages, including: (i) the anchorage of the first residue (C terminal) to resin through the side-chain aldehyde function; (ii) the selected glycerol polystyrene resin acts as a protective group of aldehyde for preventing the formation of sensitive cyclic

[1]The Kitasato Institute, Kitasato Institute for Life Science and Graduate School of Infection Control Sciences, Kitasato University, Minato-ku, Tokyo, Japan and [2]School of Pharmacy, Kitasato University, Minato-ku, Tokyo, Japan
Correspondence: Professor T Sunazuka or Professor S Ōmura, The Kitasato Institute, Kitasato Institute for Life Science and Graduate School of Infection Control Sciences, Kitasato University, 5-9-1 Shirokane, Minato-ku, Tokyo 108-8641, Japan
E-mails: sunazuka@lisci.kitasato-u.ac.jp or omuras@insti.kitasato-u.ac.jp
Received 29 May 2009; revised 12 June 2009; accepted 15 June 2009; published online 3 July 2009

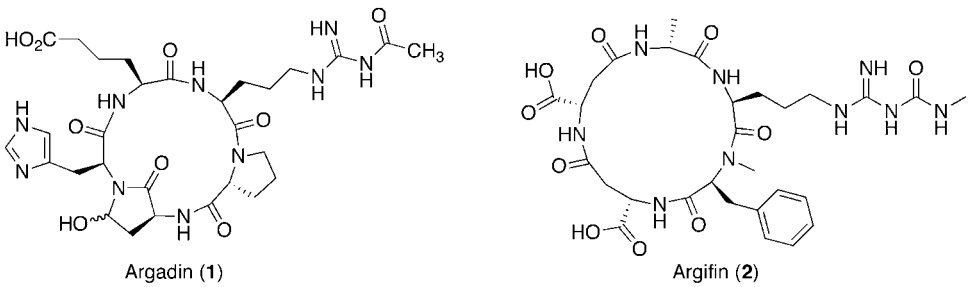

	IC_{50} (μM)		
	*Sm*ChiA	*Sm*ChiB	*Sm*ChiC$_1$
Argadin (**1**)	0.016 ± 0.0040	0.033 ± 0.0028	>30
Argifin (**2**)	0.025 ± 0.0024	6.4 ± 1.0	>30

Figure 1 Argadin (**1**) and Argifin (**2**) and the IC_{50} values against *Serratia marcescens* chitinases (*Sm*Chi) A, B and C_1.

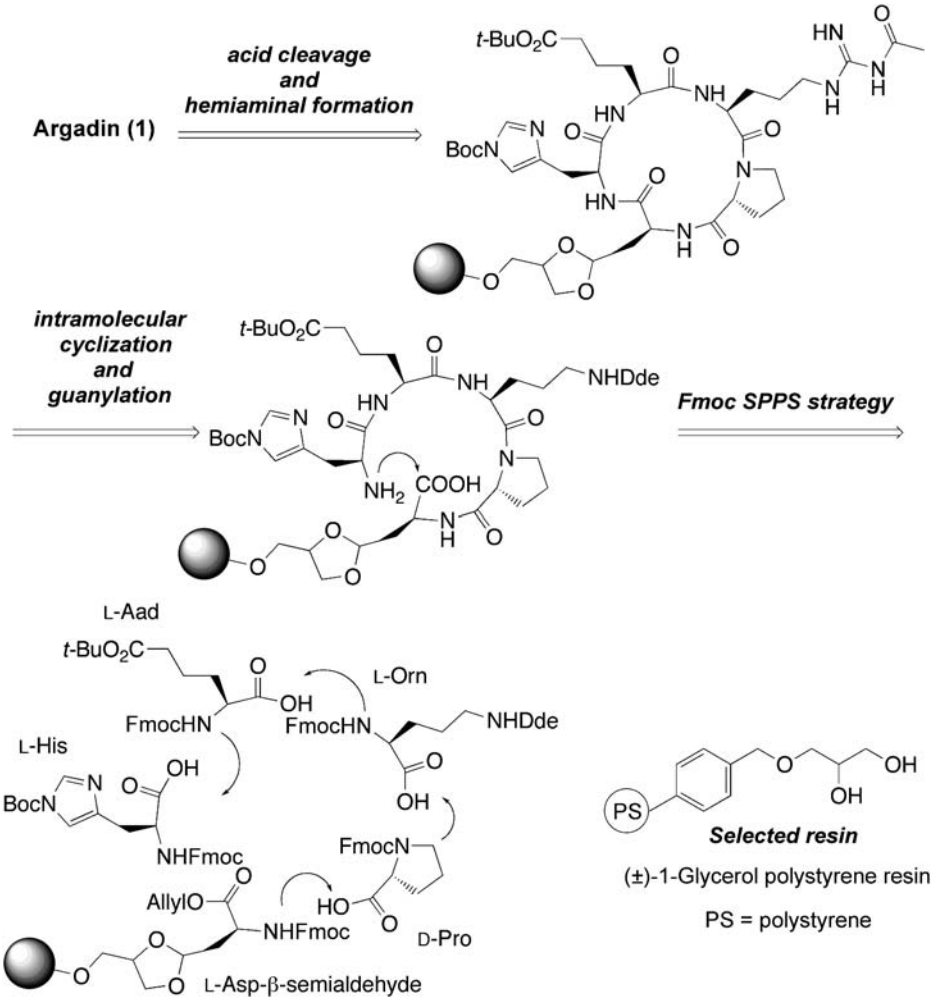

Scheme 1 Synthetic plan of **1**. Boc, *t*-butoxycarbonyl; Dde, 1-(4,4-dimethyl-2,6-dioxocyclohex-1-ylidene)ethyl; Fmoc, 9-fluorenylmethoxycarbonyl; SPPS, solid-phase peptide synthesis.

hemiaminal; (iii) on resin, cyclization includes a stepwise selective deprotection of the C and N terminals, followed by intramolecular condensation; (iv) single-step operation to convert to the N^{ω}-acetylarginine residue obtained from ornithine by acetylguanylation; and (v) the whole reaction sequence can be carried out on resin, except for the cleavage from resin and hemiaminal formation at the final step.

The synthesis of **1** commenced with the loading of the solid support of the *N*-Fmoc-*O*-allyl-protected aspartic acid β-semialdehyde residue (**3**),[22] anchored by a side chain. The aldehyde in **3** was loaded onto (±)-glycerol polystyrene resin (1.40 mmol g^{-1}) in the presence of catalytic TsOH under reflux in 1,4-dioxane to yield **4** with a loading of > 1.33 mmol g^{-1} (Scheme 2). To confirm the loading yield, cleavage

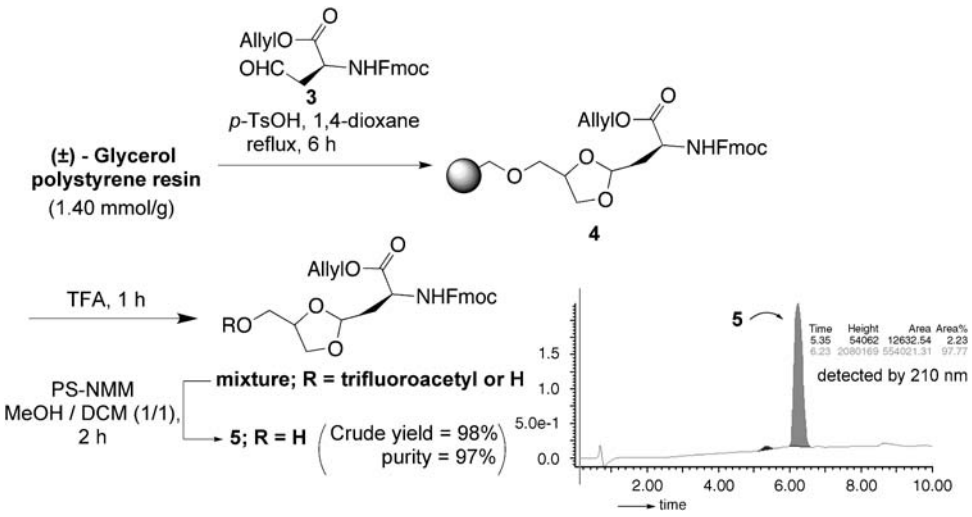

Scheme 2 Loading of **3** onto resin and liquid chromatography (LC)-UV analysis of cleaved compound **5**. Ts, *p*-toluenesulfonyl; TFA, trifluoroacetic acid; PS-NMM, polystyrene-*N*-methylmorpholine.

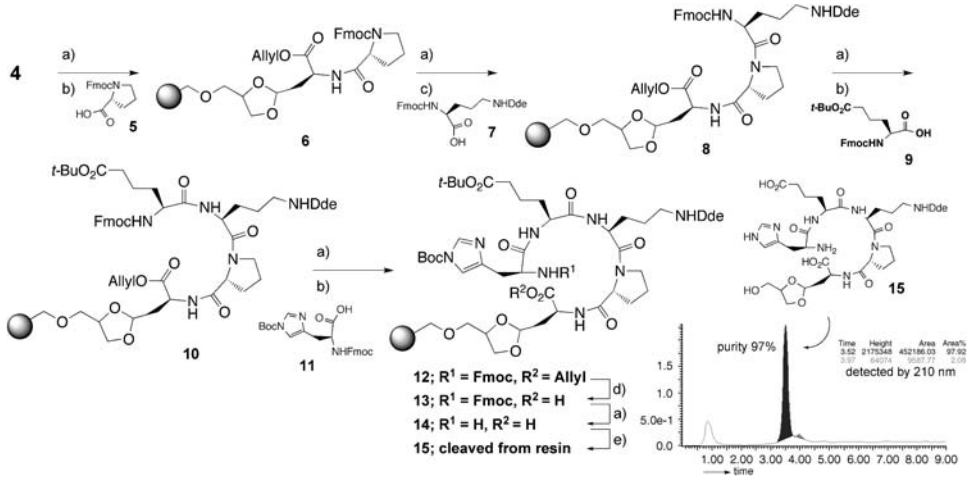

Scheme 3 Solid-phase synthetic scheme of linear pentapeptide **14** and liquid chromatography (LC)-UV analysis of cleaved compound **15**; (a) 20% piperidine/DMF, 1 h; (b) PyBOP, (DIPEA), dichloromethane (DCM)/DMF (4/1), 2 h; (c) HBTU, DIPEA, DCM/DMF (4/1), 2 h; (d) $Pd(PPh_3)_4$, dimedone, THF, 1 h; (e) (1) TFA, 1 h, (2) polystyrene-*N*-methylmorpholine (PS-NMM), MeOH/DCM (1/1), 2 h. PyBOP, (benzotriazol-1-yloxy)tripyrrolidinophosphonium hexafluorophosphate; DIPEA, diisopropylethylamine; HBTU, *O*-(benzotriazol-1-yl)-*N,N,N′,N′*-tetramethyluronium hexafluorophosphate.

from the resin **4** with 100% of TFA for 1 h, followed by treatment with morpholinomethyl polystyrene resin (polystyrene-*N*-methylmorpholine (PS-NMM)) in $MeOH/CH_2Cl_2$ (1/1) for 2 h, resulted in the desired glycerol bearing **3** (**5**) in 98% crude yield with 97% purity (calculated using the liquid chromatography (LC)-UV analysis).

The resin-bound amino acid **4** was subsequently subjected to four deprotection-coupling cycles to construct the linear pentapeptide by standard Fmoc solid-phase peptide synthesis using PyBOP ((benzotriazol-1-yloxy)tripyrrolidinophosphonium hexafluorophosphate) activation for peptide formation, except for the condensation between 1-(4,4-dimethyl-2,6-dioxocyclohex-1-ylidene)ethyl (Dde)-protected Fmoc-Orn-OH (**7**)[23,24] and D-Pro, which was accomplished using HBTU (2-(1*H*-benzotriazol-1-yl)-1,1,3,3-tetramethyluroniumhexafluorophosphate) activation. Each amino acid coupling step was monitored by the LC-UV analysis for the cleaved material using the acid deprotection processes. After the synthesis of the linear pentapeptide (**12**) was accomplished, deprotection on both the C and N terminals was achieved by subjecting the resin-bound **12** to $Pd(PPh_3)_4$ treatment in the presence of dimedone in DMF under Ar atmosphere to eliminate the allyl function. Subsequently, the Fmoc group was removed by piperidine to afford the precursor of the cyclic peptide compound (**14**), which was then converted to the crude product (**15**) with 97% purity, as determined by the LC-UV analysis (as shown in Scheme 3).

Macrolactamization of **14** under the PyBOP activation condition for 1 h of reaction time proceeded with low efficiency to yield the cyclic peptide **16**, which was converted to final Argadin (**1**) with very low quantity (<1% isolated yield after HPLC separation) by submitting a 3-reaction sequence, deprotection of Dde by 2% NH_2NH_2 in DMF, acetylguanylation using 1-*H*-pyrazole-1-[*N*-(*tert*-butoxycarbonyl)]-*N′*-acetylcarboxamidine (**18**),[25] followed by the formation of hemiaminal accompanied by total deprotection, including resin cleavage, to roughly elucidate the conversion ratio from **14** to **15** (Scheme 4). Although the two-cycle repetition reaction for lactamiza-

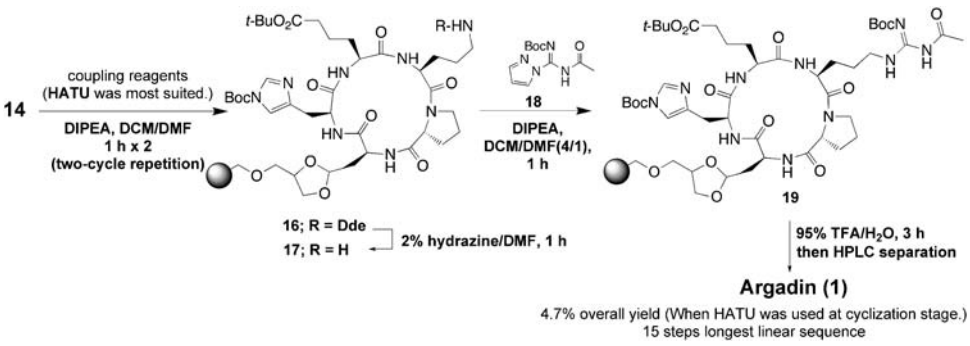

Scheme 4 Completion of solid-phase total synthesis of **1**. HATU=*O*-(7-azabenzotriazol-1-yl)-*N,N,N′,N′*-tetramethyluronium hexafluorophosphate; DIPEA, diisopropylethylamine.

tion with **14** (PyBOP, 1 h×2) was attempted to improve the conversion yield, the production of **1** was still low (~1% yield). To obtain a sufficient quantity of **1**, various condensation reagents, such as HBTU, *O*-(7-azabenzotriazol-1-yl)-*N,N,N′,N′*-tetramethyluronium hexafluorophosphate (HATU) and PyBrop, were tested. Optimally, when **14** was subjected to the macrolactamization using HATU in the presence of diisopropylethylamine (DIPEA) in CH_2Cl_2/DMF (4/1) for 1 h over a two-cycle repetition, Argadin (**1**) was isolated in 4.7% of the overall yield, after undergoing the three-step reaction sequence and final separation by HPLC (Scheme 4). All spectral data (^{1}H-, ^{13}C-NMR in DMSO-d_6 with 1.7% TFA and HR-MS) and activities of synthetic **1** were found to be identical with those of natural **1**. However, the optical rotations of synthetic ($[\alpha]_D$=−17.0 in H_2O; *c* 0.04) and natural **1** ($[\alpha]_D$=+52.1 in H_2O; *c* 0.1)[9] did not match, partly because of the optical rotational value of **1** being strongly influenced by the counter anion of acids, and the fact that it was difficult to create identical conditions under which to measure the optical rotation. HPLC profiles of both synthetic and natural **1** showed a 3:1 to 7:1 mixture of diastereoisomers at the hemiaminal position. The ratio of diastereomers was also influenced by acidic additives (TFA, AcOH or HCO_2H), which are usually added into a mobile phase of HPLC, and the stock solution of Argadin samples to stabilize Argadin itself. The diastereomeric ratio of hemiaminal may affect the optical rotational value of Argadin. Therefore, we examined the inhibitory activity of synthetic **1** against chitinases, and its activity was almost the same as that of natural **1**.

In conclusion, we completed the solid-phase total synthesis of Argadin (**1**) using a supported acetal resin. This synthesis was concise and required 15 steps in the longest linear sequence from (±)-glycerol polystyrene resin, with HPLC separation after cleavage from resin to yield **1** in 4.7% of the overall yield. The process allows us to speedily generate a variety of analogs in structure–activity relationship studies. Ongoing studies, aimed at the synthesis and biological evaluation of peptide analogs, designed using computer-aided rational molecular calculations[26] using information obtained from X-ray cocrystallography of Argadin-chitinase, are currently under way in our laboratories.

EXPERIMENTAL SECTION

General procedure

Fmoc-D-Pro-OH (**5**), Fmoc-Ada(O*t*-Bu)-OH (**9**) and Fmoc-(Boc)His-OH (**11**) were purchased from Watanabe Chemical Industries (Hiroshima, Japan). (±)-Glycerol polystyrene resin (1.4 mmol g^{-1}) was purchased from NovaBiochem (Tokyo, Japan). Dry pyridine, THF, DMF, MeOH, 1,4-dioxane and CH_2Cl_2 were purchased from Kanto Chemical (Tokyo, Japan). ^{1}H-NMR spectra were recorded at 400 MHz, and ^{13}C-NMR spectra were recorded at 100 MHz on Varian XL-400 (Varian; 400 MHz). The chemical shifts are expressed in p.p.m. downfield from internal solvent peaks and DMSO (2.49 p.p.m., ^{1}H-NMR), DMSO-d_6 (39.7 p.p.m., ^{13}C-NMR) and *J*-values are expressed in hertz. The coupling patterns are expressed by s (singlet), d (doublet), dd (double doublet), ddd (double double doublet), m (multiplet) or br (broad). High-resolution mass spectra were measured on a JEOL JMS-DX300 spectrometer (JEOL, Tokyo, Japan). HPLC analysis was conducted on a Waters 2795 Separation Module (Nihon Waters KK, Tokyo, Japan) with Alliance HT (column; Senshu Pak-PEGASIL ODS 2 ϕ×50 mm (Senshu Scientific Co. Ltd., Tokyo, Japan): condition of HPLC; gradient 10% MeCN (0.05% TFA)/H_2O (0.1% TFA) to 100% MeCN (0.05% TFA) over 8 min, flow 0.3 ml min^{-1}, detect 210 nm, temp 20 °C). HPLC purification of Argadin (**1**) was performed on a Hitach ELITE LaChrom (column; Senshu Pak PEGASIL ODS 20 ϕ×250 mm with a flow rate of 8 ml min^{-1}. The mobile phase was 0.05% TFA in 8% MeCN/H_2O). The solid-phase total synthesis of Argadin was carried out in a MicroKan microreactor initially filled with 30 mg of (±)-glycerol polystyrene resin-bound amino acid residue (**4**).

Loading of *N*-(9-Fluorenyl)methoxycarbonyl-(*O*Allyl)-L-Homoserinealdehyde (3) onto glycerol polystyrene resin; Fmoc-L-Hse-*O,O*-hydroxymethylethylideneacetal-*O*-PS (4)

(±)-Glycerol polystyrene resin (1.54 g, 2.0 mmol) was swelled in 1,4-dioxane (20 ml) for 30 min at room temperature. Fmoc-(*O*Allyl)-L-homoserinealdehyde (**3**)[22] (1.4 g, 4.0 mmol) and $TsOH \cdot H_2O$ (0.75 g, 0.4 mmol) was added to the solution of resin, and the reaction mixture was heated to 90 °C using a Dean—Stark trap. After heating for 8 h, the reaction was cooled to room temperature, filtered to collect the resin product, which was washed with pyridine (10 ml×2), Py/H_2O (1/1) (10 ml×2), H_2O (10 ml×2), THF (10 ml×2), DMF (10 ml×4), dichloromethane (DCM) (10 ml×4) and dried *in vacuo* to afford the desired resin-bound product **4**.

General procedure for deprotection of the Fmoc group

The MicroKan microreactor with 30 mg resin was placed into a 20 ml screw vial and swollen in DCM (1.5 ml) for 1 h and thereafter filtered. It was sequentially treated with a solution of 20% piperidine in DMF (1.5 ml). The mixture was vigorously agitated at room temperature. After being agitated for 1 h, the mixture was filtered, washed with DMF (5 ml×4), DCM (5 ml×4) and dried *in vacuo* to afford the corresponding resin-bound amine products.

General procedure for peptide coupling

The MicroKan microreactor with 30 mg resin was placed into a 20 ml screw vial and swollen in DMF (1.5 ml) for 1 h and thereafter filtered. It was treated with a cocktail of each amino acid (3.0 equiv.) [Fmoc-D-Pro-OH (**5**), Fmoc-Ada(O*t*-Bu)-OH (**9**) and Fmoc-(Boc)His-OH (**11**)], PyBop (3.0 equiv.), *N,N*-diisopropylethylamine (6.0 equiv.) in DCM/DMF (4/1, 1.5 ml), except for the case of coupling between dipeptide **6** and Fmoc-Orn(Dde)-OH (**7**) [**7** (3.0 equiv.), HBTU (3.0 equiv.) and *N,N*-diisopropylethylamine (6.0 equiv.) in DCM/DMF (4/1, 1.5 ml) for 1 h]. The mixture was vigorously agitated at room temperature. After being agitated for 2 h, the mixture was filtered, washed with

DMF (5 ml×4), DCM (5 ml×4) and dried *in vacuo* to afford the corresponding peptides.

Procedure for deprotection of the allyl group of 12

The MicroKan microreactor with **12** was placed into a 20 ml screw vial and swollen in THF (1.5 ml) for 1 h under Ar atmosphere, and the remaining THF was thereafter drained by a syringe. To the MicroKan microreactor with **12** was sequentially added a well-mixed solution of $Pd(PPh_3)_4$ (1.5 equiv.) and dimedone (10 equiv.) in THF (1.5 ml) through a syringe under Ar atmosphere. The mixture was vigorously agitated at room temperature under the Ar atmosphere. After being agitated for 1 h, the mixture was filtered, washed with THF (5 ml×4), DMF (5 ml×4), DCM (5 ml×4) and dried *in vacuo* to afford **13**.

Cyclization of 14

The MicroKan microreactor with **14** was placed into a 20 ml screw vial and swollen in DCM (1.5 ml) for 1 h and thereafter filtered. It was treated with a cocktail of HATU (2 equiv.) and DIPEA (4 equiv.) in DCM/DMF (4/1, 1.5 ml). The mixture was vigorously agitated at room temperature. After being agitated for 2 h, the mixture was filtered, washed with DMF (5 ml×4), DCM (5 ml×4) and dried *in vacuo*. The same procedure was repeated.

Procedure for deprotection of Dde in 16

The MicroKan microreactor with **16** was placed into a 20 ml screw vial and swollen in DMF (1.5 ml) for 1 h, and filtered. It was sequentially treated with a solution of 2% hydrazine monohydrate in DMF (1.5 ml). The mixture was vigorously agitated at room temperature. After being agitated for 1 h, the reaction mixture was filtered, washed with DMF (5 ml×4), DCM (5 ml×4) and dried *in vacuo* to afford **17**.

Procedure for acetylguanylation of 17

The MicroKan microreactor with **17** was placed into a 20 ml screw vial and swollen in DCM (1.5 ml) for 1 h and thereafter filtered. The MicroKan microreactor was sequentially treated with a 1.0 M solution of **18**[25] in DCM (126 µl) and *N,N*-diisopropylethylamine (43.9 µl, 252 µmol) in DCM/DMF (4/1, 1.5 ml). The mixture was vigorously agitated at room temperature. After being agitated for 2 h, the reaction mixture was filtered, washed with DMF (5 ml×4), DCM (5 ml×4) and dried *in vacuo* to afford **19**.

Cleavage from the resin and hemiaminal formation to yield 1

The MicroKan microreactor with **19** was placed into a 20 ml screw vial and swollen in DCM (1.5 ml) for 1 h and thereafter filtered. It was sequentially treated with a cocktail mixture of 95% TFA/H_2O (1.5 ml). The mixture was vigorously agitated at room temperature. After being agitated for 3 h, the reaction mixture was filtered and dried *in vacuo* to provide crude Argadin (**1**) (24 mg, 84.5%). The use of HPLC purification (8% MeCN/H_2O containing 0.05% TFA) furnished **1** (4.2 mg, 4.7%) as a colorless solid.

Synthetic Argadin

$[\alpha]_D$=17.0 (*c* 0.04, H_2O); ^{1}H-NMR (400 MHz, DMSO-d_6 with 1.7% TFA) δ: 14.19 (brs, 1H, His), 11.75 (s, 2H, η1 position of Arg), 9.14 (m, 2H, ε position of Arg), 9.00 (s, 1H, ε position of His), 8.68 (brs, 1H, η2 position of Arg), 8.61 (d, *J*=6.6 Hz, 1H, NH), 8.29 (d, *J*=8.0 Hz, 1H, NH), 7.46 (s, 1H, δ position of His), 7.19 (d, *J*=9.0 Hz, 1H, NH), 5.33 (d, *J*=6.2 Hz, 1H, γ position of Hse), 4.60 (m, 1H, α position of Pro), 4.58 (m, 1H, α position of His), 4.36 (m, 1H, α position of Hse), 4.11 (m, 1H, α position of Arg), 3.40 (m, 1H, δ position of Pro), 3.36 (m, 1H, β position of His), 3.31 (m, 1H, δ position of Pro), 3.30 (m, 1H, γ position of Pro), 3.27 (dd, *J*=9.0, 15.0 Hz, 1H, β position of His), 3.21 (m, 2H, δ position of Arg), 2.65 (m, 1H, β position of Hse), 2.20 (ddd, *J*=9.0, 17.0, 24.0 Hz, 1H, γ position of Aad), 2.12 (m, 3H, γ position of Aad, β position of Pro), 2.05 (s, 3H, acetyl), 1.74 (m, 2H, β position of Pro, γ position of Pro), 1.72 (m, 1H, β position of Arg), 1.66 (m, 2H, β position of Arg, β position of Hse), 1.58 (m, 1H, α position of Aad), 1.49 (m, 2H, γ position of Arg), 1.44 (m, 2H, β position of Aad); ^{13}C-NMR (100 MHz, DMSO-d_6 with 1.7% TFA) δ: 173.9 (ε position of Aad), 172.9 (-NHCO- of Hse), 173.2 (-COCH$_3$), 171.9 (-NHCO- of Aad), 171.4 (-NHCO- of Pro), 170.1 (-NHCO- of Arg), 169.9 (-NHCO- of His), 153.1 (ζ position of Arg), 134.5 (ε position of His), 129.4 (γ position of Aad), 117.0 (δ position of His), 78.4 (γ position of Hse), 59.4 (α position of Pro), 57.2 (α position of His), 53.2 (α position of Aad), 51.2 (α position of Arg), 48.9 (α position of Hse), 46.0 (δ position of Pro), 40.7 (δ position of Arg), 35.9 (β position of Hse), 33.1 (δ position of Aad), 31.8 (β position of Aad), 27.8 (β position of Pro), 27.2 (β position of Arg), 24.3 (γ position of Arg), 24.1 (-COCH$_3$), 23.6 (γ position of Pro), 22.5 (β position of His), 20.7 (γ position of Aad); HR-MS (PEG_ESI+_1000) calcd for $C_{29}H_{43}O_{10}N_9$: 675.3215 [M+H], found *m/z* : 675.3199 $[M+H]^+$.

Natural Argadin

$[\alpha]_D$=+52.1 (*c* 0.1, H_2O);[9] ^{1}H-NMR (400 MHz, DMSO-d_6 with 1.7% TFA) δ: 14.19 (brs, 1H, His), 11.78 (s, 2H, η1 position of Arg), 9.16 (t, *J*=4.8 Hz, 2H, ε position of Arg), 8.97 (s, 1H, ε position of His), 8.68 (brs, 1H, η2 position of Arg), 8.58 (d, *J*=6.8 Hz, 1H, NH), 8.27 (d, *J*=7.9 Hz, 1H, NH), 7.43 (s, 1H, δ position of His), 7.16 (d, *J*=9.1 Hz, 1H, NH), 5.31 (d, *J*=6.2 Hz, 1H, γ position of Hse), 4.59 (m, 1H, α position of Pro), 4.58 (m, 1H, α position of His), 4.33 (ddd, *J*=4.3, 9.1, 11.6 Hz, 1H, α position of Hse), 4.10 (m, 1H, α position of Arg), 3.41 (ddd, *J*=11.4, 11.4, 11.4 Hz, 1H, δ position of Pro), 3.36 (dd, *J*=12.6, 19.9 Hz, 1H, β position of His), 3.31 (m, 1H, δ position of Pro), 3.28 (m, 1H, γ position of Pro), 3.26 (dd, *J*=9.6, 19.9 Hz, 1H, β position of His), 3.25 (m, 2H, δ position of Arg), 2.63 (ddd, *J*=6.2, 11.6, 19.4 Hz, 1H, β position of Hse), 2.21 (ddd, *J*=9.1, 16.9, 21.3 Hz, 1H, γ position of Aad), 2.17 (ddd, *J*=9.1, 16.9, 21.3 Hz, 2H, γ position of Aad), 2.11 (m, 1H, β position of Pro), 2.10 (s, 3H, acetyl), 1.75 (m, 2H, β position of Pro, γ position of Pro), 1.73 (m, 1H, β position of Arg), 1.66 (m, 2H, β position of Arg, β position of Hse), 1.57 (m, 1H, α position of Aad), 1.50 (m, 2H, γ position of Arg), 1.43 (m, 2H, β position of Aad).

^{13}C-NMR (100 MHz, DMSO-d_6 with 1.7% TFA) δ: 174.3 (ε position of Aad), 172.9 (-NHCO- of Hse), 172.7 (-COCH$_3$), 171.4 (-NHCO- of Aad), 171.1 (-NHCO- of Pro), 170.1 (-NHCO- of Arg), 169.9 (-NHCO- of His), 153.1 (ζ position of Arg), 134.5 (ε position of His), 129.4 (γ position of Aad), 117.0 (δ position of His), 78.7 (γ position of Hse), 59.8 (α position of Pro), 57.2 (α position of His), 53.2 (α position of Aad), 51.6 (α position of Arg), 49.0 (α position of Hse), 46.0 (δ position of Pro), 40.7 (δ position of Arg), 35.9 (β position of Hse), 33.1 (δ position of Aad), 31.8 (β position of Aad), 27.9 (β position of Pro), 27.4 (β position of Arg), 24.3 (γ position of Arg), 24.1 (-COCH$_3$), 23.6 (γ position of Pro), 22.5 (β position of His), 20.7 (γ position of Aad).

ACKNOWLEDGEMENTS

This work was supported by the Grant of the 21st Century COE Program, Ministry of Education Culture, Sports, Science and Technology. AS was supported by a JSPS Research Fellowships for Young Scientists. TH acknowledges the Kitasato University research grant for young researchers. We also thank Ms A Nakagawa, Ms N Sato and Dr K Nagai (Kitasato University) for various instrumental analyses.

1 Boot, R. G. *et al.* Identification of a novel acidic mammalian chitinase distinct from chitotriosidase. *J. Biol. Chem.* **276,** 6770–6778 (2001).
2 Shahabuddin, M., Toyoshima, T., Aikawa, M. & Kaslow, D. C. Transmission-blocking activity of a chitinase inhibitor and activation of malarial parasite chitinase by mosquito protease. *Proc. Natl. Acad. Sci. USA* **90,** 4266–4270 (1993).
3 Shibata, Y., Foster, L. A., Bradfield, J. F. & Myrvik, Q. N. Oral administration of chitin down-regulates serum IgE levels and lung eosinophilia in the allergic mouse. *J. Immunol.* **164,** 1314–1321 (2000).
4 Matsuura, H *et al.* Nucleotide sequences of genes encoding allosamidin-sensitive and -insensitive chitinases produced by allosamidin-producing *Streptomyces*. *Biosci. Biotechnol. Biochem.* **67,** 2002–2005 (2003).
5 Hollis, T. *et al.* The X-ray structure of a chitinase from the pathogenic fungus *Coccidioides immitis*. *Protein Sci.* **9,** 544–551 (2000).
6 Sakuda, S., Isogai, A., Matsumoto, S. & Suzuki, A. Search for microbial insect growth regulators. II. Allosamidin, a novel insect chitinase inhibitor. *J. Antibiot.* **40,** 296–300 (1987).
7 Vinetz, J. M. *et al.* Chitinases of the avian malaria parasite *Plasmodium gallinaceum*, a class of enzymes necessary for parasite invasion of the mosquito midgut. *J. Biol. Chem.* **275,** 10331–10341 (2000).

8 Zhu, Z. *et al.* Acidic mammalian chitinase in asthmatic Th2 inflammation and IL-13 pathway activation. *Science* **304,** 1678–1682 (2004).
9 Arai, N. *et al.* Argadin, a new chitinase inhibitor, produced by *Clonostachys sp.* FO-7314. *Chem. Pharm. Bull.* **48,** 1442–1446 (2000).
10 Ōmura, S. *et al.* Argifin, a new chitinase inhibitor, produced by *Gliocladium sp.* FTD-0668. I. Taxonomy, fermentation, and biological activities. *J. Antibiot.* **53,** 603–608 (2000).
11 Arai, N., Shiomi, K., Iwai, Y. & Ōmura, S. Argifin, a new chitinase inhibitor, produced by *Gliocladium sp.* FTD-0668. II. Isolation, physico-chemical properties, and structure elucidation. *J. Antibiot.* **53,** 609–614 (2000).
12 Shiomi, K. *et al.* Structure of argifin, a new chitinase inhibitor produced by *Gliocladium sp. Tetrahedron Lett.* **41,** 2141–2143 (2000).
13 Suzuki, K. *et al.* Chitinases A, B, and C1 of *Serratia marcescens* 2170 produced by recombinant *Escherichia coli*: enzymatic properties and synergism on chitin degradation. *Biosci. Biotechnol. Biochem.* **66,** 1075–1083 (2002).
14 Horn, S. J. *et al.* Comparative studies of chitinases A, B and C from *Serratia marcescens. Biocatal. Biotransfor.* **24,** 39–53 (2006).
15 Rao, F. V. *et al.* Specificity and affinity of natural product cyclopentapeptide inhibitors against *A. fumigatus*, human, and bacterial chitinases. *Chem. Biol.* **12,** 65–76 (2005).
16 Houston, D. R. *et al.* High-resolution structures of a chitinase complexed with natural product cyclopentapeptide inhibitors: mimicry of carbohydrate substrate. *Proc. Natl. Acad. Sci. USA* **99,** 9127–9132 (2002).
17 Dixon, M. J., Andersen, O. A., van Aalten, D. M. F. & Eggleston, I. M. First synthesis of Argadin: a nanomolar inhibitor of family-18 chitinases. *Eur. J. Org. Chem.* 5002–5006 (2006).
18 Dixon, M. J., Andersen, O. A., van Aalten, D. M. F. & Eggleston, I. M. An efficient synthesis of argifin: a natural product chitinase inhibitor with chemotherapeutic potential. *Bioorg. Med. Chem. Lett.* **15,** 4717–4721 (2005).
19 Dixon, M. J. *et al.* Solid-phase synthesis of cyclic peptide chitinase inhibitors: SAR of the argifin scaffold. *Org. Biomol. Chem.* **7,** 259–268 (2009).
20 Sunazuka, T. *et al.* Argifin; efficient solid phase total synthesis and evaluation of analogues of acyclic peptides. *Bioorg. Med. Chem.* **17,** 2751–2758 (2009).
21 Hirose, T. *et al.* Chitinase inhibitors: extraction of the active framework from natural argifin and use of *in situ* click chemistry. *J. Antibiot.* **62,** 277–282 (2009).
22 Bayer, T., Riemer, C. & Kessler, H. A new strategy for the synthesis of cyclopeptides containing diaminoglutaric acid. *J. Peptide Sci.* **7,** 250–261 (2001).
23 Bycroft, B. W., Chan, W. C., Chhabra, S. R. & Hone, N. D. A novel lysine-protecting procedure for continuous flow solid phase synthesis of branched peptides. *J. Chem. Soc. Chem. Commun.* 778–779 (1993).
24 Chhabra, S. R. *et al.* An appraisal of new variants of Dde amine protecting group for solid phase peptide synthesis. *Tetrahedron Lett.* **39,** 1603–1606 (1998).
25 Hong, Y. *et al.* Preparation of amidino-urea serotonin receptor ligands. *PCT Int. Appl.* WO2002036554 A2 20020510 (2002).
26 Gouda, H. *et al.* Computer-aided rational molecular design of argifin-derivatives with more potent inhibitory activity against chitinase B from *Serratia marcescens. Bioorg. Med. Chem. Lett.* **19,** 2630–2633 (2009).

The Journal of Antibiotics (2009) 62, 501–505

www.nature.com/ja

ORIGINAL ARTICLE

Bingchamides A and B, two novel cyclic pentapeptides from the *Streptomyces bingchenggensis*: fermentation, isolation, structure elucidation and biological properties

Wen-Sheng Xiang[1], Ji-Dong Wang[2], Xiang-Jing Wang[1] and Ji Zhang[1]

Two novel cyclic pentapeptides, bingchamides A (1) and B (2), have been isolated from the organic extracts of the mycelium of *Streptomyces bingchenggensis*. The structures of 1 and 2 were elucidated on the basis of extensive 1D and 2D NMR, as well as HRESI-MS, electrospray ionization-MS, UV and IR spectroscopic data analysis. Bingchamides A (1) and B (2) exhibited *in vitro* cytotoxicity toward human colon carcinoma cell line HCT-116 with the IC_{50} values of 14.1 and 18.0 μg ml^{-1}, respectively. The bingchamides A (1) and B (2) scaffolds are probably promising structures for the development of new antitumor agents.
The Journal of Antibiotics (2009) **62,** 501–505; doi:10.1038/ja.2009.60; published online 17 July 2009

Keywords: antitumor activity; bingchamides A and B; cyclic pentapeptides; *Streptomyces bingchenggensis*

INTRODUCTION

In the course of screening for new biologically active compounds from microbial sources, an actinomycete strain, *Streptomyces bingchenggensis*, was isolated from a soil sample collected in Harbin, China. The fermentation broths of *S. bingchenggensis* possess not only potent acaricidal and nematocidal activity, but also antitumor activity. In the previous research, we isolated compounds with potent acaricidal and nematocidal activity, milbemycins β_{13}, β_{14}, α_{28}, α_{29}, α_{30}, secomilbemycins A, B,[1–3] and a novel macrolide compound, ST906[4] with antitumor activity, from *S. bingchenggensis*. We investigated the fermentation broths of this microorganism in more detail and have isolated two new cyclic pentapeptide compounds, bingchamides A (**1**) and B (**2**, Figure 1). The structures of **1** and **2** were elucidated on the basis of extensive 1D and 2D NMR, as well as HRESI-MS, electrospray ionization (ESI)-MS, UV and IR spectroscopic data analysis. Bingchamides A (**1**) and B (**2**) possessed potent cytotoxicity against human cancer cell lines *in vitro*, and are structurally related to sansalvamide A (**3**, Figure 1), which is also a potent cytotoxic compound isolated from a marine fungus, *Fusarium* spp.[5] We describe in this paper the fermentation, isolation, structure elucidation and biological properties of **1** and **2**. To evaluate their anticancer activities *in vitro*, we used the drug-resistant human cancer cell line HCT-116.[6–10]

RESULTS AND DISCUSSION

Structural elucidation

Compound **1** was obtained as a colorless oil with the UV absorptions at λ_{max} of 232 and 275 nm. The molecular formula of **1** was established as $C_{40}H_{51}N_5O_5$ on the basis of HRESI-MS and NMR analysis, which indicated the presence of 18 degrees of unsaturation. The IR absorption at 1651 cm^{-1} indicated the presence of amide functionalities. In the ^{13}C NMR spectrum of **1**, five signals were observed between δ 169 and 174, values that are typically assigned to the carbonyls of a peptide. In total, five ^{13}C NMR signals between δ 51 and 63 were characteristic of the α-carbons of amino acid residues. The assignment of five amide groups accounted for all of the nitrogen, oxygen and five of the degrees of unsaturation required by the molecular formula. A total of 12 signals in the aromatic region of the ^{13}C NMR spectrum between δ 126 and 138 were characteristic of three mono-substituted phenyl groups, and suggested the presence of three phenylalanine (Phe) residues, which accounted for an additional 12 unsaturations, and left one remaining unsaturation, requiring that **1** possesses one ring. Application of 2D NMR techniques (^1H–^1H COSY, heteronuclear multiple quantum coherence (HMQC) and heteronuclear multiple bond correlation (HMBC)), which allowed for the identification of all of the amino acid residues of **1**, revealed the presence of leucine (Leu), isoleucine (Ile), two phenylalanines (Phe-1 and Phe-2) and one N-Me phenylalanine (N-Me-Phe). Two- and three-bond HMBC correlations from the α- and/or β-protons of each residue to their neighboring carbonyl carbons and the NOESY experiments were useful in assigning the carbonyl signals and in establishing the amino acid sequence of **1** (Figure 2). The three-bond HMBC correlation from the β-protons (δ 2.80, 3.16) of N-Me-Phe to the carbonyl carbon at δ 169.5 assigned the carbonyl carbon belonging to the residue of N-Me-Phe. The observed HMBC correlation from δ_H 1.45 to δ_C 173.4 and

[1]School of Life Science, Northeast Agricultural University, Harbin, China and [2]Zhejiang Hisun Pharmaceutical, Taizhou, Zhejiang, China
Correspondence: Professor X-J Wang, School of Life Science, Northeast Agricultural University, Harbin 150030, China.
E-mail: wangxiangjing2008@yahoo.com.cn
Received 11 March 2009; revised 17 June 2009; accepted 25 June 2009; published online 17 July 2009

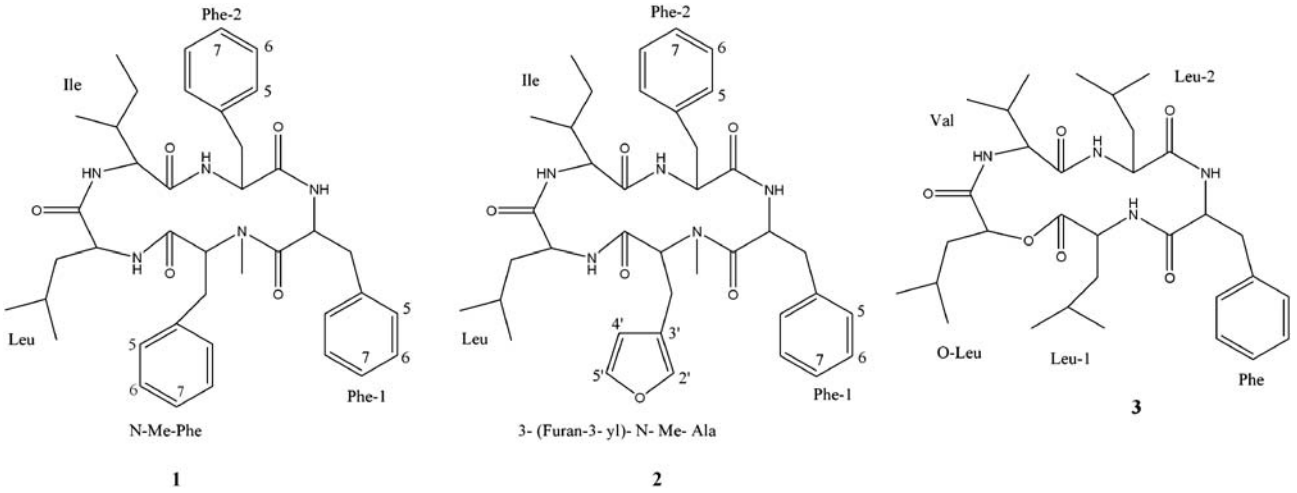

Figure 1 The structures of bingchamides A (**1**), B (**2**) and sansalvamide A (**3**).

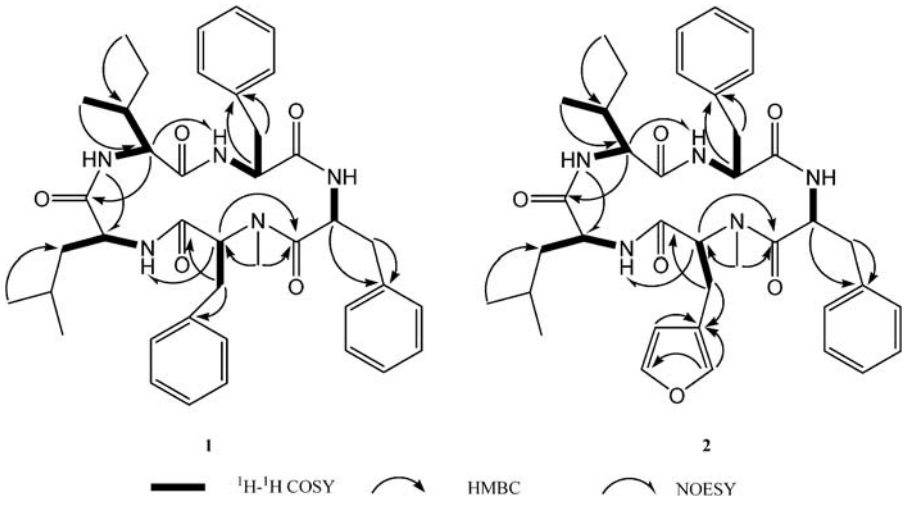

Figure 2 The key ^{1}H–^{1}H COSY, HMBC and NOESY correlations of **1** and **2**.

from δ_H 2.93 to δ_C 171.8 assigned the carbonyl carbons belonging to the residue of Leu and Phe-1**,** respectively. The remaining two overlapped carbon signals at δ 170.7 were the carbonyl carbons of the residues of Phe-2 and Ile. In its HMBC spectrum, correlation of the proton signal of N-Me (δ 2.69) and the amide carbonyl carbon at δ 171.8 established the partial sequence Phe-1→N-Me-Phe. The long-range ^{1}H–^{13}C correlation between δ_H 3.33 and δ_C 173.4 and 170.7 established the partial sequence Leu→Ile. By the ^{1}H–^{1}H COSY spectrum, four NH proton signals were assigned to their respective amino acid residues (Table 1). The key NOESY signal between δ 5.21 and δ 6.77 connected the N-Me-Phe to Leu. The sequence of four amino acid residues (Phe-1, N-Me-Phe, Leu and Ile) was completed. Consequently, the remaining Phe-2 connected with Ile and Phe-1, and was acylated by Ile. Thus, the overall sequence for **1** was established in the only way possible.

The stereochemistry of **1** remained unknown because of the absence of correlation signals of the five α-protons of the five amino acid residues in the NOESY experiment and the poor amount of **1**. To confirm the structure of **1** and establish its conformation, chemical synthesis of **1** is ongoing.

Compound **2** was also obtained as a colorless oil. The molecular formula of **2** was deduced from HRESI-MS *m/z* 694.3593 ($(M+Na)^+$, calcd for $C_{38}H_{49}N_5O_6Na$, 694.3581) in conjunction with ^{13}C NMR spectral data. Its ^{13}C NMR data displayed five characteristic α-carbon signals of amino acid residues between δ 51 and 63, and the five carbonyl signals between δ 169 and 174 were assigned to the amide carbonyl carbons of a pentapeptide. Detailed comparison of the ^{1}H and ^{13}C NMR data of **2** with those of **1** revealed that four of five amino acid residues of **2** were identical to those of **1** (Phe-1, Phe-2, Leu and Ile). By further analysis of the HMBC and NOESY correlations (Figure 2), the sequence of the four amino acid residues in **2** was the same as shown in **1**. Comparison of the ^{1}H and ^{13}C NMR data of the remaining amino acid residue in **2** with those of N-Me-Phe in **1** revealed that the difference between them was only in the aromatic moiety. The four carbon signals at δ 142.9, 139.6, 119.5 and 110.4, and an unassigned oxygen atom in conjunction with the HMBC correlations from δ_H 6.04 to δ_C 119.5, 139.6, 142.9, from δ_H 6.97 to δ_C 119.5, 110.4, 142.9, from δ_H 7.22 to δ_C 119.5, 110.4, 139.6 established the presence of a furan ring. The long-range ^{1}H–^{13}C correlations observed between δ_H 2.67, 2.87 and δ_C 119.5, 139.6 established the remaining

Table 1 NMR spectral data for 1 and 2 in $CDCl_3$

	1				***2***		
Position	*^{13}C*	*^{1}H (J)*	*Key HMBC correlations*	*Position*	*^{13}C*	*^{1}H (J)*	*Key HMBC correlations*
Phe-1				*Phe-1*			
1	171.8 s*			1	171.7 s		
2	51.4 d	4.96 m	171.8, 137.1	2	51.6 d	5.00 m	171.7
3	37.9 t	2.93 overlapped		3	37.9 t	2.94 dd (13.2, 5.3)	137.2, 171.7
		3.18 dd (13.3, 5.5)	137.1			3.20 dd (13.2, 9.4)	137.2
4	137.1 s			4	137.2 s		
5/9	129.5 d[a]	7.02–7.28 m		5/9	129.5 d	7.17–7.31 m	
6/8	128.6 d[a]	7.02–7.28 m		6/8	128.9 d[d]	7.17–7.31 m	
7	126.7 d[b]	7.02–7.28 m		7	126.7 d[e]	7.17–7.31 m	
NH		7.36 d (8.7)		NH		7.36 d (8.7)	
Phe-2				*Phe-2*			
1	170.7 s			1	170.6 s		
2	56.8 d	4.46 m	170.7, 136.2	2	56.3 d	4.53 m	17.06, 136.2
3	37.3 t	3.13 m	136.2	3	37.5 t	3.13 m	136.2, 56.3
4	136.2 s[c]			4	136.2 s		
5/9	129.0 d[a]	7.02–7.28 m		5/9	129.0 d	7.17–7.31 m	
6/8	128.6 d[a]	7.02–7.28 m		6/8	128.4 d[d]	7.17–7.31 m	
7	126.6 d[b]	7.02–7.28 m		7	127.3 d[e]	7.17–7.31 m	
NH		6.87 d (7.6)		NH		6.88 d (8.5)	
Ile				*Ile*			
1	170.7 s			1	170.6 s		
2	62.2 d	3.33 dd (10.6, 7.8)	173.4, 170.7	2	62.4 d	3.29 dd (7.7)	173.5, 170.6
3	33.2 d	2.01 m		3	33.0 d	2.03 m	
4	25.1 t	1.40 m		4	25.2 t	1.42 m	
		0.97 m				0.99 m	
5	10.2 q	0.81 t (7.4)	25.1, 33.2	5	10.0 q	0.82 t (7.4)	25.2, 33.0
6	15.4 q	0.56 d (6.6)	33.2, 62.2	6	15.5 q	0.57 d (6.6)	33.0, 62.4
NH		7.33 d (7.8)		NH		7.52 d (7.7)	
Leu				*Leu*			
1	173.4 s			1	173.5 s		
2	51.8 d	4.35 m	173.4	2	51.7 d	4.40 m	173.5
3	40.6 t	1.45 m	173.4	3	40.8 t	1.48 m	173.5
4	24.7 d	1.45 m		4	24.8 d	1.54 m	
5	21.9 q	0.82 d (6.0)	40.6, 24.7	5	21.8 q	0.86 d (6.3)	40.8, 24.8
6	22.6 q	0.86 d (6.1)	40.6, 24.7	6	22.7 q	0.96 d (6.4)	40.8, 24.8
NH		6.77 d (9.5)		NH		6.91 d (9.9)	
N-Me-Phe				*3-(Furan-3-yl)-N-Me-Ala*			
1	169.5 s			1	169.5 s		
2	56.5 d	5.21 d (8.0)	169.5, 171.8	2	55.6 d	5.11 t (8.0)	169.5, 171.7
3	32.4 t	2.80 dd (14.5, 8.0)	169.5, 136.3	3	22.1 t	2.67 overlapped	
		3.16 overlapped				2.87 dd (15.4, 8.0)	169.5, 119.5
4	136.3 s[c]			2′	139.6 d	6.97 s	110.4, 119.5, 142.9
5/9	128.9 d[a]	7.02–7.28 m		3′	119.5 s		
6/8	128.3[a] d	7.02–7.28 m		4′	110.4 d	6.04 dd (1.6, 0.7)	119.5, 139.6, 142.9
7	127.3[b] d	7.02–7.28 m		5′	142.9 d	7.22 overlapped	110.4, 119.5, 139.6
N-Me	30.0 q	2.69 s	169.5, 171.8	N-Me	29.6 q	2.66 s	169.5, 171.7

*By DEPT sequence.
[a,b,c,d,e] Values for these assignments may be interchanged.

amino acid residue as 3-(furan-3-yl)-N-Me-alanine (3-(furan-3-yl)-N-Me-Ala). Consequently, the gross structure of **2** was elucidated as the similar sequence of **1** except that the residue of 3-(furan-3-yl)-N-Me-Ala in **2** replaced the residue of N-Me-Phe in **1**. A furan ring incorporated into a cyclic peptide structure as a natural product is rare.[11,12]

Biological activity

We examined the inhibitory activity of bingchamides A (**1**) and B (**2**) against the growth of human colon carcinoma cell line HCT-116 using the CCK-8 colorimetric method as described in Methods. Compound **1** and **2** dose-dependently inhibited the growth of HCT-116 cells with IC50 value of 14.1 and 18.0 $\mu g\,ml^{-1}$, respectively.

Natural products are excellent sources of potential new drug leads. These novel structures are important for the development of original therapeutic leads that target new biological pathways.[13] Sansalvamide A is one such natural product (**3**, Figure 1). A number of analogs have been made. These sansalvamide A derivatives[6–10,14–20] have shown that they are privileged structures and exhibit potency against multiple targets in numerous cancer cell lines. The examples of potent cytotoxicity against pancreatic, colon, breast, prostate and melanoma cancers clearly indicate the potential of this compound class as a platform useful in targeting these cancers. The structures of bingchamides A (**1**) and B (**2**) are similar to sansalvamide A, and they all belong to cyclic pentapeptides. However, there are significant differences among them. This shows that like sansalvamide A, bingchamides A (**1**) and B (**2**) scaffolds are probably promising structures for the development of new antitumor agents.

METHODS

General

UV spectra were obtained on a Varian CARY 300 BIO spectrophotometer (Varian, Palo Alto, CA, USA); IR spectra were recorded on a Nicolet Magna FT-IR 750 spectrometer (Nicolet, Madison, WI, USA) (ν_{max} in cm^{-1}); and ^1H and ^{13}C NMR spectra were measured with a Bruker DRX-400 (400 MHz for ^1H and 100 MHz for ^{13}C) spectrometer (Bruker, Billerica, MA, USA). Chemical shifts are reported in parts per million (δ), using the residual $CHCl_3$ (δ_H 7.26 p.p.m.; δ_C 77.0) as an internal standard, coupling constant (J) in Hz. ^1H and ^{13}C NMR assignments were supported by ^1H–^1H COSY, HMQC and HMBC experiments. The ESI-MS and HRESI-MS spectra were taken on a Q-TOF Micromass LC–MS–MS (Waters Corporation, Milford, MA, USA) mass spectrometer. Optical rotation was measured on a Perkin-Elmer 341 Polarimeter (Perkin-Elmer, Fremont, CA, USA). Reversed phase-HPLC was conducted on an Agilent 1100 series (Agilent, Santa Clara, CA, USA). Commercial silica gel (Qing Dao Hai Yang Chemical Group, Qing Dao, China, 100–200 and 200–300 mesh) was used for column chromatography. Spots were detected on TLC under UV or by heating after spraying with sulfuric acid-ethanol, 5:95 (v/v).

Microorganism

The producing organism, *S. bingchenggensis*, was isolated from a soil sample collected in Harbin, China. *S. bingchenggensis* has been deposited at the China General Microbiology Culture Collection Center (Accession no: CGMCC1734), Institute of Microbiology, Chinese Academy of Sciences, and we have determined the 16S rDNA sequence (Accession no: DQ449953 in GenBank, National Center for Biological Information).

Fermentation

The seed for preculture was spores. The medium for sporulation contained sucrose (Bei Jing Ao Bo Xing, Beijing, China) 4 g, yeast extract (Bei Jing Ao Bo Xing) 2 g, malt extract (Bei Jing Ao Bo Xing) 5 g and skim milk (Nmyili, Huhehaote, China) 1 g in 1 l water. The pH was adjusted to 7.0 with 1 M NaOH, 20 g of agar was added and this mixture was sterilized at 121 °C for 30 min. The spore suspension was prepared from the agarplates (20 ml) incubated at 28 °C for 7–8 days.

A spore suspension of the culture of strain *S. bingchenggensis*, 1 ml, was transferred to a 250-ml Erlenmeyer flask that contained 25 ml of the seed medium containing sucrose 0.25 g, polypepton (Bei Jing Ao Bo Xing) 0.1 g and K_2HPO_4 1.25 mg. The inoculated flasks were incubated at 28 °C for 42 h on a rotary shaker at 250 r.p.m. Then 8.0 ml of the culture was transferred into 1-l Erlenmeyer flask containing 100 ml of the producing medium consisting of sucrose (Bei Jing Ao Bo Xing) 8.0%, soybean powder (Comwin, Beijing, China) 1.0%, yeast extract (Bei Jing Bo Xing) 0.2%, meat extract (Bei Jing Ao Bo Xing) 0.1%, $CaCO_3$ (Bei Jing Hong Xin, Beijing, China) 0.3%, K_2HPO_4 0.03 %, $MgSO_4 \cdot 7H_2O$ 0.1% and $FeSO_4 \cdot 7H_2O$ 0.005%, pH 7.2 before sterilization. Fermentation was carried out at 28 °C for 8 days in a rotary shaker at 250 r.p.m.

Isolation and purification

The fermentation broth (30 l) was filtered. The resulting cake was washed with water, and both filtrate and wash were discarded. Methanol (5 l) was used to extract the washed cake. The MeOH extract was concentrated to approximately 1 l under reduced pressure and the resulting concentrate was extracted three times with an equal volume of EtOAc. The combined EtOAc phase was concentrated under reduced pressure to yield 50 g of oily substances. The residual oily substance was chromatographed on silica gel and eluted with petroleum ether–acetone (95:5–50:50) to give five fractions. The semi-preparative HPLC (Agilent 1100, Zorbax SB-C18, 5 µm, 250×9.4 mm i.d.) was further applied to obtain pure compounds. The eluates were monitored with a photodiode array detector at 220 nm and the flow rate was 1.5 ml min^{-1} at room temperature. The fifth fraction (petroleum ether–acetone 1:1) with anticancer activity was separated by semi-preparative HPLC using a solvent of 85% CH_3CN/H_2O to afford **1** (11.1 min, 13.0 mg) and **2** (9.8 min, 9.5 mg).

Physico-chemical properties of compounds 1. Bingchamide A (**1**) $C_{40}H_{51}N_5O_5$, colorless oil; $[\alpha]^{25}_D$+103.6° (c 0.03, EtOH); UV ($CHCl_3$) λ_{max} nm (log ε): 232 (4.8), 275 (3.6); IR (KBr), ν_{max} cm^{-1}: 3479, 2922, 1651, 1522, 1456, 1124, 699; ^1H NMR ($CDCl_3$, 400 MHz) and ^{13}C NMR ($CDCl_3$, 100 MHz) see Table 1; ESI-MS *m/z* 682 $[M+H]^+$; HRESI-MS *m/z* 704.3807 ($[M+Na]^+$, calcd for $C_{40}H_{51}N_5O_5Na$, 704.3788).

Physico-chemical properties of compounds 2. Bingchamide B (**2**) $C_{38}H_{49}N_5O_6$, colorless oil; $[\alpha]^{25}_D$+111.8° (*c* 0.02, EtOH); UV ($CHCl_3$) λ_{max} nm (log ε): 231 (4.8), 276 (3.7); IR (KBr), ν_{max} cm^{-1}: 3276, 2928, 1663, 1528, 1458, 1026, 874, 701; ^1H NMR ($CDCl_3$, 400 MHz) and ^{13}C NMR ($CDCl_3$, 100 MHz) see Table 1; ESI-MS *m/z* 672 $[M+H]^+$; HRESI-MS *m/z* 694.3593 ($[M+Na]^+$, calcd for $C_{38}H_{49}N_5O_6Na$, 694.3581).

Biological assays

The cytotoxicity of compound on tumor cells was assayed according to the published procedures.[21] Human colon carcinoma cell line HCT-116 was routinely cultured in Dulbecco's Modified Eagle Media containing 10% calf serum at 37 °C for 4 h in a humidified atmosphere of 5% CO_2 incubator. The adherent cells at their logarithmic growth stage were digested, and were inoculated onto 96-well culture plate at a density of 1.0×10^4 per well for the determination of proliferation. Test samples were added to the medium, and incubation was continued for 72 h. Coloration substrate, cell-counting kit-8 (CCK-8, Dojindo, Kumamoto, Japan), was added to the medium followed by further incubation for 3 h. Absorbance at 450 nm with a 600 nm reference was measured thereafter. Media and DMSO control wells, in which compound was absent, were included in all the experiments to eliminate the influence of DMSO. The inhibitory rate of cell proliferation was calculated by the following formula:

$$\text{Growth inhibition}(\%) = [OD_{control} - OD_{treated}]/OD_{control} \times 100$$

The cytotoxicity of compound on tumor cells was expressed as IC_{50} values (the drug concentration reducing by 50% the absorbance in treated cells, with respect to untreated cells) and was calculated by LOGIT method.

ACKNOWLEDGEMENTS

This study was supported by the National Natural Science Foundation of China (Grant nos. 30571234 and 30771427), the National Key Technology R&D Program (Grant no. 2006BAD31B) and the Program for New Century Excellent Talents in University.

1 Xiang, W. S., Wang, J. D., Wang, X. J. & Zhang, J. Two new-class milbemycins from *Streptomyces bingchenggensis* Fermentation, isolation, structure elucidation and biological properties. *J. Antibiot.* **60,** 351–356 (2007).

2 Xiang, W. S., Wang, J. D., Wang, X. J., Zhang, J. & Wang, Z. Further new milbemycin antibiotics from *Streptomyces bingchenggensis*. *J. Antibiot.* **60,** 608–613 (2007).
3 Xiang, W. S., Wang, J. D., Fan, H. M., Wang, X. J. & Zhang, J. New Seco-milbemycins from *Streptomyces bingchenggensis*: fermentation, isolation and structure elucidation. *J. Antibiot.* **60,** 27–32 (2008).
4 Xiang, W. S., Wang, J. D., Wang, X. J. & Zhang, J. A novel macrolide compound from *Streptomyces bingchenggensis* fermentation, isolation, structure elucidation and biological properties. *J. Antibiot.* **62,** 229–231 (2009).
5 Hwang, Y. *et al.* Mechanism of inhibition of a poxvirus topoisomerase by the marine natural product sansalvamide. *A. Mol. Pharmacol.* **6,** 1049–1053 (1999).
6 Lee, Y. & Silverman, R. B. Rapid, high-yield, solid-phase synthesis of the antitumor antibiotic sansalvamide A using a side-chain-tethered phenylalanine building block. *Org. Lett.* **2,** 3743–3746 (2000).
7 Gu, W., Liu, S. & Silverman, R. B. Solid-phase, Pd-catalyzed siliconaryl carbon bond formation. Synthesis of sansalvamide A peptide. *Org. Lett.* **4,** 4171–4174 (2002).
8 Carroll, C. L. *et al.* Synthesis and cytotoxicity of novel sansalvamide A derivatives. *Org. Lett.* **7,** 3481–3484 (2005).
9 Otrubova, K. *et al.* Synthesis and novel structure-activity relationships of potent sansalvamide A derivatives. *Chem. Commun.* **9,** 1033–1034 (2006).
10 Otrubova, K., McGuire, K. L. & McAlpine, S. R. Scaffold targeting drug-resistant colon cancers. *J. Med. Chem.* **9,** 1999–2002 (2007).
11 Tan, N. H. & Zhou, J. Plant Cyclopeptides. *Chem. Rev.* **106,** 840–895 (2006).
12 Liu, Y. Q. *et al.* Design and synthesis of cyclo[-Arg-Gly-Asp-ψ(triazole)-Gly-Xaa-] peptide analogues by click chemistry. *Tetrahedron* **47,** 10728–10734 (2008).
13 Harvey, A. L. Natural products in drug discovery. *Drug Discov. Today* **13,** 895–901 (2008).
14 Otrubova, K., Lushington, G., McGuire, K. L. & McAlpine, S. R. Comprehensive study of sansalvamide A derivatives and their structure-activity relationships against drug-resistant colon cancer cell lines. *J. Med. Chem.* **3,** 530–544 (2008).
15 Davis, M. R. *et al.* Synthesis and cytotoxicity of a new class of potent decapeptide macrocycles. *Org. Lett.* **2,** 177–180 (2008).
16 Pan, P. S., McGuire, K. L. & McAlpine, S. R. Identification of Sansalvamide A analog potent against pancreatic cancer cell lines. *Bioorg. Med. Chem. Lett.* **18,** 5072–5077 (2007).
17 Rodriguez, R. A. *et al.* Synthesis of second-generation sansalvamide A derivatives: novel templates as potential antitumor agents. *J. Org. Chem.* **6,** 1980–2002 (2007).
18 Styers, T. J. *et al.* Synthesis of Sansalvamide A derivatives and their cytotoxicity in the MSS colon cancer cell line HT-2. *Bioorg. Med. Chem.* **16,** 5625–5631 (2006).
19 Otrubova, K. *et al.* Synthesis and novel structure-activity relationships of potent sansalvamide A derivatives. *Chem. Commun.* **9,** 1033–1034 (2006).
20 Ujiki, M. B. *et al.* A novel peptide sansalvamide analogue inhibits pancreatic cancer cell growth through G0/G1 cell-cycle arrest. *Biochem. Biophys. Res. Commun.* **4,** 1224–1228 (2006).
21 Wijnhoven, B. P. *et al.* Human oesophageal adenocarcinoma cell lines JROECL 47 and JROECL 50 are admixtures of the human colon carcinoma cell line HCT 11. *Br. J. Cancer.* **9,** 1510–1512 (2000).

The Journal of Antibiotics (2009) 62, 507–512

www.nature.com/ja

ORIGINAL ARTICLE

The cytotoxic macrolide FD-891 induces caspase-8-dependent mitochondrial release of cytochrome *c* and subsequent apoptosis in human leukemia Jurkat cells

Susumu Inaba[1], Tadashi Eguchi[2], Atsushi Motegi[2], Kazutoshi Mizoue[3], Takeo Usui[4], Kazuo Nagai[5] and Takao Kataoka[1,6]

The 16-membered macrolide FD-891 exerts cytotoxicity toward several cancer cell lines. In this study, we showed that FD-891 induces apoptosis in various human cancer cell lines. Human leukemia Jurkat cells were highly sensitive to FD-891, exhibiting caspase activation and mitochondrial release of cytochrome *c* into the cytosol at early time points after exposure to FD-891. By contrast, Jurkat cells deficient in caspase-8 were resistant to FD-891-induced apoptosis and manifested little induction of cytochrome *c* release as well as caspase-9 processing. Consistent with these results, the overexpression of the Bcl-2 family member Bcl-x_L or the caspase-8 modulator c-FLIP$_L$ markedly prevented FD-891-induced apoptosis. These results clearly demonstrate that FD-891 triggers caspase-8-dependent mitochondrial release of cytochrome *c* and subsequent apoptosis in Jurkat cells.
The Journal of Antibiotics (2009) **62,** 507–512; doi:10.1038/ja.2009.62; published online 10 July 2009

Keywords: apoptosis; caspase-8; cytochrome *c*; cytotoxicity; FD-891; macrolide

INTRODUCTION

Apoptosis is a physiological process that has an important role in the homeostasis of mature tissues. Caspases are a family of cysteine proteinases that are essential for apoptosis and act by cleaving selected substrates.[1–3] Initiator caspase-8 is converted into active forms via dimerization and self-processing, and subsequently cleaves various substrates, such as effector caspases and BH3-only protein Bid, to produce their active forms.[1–3] Truncated Bid is translocated to mitochondria where it initiates the release of pro-apoptotic proteins into the cytosol.[4,5] Mitochondrial pro-apoptotic proteins, such as cytochrome *c*, are confined to intermembrane space and liberated into the cytosol in response to apoptotic stimuli.[6,7] Cytochrome *c* collaborates with adaptor protein Apaf-1 to activate initiator caspase-9.[8–10] Effector caspases-3, -6, and -7 are processed into their active forms by activated caspase-9 and the activated caspases mediate the proteolytic cleavage of cellular proteins required for apoptosis.[11]

The cytotoxic macrolide FD-891 was originally isolated from the fermentation broth of *Streptomyces graminofaciens* A-8890.[12,13] The absolute structure of FD-891 was determined in our earlier work (Figure 1a)[14,15] and its planar structure turned out to be the same as that of BE-45653.[16] The total synthesis of FD-891 was recently reported.[17–19] It has been shown that FD-891 exerts cytotoxicity toward several cancer cell lines.[12,19] Moreover, as regards immunosuppressive activity, FD-891 prevents cytotoxic T lymphocyte (CTL) mediated killing pathway.[20] In this study, we investigated the molecular mechanism underlying the cytotoxicity of FD-891. Our present results demonstrate that FD-891 triggers caspase-8-dependent mitochondrial release of cytochrome *c* and subsequent apoptosis in a human leukemia cell line highly sensitive to FD-891.

MATERIALS AND METHODS

Cells

Human lung carcinoma A549 cells, human fibrosarcoma HT-1080 cells and human rhabdomyosarcoma Kym-1 cells were obtained from the Health Science Research Resources Bank (Osaka, Japan). Caspase-8-deficient Jurkat cell clone (I9.2),[21] c-FLIP$_L$-transfected Jurkat cell clone (JFL2),[22] and Bcl-x_L-transfected Jurkat cell clone (Jurkat-Bcl-x_L #1)[23] were described previously. Human cancer cell lines were maintained in RPMI-1640 medium (Invitrogen, Carlsbad, CA, USA) supplemented with 10% (v/v) heat-inactivated fetal calf serum (JRH Bioscience, Lenexa, KS, USA), penicillin G (100 U ml^{-1}) (Sigma-Aldrich, St Louis, MO, USA) and streptomycin (100 μg ml^{-1}) (Sigma-Aldrich).

Reagents

FD-891 was purified from the fermentation broth of *S. graminofaciens* A-8890 as previously described.[12] Doxorubicin, etoposide and vincristine were purchased from Sigma-Aldrich.

[1]Center for Biological Resources and Informatics, Tokyo Institute of Technology, Nagatsuta-cho, Midori-ku, Yokohama, Japan; [2]Department of Chemistry and Materials Science, Tokyo Institute of Technology, O-okayama, Meguro-ku, Tokyo, Japan; [3]Taisho Pharmaceutical Co. Ltd., Yoshino-cho, Kita-ku, Saitama-shi, Saitama, Japan; [4]Graduate School of Life and Environmental Sciences, University of Tsukuba, Tennodai, Tsukuba, Ibaraki, Japan; [5]Department of Biological Chemistry, Chubu University, Matsumoto-cho, Kasugai, Aichi, Japan and [6]Department of Applied Biology, Kyoto Institute of Technology, Matsugasaki, Sakyo-ku, Kyoto, Japan
Correspondence: Professor T Kataoka, Department of Applied Biology, Kyoto Institute of Technology, Matsugasaki, Sakyo-ku, Kyoto 606-8585, Japan.
E-mail: takao.kataoka@kit.ac.jp
Received 3 June 2009; revised 8 June 2009; accepted 18 June 2009; published online 10 July 2009

Antibodies

Antibodies to caspase-3 (H-277; Santa Cruz Biotechnology, Santa Cruz, CA, USA), caspase-6 (3E8; Medical & Biological Laboratories (MBL), Nagoya, Japan), caspase-7 (11E4; Sigma-Aldrich), caspase-8 (5F7; MBL), caspase-9 (5B4; MBL), cytochrome *c* (7H8.2C12; BD Biosciences, Franklin Lakes, NJ, USA), and PARP (C-2-10; Sigma-Aldrich) were commercially obtained.

Assay for cell viability

Cells were pulsed with 500 μg ml^{-1} of 3-(4,5-dimethylthiazol-2-yl)-2,5-diphenyl tetrazolium bromide (MTT) for 4 h. MTT formazan was solubilized with 10% sodium dodecyl sulfate (SDS) overnight. Absorbance at 595 nm was measured with a Model 680 microplate reader (Bio-Rad Laboratories, Hercules, CA, USA). Cell viability (%) was calculated as [(experimental absorbance–background absorbance)/(control absorbance –background absorbance)]×100.

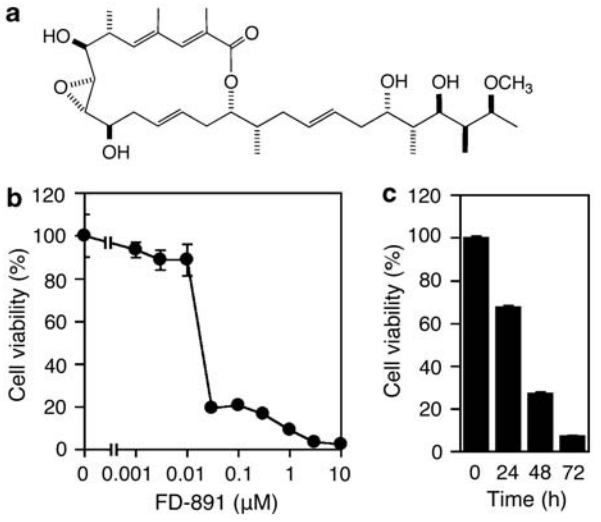

Figure 1 FD-891 inhibits cell proliferation. (**a**) Structure of FD-891. (**b** and **c**) Jurkat cells were incubated with various concentrations of FD-891 for 72 h (**b**). Jurkat cells were incubated with FD-891 (1 μM) for the indicated times (**c**). Cell viability (%) was measured by MTT assay. Data points represent means ± s.d. of triplicate cultures.

Assay for apoptosis

Cells were fixed with PBS containing 4% paraformaldehyde at 4 °C overnight, and then stained with 300 μM Hoechst 33342 (Calbiochem, San Diego, CA, USA). Nuclear morphology was observed under a fluorescence light microscope (Axiovert 200 M; Carl Zeiss, Jena, Germany). Apoptotic cells (%) were calculated as (condensed nuclei/total nuclei)×100.

Preparation of cell lysates

Cells were washed with PBS and lysed in Triton X-100 lysis buffer consisting of 50 mM Tris-HCl (pH 7.4), 1% Triton X-100, 2 mM DTT, 2 mM sodium orthovanadate, and the protease inhibitor mixture Complete (Roche Diagnostics,

Table 1 Effect of FD-891 on proliferation of human cancer cell lines

Cell line	*Source*	*IC_{50} (nM)*
A549	Lung carcinoma	310 ± 70
HeLa	Cervix adenocarcinoma	140 ± 70
HL-60	Acute promyelocytic leukemia	35 ± 29
HT-1080	Fibrosarcoma	130 ± 70
Jurkat	Acute T cell leukemia	32 ± 24
K-562	chronic myelogenous leukemia	1000 ± 710
Kym-1	Rhabdosarcoma	250 ± 80
MCF7	Breast adenocarcinoma	220 ± 100
Raji	Burkitt's lymphoma	170 ± 140
THP-1	Acute monocytic lymphoma	30 ± 20
U-937	Histiocytic lymphoma	41 ± 34

Human cancer cell lines were incubated with serial dilution of FD-891 for 3 days. Cell viability (%) was measured by MTT assay. The IC_{50} values (mean ± s.d.) were calculated from three to four independent experiments.

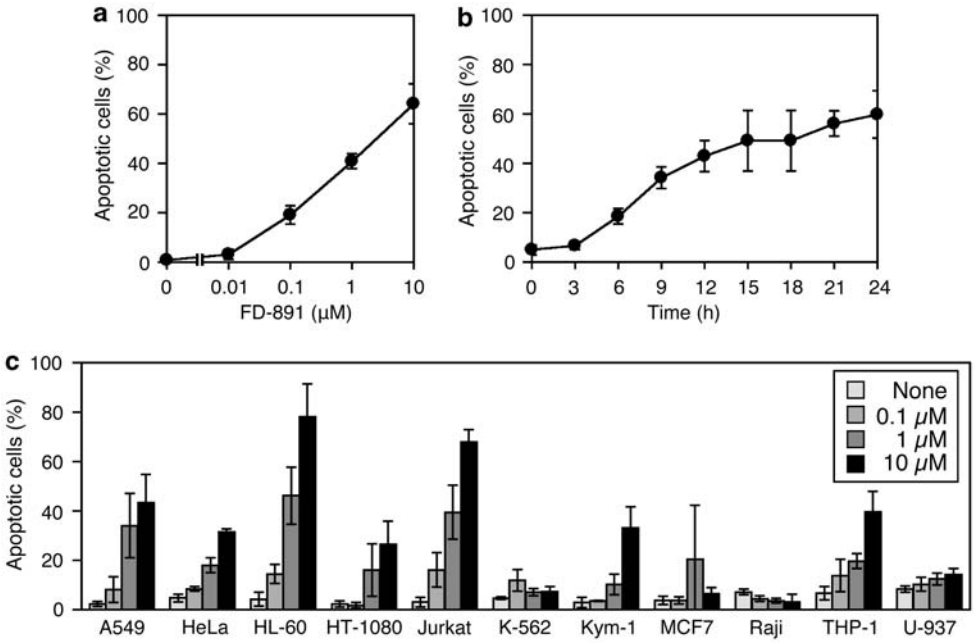

Figure 2 FD-891 induces apoptosis. (**a** and **b**) Jurkat cells were incubated with various concentrations of FD-891 for 24 h (**a**). Jurkat cells were incubated with FD-891 (1 μM) for the indicated times (**b**). Apoptotic cells (%) were measured by Hoechst 33342 staining. Data points represent means ± s.d. of triplicate determinations. (**c**) Human cancer cell lines were incubated with various concentrations of FD-891 for 24 h. Apoptotic cells (%) were measured by Hoechst 33342 staining. The results are expressed as means ± s.d. of three independent experiments.

Mannheim, Germany). Postnuclear lysates were collected as supernatants by centrifugation (10 000 *g*, 5 min). Alternatively, cells were washed with PBS and lysed with digitonin lysis buffer (10 mM Hepes-KOH (pH 7.2), 100 μM digitonin, 250 mM sucrose, 1 mM DTT, 5 mM EGTA, 2 mM $MgCl_2$, 50 mM NaCl and the protease inhibitor mixture Complete) on ice for 15 min. After centrifugation (10 000 *g*, 5 min), cell lysates containing the cytosol were recovered as supernatants. Pellets were washed once with digitonin lysis buffer and treated with Triton X-100 lysis buffer on ice for 15 min. After centrifugation (10 000 *g*, 5 min), cell lysates containing the mitochondria were collected as supernatants (mitochondrial fraction).

Western blotting

Protein samples (30 μg per lane) were separated by SDS-PAGE and transferred onto Hybond-ECL nitrocellulose membranes (GE Healthcare, Piscataway, NJ, USA). The transferred membranes were stained with Ponceau S and checked for equal loading of proteins before antibody reaction. The membranes were incubated with primary antibodies and then with horseradish peroxidase-conjugated secondary antibodies (Jackson ImmunoResearch, West Grove, PA, USA), followed by analysis using ECL western blotting detection reagents (GE Healthcare).

RESULTS

FD-891 inhibits proliferation of human cancer cell lines

It has been shown that FD-891 exerts cytotoxicity toward several cancer cell lines.[12,19] To investigate the inhibition specificity of FD-891 on cancer cell proliferation, various human cancer cell lines were incubated in the presence of FD-891 for 72 h and cell viability was measured by the MTT assay. Although FD-891 prevented cell proliferation at IC_{50} values of 130 to 1000 nM in most of the cancer cell lines, four leukemia cell lines (HL-60, Jurkat, THP-1 and U-937) were highly sensitive to FD-891 at IC_{50} values of approximately 30 to 40 nM (Table 1). In Jurkat cells, FD-891 decreased cell viability by more than 80% at concentrations higher than 100 nM when incubated for 72 h (Figure 1b). Kinetic studies revealed that FD-891 gradually reduced cell viability during incubation for 24 to 72 h (Figure 1c).

FD-891 induces apoptosis of human cancer cell lines

To investigate whether FD-891 is able to induce apoptosis, Jurkat cells were incubated with various concentrations of FD-891 for 24 h and nuclear morphological changes were analyzed by fluorescence microscopy after Hoechst 33342 staining. FD-891 at concentrations higher than 100 nM was found to induce nuclear condensation and fragmentation characteristic of apoptosis within 24 h (Figure 2a). Kinetic studies revealed that FD-891 initiated apoptosis within 6 h and that the number of apoptotic cells steadily increased during 24 h incubation (Figure 2b). Various human cancer cell lines were also found to undergo apoptosis upon treatment with FD-891. FD-891 was able to induce apoptosis very strongly in two leukemia cell lines (that is, Jurkat and HL-60), whereas it induced moderate-to-weak apoptosis in

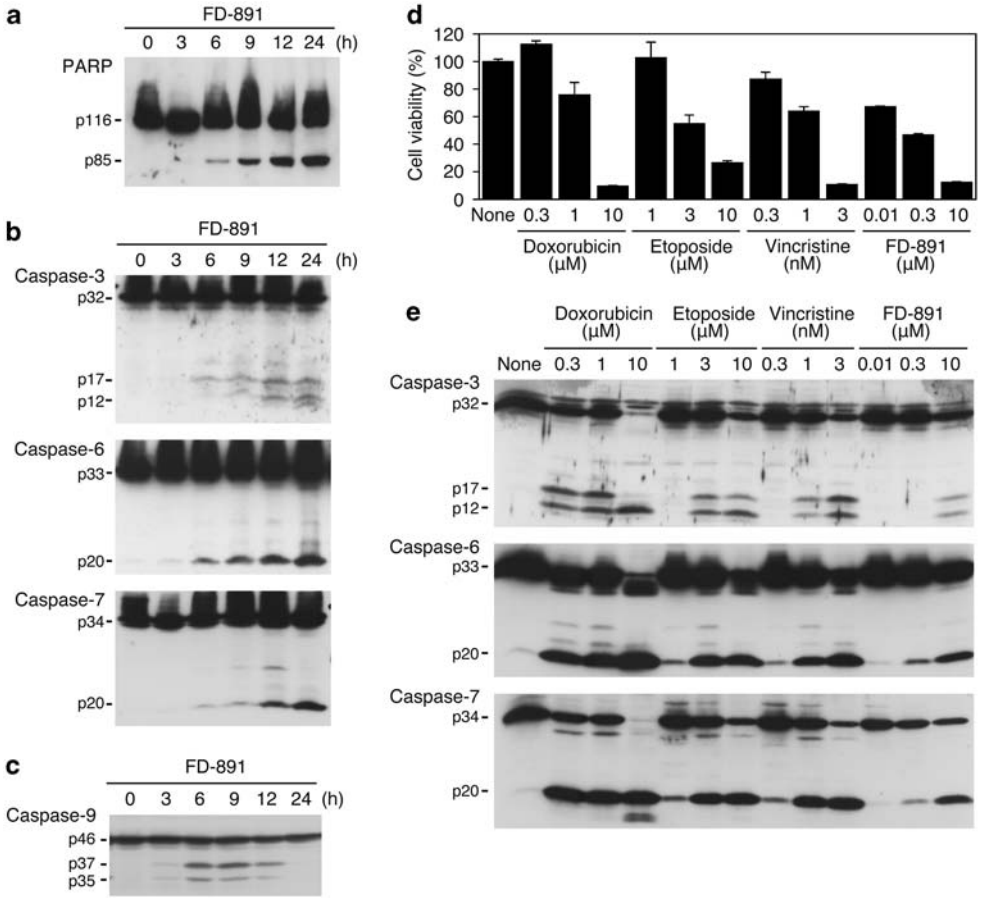

Figure 3 FD-891 induces activation of effector caspases. (**a**–**c**) Jurkat cells were incubated with FD-891 (1 μM) for the indicated times. The expression of PARP (**a**), caspases-3, -6, -7 (**b**), and caspase-9 (**c**) was analyzed by western blotting. (**d**) Jurkat cells were incubated with various concentrations of doxorubicin, etoposide, vincristine, and FD-891 for 24 h. Cell viability (%) was measured by MTT assay. The results are means ± s.d. of triplicate cultures. (**e**) Jurkat cells were incubated with various concentrations of doxorubicin, etoposide, vincristine and FD-891 for 24 h. The expression of caspases-3, -6 and -7 was analyzed by western blotting.

the other cancer cell lines (Figure 2c). Therefore, the results suggest that the induction of apoptosis is correlated with the inhibitory effect of FD-891 on cell proliferation at least in Jurkat and HL-60 cells. However, non-apoptotic cells harboring two nuclei apparently accumulated in FD-891-treated cells (unpublished observation). Therefore, as previously reported,[19] it seems that FD-891 induces cell cycle arrest at the G_2/M phase, and this biological effect may also contribute to its inhibitory effect on cell proliferation. In this study, the molecular mechanism underlying FD-891-induced apoptosis in Jurkat cells was further addressed.

FD-891 induces activation of caspases

Poly(ADP-ribose)polymerase (PARP) is a nuclear protein that is processed by effector caspases during apoptosis.[24] When Jurkat cells were incubated with FD-891, full-length PARP (116 kDa) was processed into the cleaved form (85 kDa) during 6 to 24 h incubation (Figure 3a). Likewise, caspase-3, caspase-6 and caspase-7 were processed into their active forms in FD-891-treated cells with similar kinetics (Figure 3b). Initiator caspase-9 was also processed into p35 and p37 fragments at earlier time points than other effector caspases when Jurkat cells were exposed to FD-891 (Figure 3c). We previously reported that chemotherapeutic agents, such as doxorubicin, etoposide and vincristine, induce apoptosis in Jurkat cells.[25] Similar to FD-891, doxorubicin, etoposide and vincristine were able to induce the processing of caspase-3, caspase-6 and caspase-7 into their active forms (Figure 3e). However, at the concentrations that reduced cell viability to approximately 50% within 24 h, these chemotherapeutic drugs were able to induce the activation of effector caspases more effectively than FD-891 (Figures 3d and e). Thus, the results suggest that FD-891 may induce caspase activation in a manner distinct from doxorubicin, etoposide and vincristine.

FD-891 induces mitochondrial release of cytochrome *c*

Mitochondria has an essential role in the induction of apoptosis by releasing pro-apoptotic proteins, such as cytochrome *c*, into the cytosol.[6,7] Upon treatment with FD-891, cytochrome *c* was released from the mitochondria into the cytosol in Jurkat cells (Figure 4a). The Bcl-2 family of proteins regulates cytochrome *c* release and subsequent induction of apoptosis.[6,7] The overexpression of Bcl-x_L markedly inhibited apoptosis induced by FD-891 (Figure 4b). These results suggest that the mitochondrial release of cytochrome *c* is required for FD-891-induced apoptosis.

Caspase-8 is required for mitochondrial release of cytochrome *c* during FD-891-induced apoptosis

Caspase-8 is an initiator caspase that undergoes self-processing into its active forms in response to various stimuli.[1–3] In Jurkat cells, caspase-8 was processed into p43/p41 fragments during FD-891-induced apoptosis (Figure 5a). However, in contrast to Fas ligand (FasL) stimulation, p18 large fragments were barely detectable in FD-891-treated cells (Figure 5a). To address if caspase-8 is required for FD-891-induced apoptosis, Jurkat cells deficient in caspase-8 were compared with wild-type cells for the induction of apoptosis upon exposure to FD-891. Caspase-8-deficient cells manifested resistance to FD-891-induced apoptosis (Figure 5b). The overexpression of the caspase-8 modulator c-$FLIP_L$ also conferred resistance to FD-891-induced apoptosis in Jurkat cells (Figure 5c), supporting the notion that caspase-8 is required for FD-891-induced apoptosis. In caspase-8-deficient cells, FD-891 barely induced the release of cytochrome *c* into the cytosol (Figure 5d). Consistently, caspase-9 processing was also inhibited in caspase-8-deficient cells treated with FD-891 (Figure 5e).

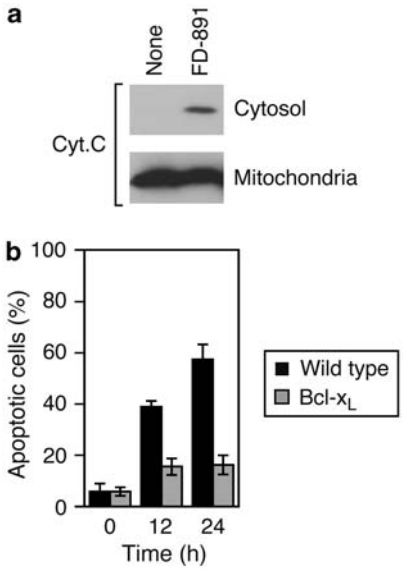

Figure 4 FD-891 induces mitochondrial release of cytochrome *c*. (**a**) Jurkat cells were incubated with FD-891 (1 μM) for 12 h. Cell lysates containing the cytosol and the mitochondria were prepared. The expression of cytochrome *c* was analyzed by western blotting. (**b**) Wild-type Jurkat cells (black bars) and Bcl-x_L-transfected Jurkat cell clone (gray bars) were incubated with FD-891 (1 μM) for the indicated times. Apoptotic cells (%) were measured by Hoechst 33342 staining. The results are expressed as means ± s.d. of triplicate determinations.

Together, the results demonstrate that caspase-8 is required for the release of cytochrome *c* to the cytosol and the subsequent activation of caspase-9.

DISCUSSION

FD-891 was found to induce apoptosis in several human cancer cell lines. In Jurkat cells that were highly sensitive to FD-891, the activation of caspases as well as the mitochondrial release of cytochrome *c* to the cytosol was induced at early time points after treatment with FD-891. Unlike wild-type Jurkat cells, FD-891 barely induced the activation of caspase-9 and the mitochondrial release of cytochrome *c* in caspase-8-deficient Jurkat cells. The overexpression of Bcl-x_L or c-$FLIP_L$ rendered Jurkat cells resistant to FD-891-induced apoptosis. Thus, our present results clearly demonstrate that FD-891 induces caspase-8-dependent mitochondrial release of cytochrome *c* to the cytosol and subsequent apoptosis in Jurkat cells.

It has been shown that FD-891 inhibits cell proliferation in cancer cell lines.[12,19] Consistent with these findings, we have shown that FD-891 is able to inhibit cell proliferation in many human cancer cell lines at IC_{50} values of 0.03 to 1 μM. Human leukemia cell lines, such as Jurkat cells and HeLa cells, were highly sensitive to FD-891 and underwent rapid apoptosis upon treatment with FD-891. However, in some cancer cell lines, FD-891 barely induced apoptosis even at 10 μM, suggesting that the FD-891-induced apoptosis is cell type-specific. It has been shown that FD-891 induces accumulation of cancer cells at the G_2/M phase during the cell cycle.[19] Therefore, it seems likely that FD-891 predominantly induces cell cycle arrest, thereby inhibiting cell proliferation in cancer cell lines refractory to apoptosis.

Chemotherapeutic drugs, such as doxorubicin, etoposide and vincristine, are known to induce caspase-dependent apoptosis in various types of cancer cells. We previously showed that the over-

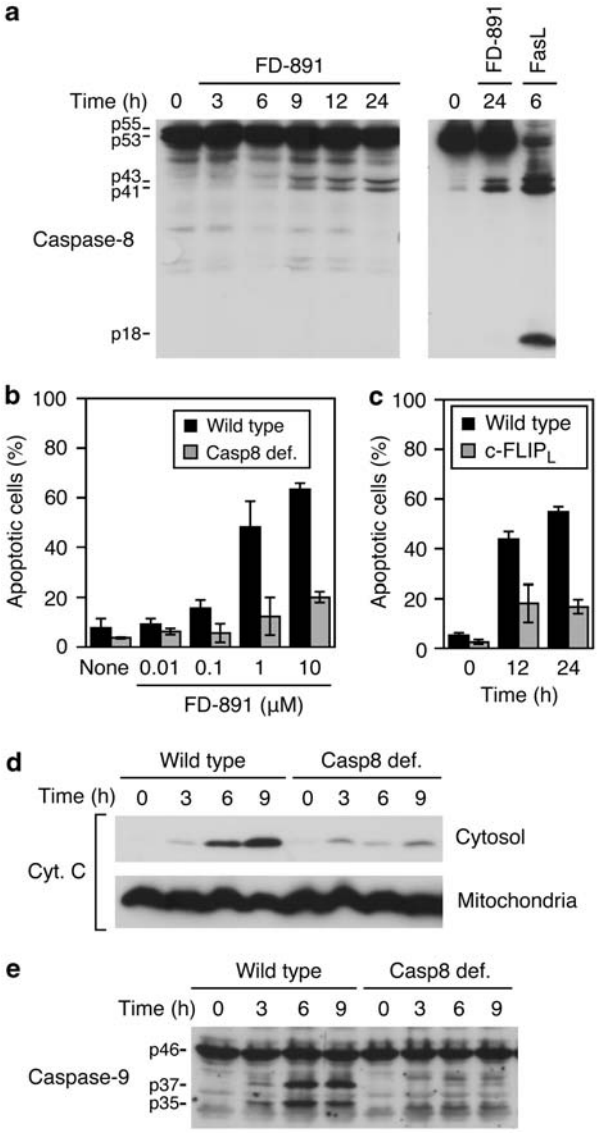

Figure 5 Caspase-8 is required for cytochrome *c* release and caspase-9 activation during FD-891-induced apoptosis. (**a**) Jurkat cells were incubated with or without FD-891 (1 μM) or FasL (200 ng ml^{-1}) for the indicated times. The expression of caspase-8 was analyzed by western blotting. (**b**) Wild-type Jurkat cells (black bars) and caspase-8-deficient Jurkat cells (gray bars) were incubated with various concentrations of FD-891 for 24 h. Apoptotic cells (%) were measured by Hoechst 33342 staining. The results are means ± s.d. of triplicate determinations. (**c**) Wild-type Jurkat cells (black bars) and c-FLIP$_L$-transfected Jurkat cell clone JFL2 (gray bars) were incubated with FD-891 (1 μM) for the indicated times. Apoptotic cells (%) were measured by Hoechst 33342 staining. The results are means ± s.d. of triplicate determinations. (**d**) Wild-type Jurkat cells and caspase-8-deficient Jurkat cells were incubated with FD-891 (1 μM) for the indicated times. Cell lysates containing the cytosol and the mitochondria were prepared. The expression of cytochrome *c* was analyzed by western blotting. (**e**) Wild-type Jurkat cells and caspase-8-deficient Jurkat cells were incubated with FD-891 (1 μM) for the indicated times. The expression of caspase-9 was analyzed by western blotting.

expression of c-FLIP$_L$ does not prevent apoptosis induced by doxorubicin, etoposide and vincristine in Jurkat cells,[25] indicating that caspase-8 is dispensable for apoptosis induced by these chemotherapeutic drugs. However, it seems that caspase-8 activation is required for FD-891-induced apoptosis, as c-FLIP$_L$ overexpression or caspase-8 deficiency markedly prevented FD-891-induced apoptosis. Therefore, as the main apoptosis-signaling pathway, FD-891 is likely to induce the mitochondrial release of cytochrome *c* as well as caspase-9 processing through caspase-8 activation.

In addition to the cytotoxicity toward cancer cells, we have previously shown that FD-891 prevents the interaction between CTLs and target cells, thereby inhibiting CTL-mediated killing pathways.[20] Structurally related 16- and 18-membered macrolides (bafilomycin A$_1$ and concanamycin A, respectively), known as inhibitors of vacuolar-type H$^+$-ATPase, manifested inhibitory profiles different from FD-891 in the CTL-mediated killing pathway,[26] in agreement with the fact that FD-891 does not affect vacuolar acidification.[20] The mechanism of action of FD-891 is also distinct from that of known chemotherapeutic drugs (doxorubicin, etoposide and vincristine). To understand anti-cancer and immunosuppressive activities at the molecular level, the molecular target(s) of FD-891 should be identified.

ACKNOWLEDGEMENTS

This work was supported by a Grant-in-Aid for Scientific Research from the Ministry of Education, Culture, Sports, Science and Technology (MEXT), Japan.

1 Riedl, S. J. & Shi, Y. Molecular mechanisms of caspase regulation during apoptosis. *Nat. Rev. Mol. Cell Biol.* **5,** 897–907 (2004).
2 Siegel, R. M. Caspases at the crossroads of immune-cell life and death. *Nat. Rev. Immunol.* **6,** 308–317 (2006).
3 Krammer, P. H., Arnold, R. & Lavrik, I. N. Life and death in peripheral T cells. *Nat. Rev. Immunol.* **7,** 532–542 (2007).
4 Luo, X., Budihardjo, I., Zou, H., Slaughter, C. & Wang, X. Bid, a Bcl2 interacting protein, mediates cytochrome c release from mitochondria in response to activation of cell surface death receptors. *Cell* **94,** 481–490 (1998).
5 Li, H., Zhu, H., Xu, C. & Yuan, J. Cleavage of BID by caspase 8 mediates the mitochondrial damage in the Fas pathway of apoptosis. *Cell* **94,** 491–501 (1998).
6 Chipuk, J. E., Bouchier-Hayes, L. & Green, D. R. Mitochondrial outer membrane permeabilization during apoptosis: the innocent bystander scenario. *Cell Death Differ.* **13,** 1396–1402 (2006).
7 Garrido, C. *et al.* Mechanisms of cytochrome *c* release from mitochondria. *Cell Death Differ.* **13,** 1423–1433 (2006).
8 Pop, C., Timmer, J., Sperandio, S. & Salvesen, G. S. The apoptosome activates caspase-9 by dimerization. *Mol. Cell* **22,** 269–275 (2006).
9 Schafer, Z. T. & Kornbluth, S. The apoptosome: physiological, developmental, and pathological modes of regulation. *Dev. Cell* **10,** 549–561 (2006).
10 Bao, Q. & Shi, Y. Apoptosome: a platform for the activation of initiator caspases. *Cell Death Differ.* **14,** 56–65 (2007).
11 Taylor, R. C., Cullen, S. P. & Martin, S. J. Apoptosis: controlled demolition at the cellular level. *Nat. Rev. Mol. Cell Biol.* **9,** 231–241 (2008).
12 Seki-Asano, M. *et al.* Isolation and characterization of new 18-membered macrolides FD-891 and FD-892. *J. Antibiot.* **47,** 1226–1233 (1994).
13 Seki-Asano, M., Tsuchida, Y., Hanada, K. & Mizoue, K. Structures of new 18-membered macrolides FD-891 and FD-892. *J. Antibiot.* **47,** 1234–1241 (1994).
14 Eguchi, T. *et al.* Stereostructure of a novel cytotoxic 18-membered macrolactone antibiotic FD-891. *Org. Lett.* **4,** 3383–3386 (2002).
15 Eguchi, T., Yamamoto, K., Mizoue, K. & Kakinuma, K. Structure revision of FD-891, a 16-membered macrolide antibiotic. *J. Antibiot.* **57,** 156–157 (2004).
16 Ogawa, H., Nakajima, S., Suzuki, H., Ojiri, K. & Suda, H. Antitumor agent BE-45653 manufacture with Streptomyces. *Jpn. Kokai Tokkyo Koho* 09087285 (1997).
17 Crimmins, M. T. & Caussanel, F. Enantioselective total synthesis of FD-891. *J. Am. Chem. Soc.* **128,** 3128–3129 (2006).
18 García-Fortanet, J., Murga, J., Carda, M. & Marco, J. A. Stereoselective synthesis of the cytotoxic macrolide FD-891. *Org. Lett.* **8,** 2695–2698 (2006).
19 García-Fortanet, J. *et al.* The total synthesis and biological properties of the cytotoxic macrolide FD-891 and its non-natural (Z)-C12 isomer. *Chem. Eur. J.* **13,** 5060–5074 (2007).
20 Kataoka, T. *et al.* FD-891, a structural analogue of concanamycin A that does not affect vacuolar acidification or perforin activity, yet potently prevents cytotoxic T lymphocyte-mediated cytotoxicity through the blockage of conjugate formation. *Immunology* **100,** 170–177 (2000).
21 Juo, P., Kuo, C. J., Yuan, J. & Blenis, J. Essential requirement for caspase-8/FLICE in the initiation of the Fas-induced apoptotic cascade. *Curr. Biol.* **8,** 1001–1008 (1998).

22 Irmler, M. *et al.* Inhibition of death receptor signals by cellular FLIP. *Nature* **388,** 190–195 (1997).
23 Kadohara, K. *et al.* Acetoxycycloheximide (E-73) rapidly induces apoptosis mediated by the release of cytochrome *c* via activation of c-Jun N-terminal kinase. *Biochem. Pharmacol.* **69,** 551–560 (2005).
24 Nicholson, D. W. Caspase structure, proteolytic substances, and function during apoptotic cell death. *Cell Death Differ.* **6,** 1028–1042 (1999).
25 Kataoka, T. *et al.* FLIP prevents apoptosis induced by death receptors but not by perforin/granzyme B, chemotherapeutic drugs, and gamma irradiation. *J. Immunol.* **161,** 3936–3942 (1998).
26 Kataoka, T. *et al.* Identification of low molecular weight probes on perforin- and Fas-based killing mediated by cytotoxic T lymphocytes. *Biosci. Biotech. Biochem.* **60,** 1726–1728 (1996).

The Journal of Antibiotics (2009) 62, 513–518

www.nature.com/ja

ORIGINAL ARTICLE

Piceamycin and its *N*-acetylcysteine adduct is produced by *Streptomyces* sp. GB 4-2*

Dirk Schulz[1,6], Jonny Nachtigall[2,6], Julia Riedlinger[1], Kathrin Schneider[2], Karl Poralla[1], Johannes F Imhoff[3], Winfried Beil[4], Graeme Nicholson[5], Hans-Peter Fiedler[1] and Roderich D Süssmuth[2]

Piceamycin, a new macrolactam polyketide antibiotic, was detected by HPLC-diode array screening in extracts of *Streptomyces* sp. GB 4-2, which was isolated from the mycorrhizosphere of Norway spruce. The structure of piceamycin was determined by mass spectrometry and NMR experiments. It showed inhibitory activity against Gram-positive bacteria, selected human tumor cell lines and protein tyrosine phosphatase 1B.
The Journal of Antibiotics (2009) **62,** 513–518; doi:10.1038/ja.2009.64; published online 17 July 2009

Keywords: macrolactam antibiotic; polyketide; protein tyrosine phosphatase 1B inhibitor; *Streptomyces*; structural elucidation

INTRODUCTION

The rhizosphere is a highly complex and evidently balanced community of symbiotic and parasitic organisms composed by the coexistence of plants, mycorrhiza-forming soil fungi and mycorrhiza-promoting bacteria, on the one hand, and phytopathogenic fungi and bacteria on the other.[2] On account of the attack and defense mechanisms within this community, a huge variety of signaling factors, growth-promoting metabolites, antifungals and phytotoxins produced by the various partners of this interaction have been reported.[3,4] Recently, we described the mycorrhiza growth-promoting factor, auxofuran, which was produced by the mycorrhiza helper bacterium, *Streptomyces* sp. AcH 505, isolated from the mycorrhizosphere of Norway spruce.[5,6] In addition, the same streptomycete produced two antifungal naphthoquinone antibiotics, WS-5995 B and C, which inhibited the growth of the spruce-pathogenic fungus, *Heterobasidion annosum*.

Streptomyces sp. GB 4-2 was isolated from the mycorrhizosphere of Norway spruce (*Picea abies*). In contrast to *Streptomyces* sp. AcH 505, strain GB 4-2 does not act as a mycorrhiza helper bacterium but promotes the growth of the phytopathogenic fungus, *Heterobasidion abietinum* and induces in parallel plant defense responses. Host responses indicated that strain GB 4-2 induced both local and systemic defense responses in Norway spruce.[7] Furthermore, strain GB 4-2 was found to give a response against the attack of *Heterobasidion* toward the host plant by a two-step enzymatic detoxification of the fungal phytotoxin fomannoxin, which will be reported in a forthcoming publication.

In this report, we describe the fermentation, isolation, structural elucidation and biological activity of piceamycin (**1**), a novel macrocyclic lactam antibiotic, and its *N*-acetylcysteine adduct (**2**) produced by the strain, GB 4-2. The structures of **1** and **2** are shown in Figure 1. Piceamycin (**1**) shows remarkable inhibitory activities against Gram-positive bacteria, human tumor cell lines and human recombinant protein tyrosine phosphatase 1B. The function of **1** within the interaction between the producing strain, Norway spruce, and the parasitic fungus, *Heterobasidion*, is not yet understood, because the compound does not show inhibitory effects against *Heterobasidion* and neither does it induce local and systemic defense response in Norway spruce.

RESULTS

Taxonomy of the producing strain

The morphological and chemical properties of strain GB 4-2 designated the strain as belonging to the genus *Streptomyces*.[8,9] The strain divided on agar plates into a grey-sporulating wild-type and a yellow-orange colored mutant with sparsely developed white aerial mycelium. In submerged cultures, only the yellow-orange mutant was observed. The peptidoglucan was rich in LL-diaminopimelic acid and hexa- and octahydrogenated menaquinones with nine isoprene units were the predominant isoprenologs. Partial sequencing of the 16S rRNA gene of strain GB 4-2 was described by Lehr *et al.*[7] and confirmed its taxonomic classification to the genus *Streptomyces*.

Screening, fermentation and isolation

Streptomycetes isolated from the rhizosphere of various plants were grown in submerged culture in different complex media, and extracts were prepared from mycelia and culture filtrates at various fermentation

[1]Mikrobiologisches Institut, Universität Tübingen, Tübingen, Germany; [2]Institut für Chemie, Technische Universität Berlin, Berlin, Germany; [3]Kieler Wirkstoffzentrum KiWiZ am Institut für Meereswissenschaften IFM-GEOMAR, Kiel, Germany; [4]Institut für Pharmakologie, Medizinische Hochschule Hannover, Hannover, Germany and [5]Institut für Organische Chemie, Universität Tübingen, Tübingen, Germany
[6]These authors contributed equally to this work.
Correspondence: Professor H-P Fiedler, Mikrobiologisches Institut, Auf der Morgenstelle 28, Universität Tübingen, 72076 Tübingen, Germany.
E-mail: hans-peter.fiedler@uni-tuebingen.de or
Professor RD Süssmuth, Institut für Chemie, Technische Universität Berlin, Straße des 17. Juni 124, 10623 Berlin, Germany.
E-mail: suessmuth@chem.tu-berlin.de
*Art. no. 50 in 'Biosynthetic Capacities of Actinomycetes'. Art. no. 49: see Hohmann *et al.*[1]
Received 9 April 2009; revised 25 June 2009; accepted 29 June 2009; published online 17 July 2009

times. The extracts were screened by HPLC-diode array monitoring in combination with our in-house developed HPLC-UV-Vis database[10] to detect novel secondary metabolites. Strain GB 4-2 gained our interest because of the presence of two peaks in the culture filtrate extract at retention times of 8.2 and 10.1 min, as shown in Figure 2, having characteristic UV-visible spectra that differed from those of 867 reference compounds stored in our database.

During a 10-l fermentation strain GB 4-2 began production of **1** after 48 h and reached a maximal yield of 170 mg l^{-1} at 96 h of incubation. **2** was produced simultaneously with **1**, though in a reduced amount. **1** was isolated from the culture filtrate by extraction with ethyl acetate and purified by chromatography on a diol-modified silica gel column followed by subsequent chromatography on Sephadex LH-20 and Toyopearl HW-40 columns. Pure **1** was obtained by preparative reversed-phase (RP)-HPLC as an orange powder.

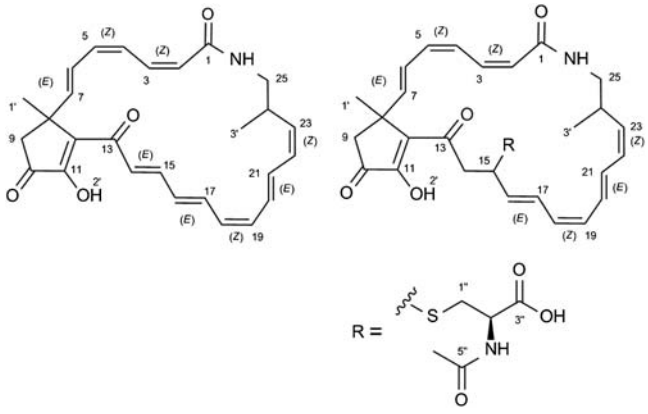

Figure 1 Structures of piceamycin (**1**) and its *N*-acetylcysteine adduct (**2**).

2 was isolated from the culture filtrate by separation on an Amberlite XAD-16 column and was purified by subsequent chromatography on Sephadex LH-20 and Toyopearl HW-40S columns. Pure **2** was obtained by preparative RP-HPLC as pale-yellow powder.

Structural elucidation

The physico-chemical properties of **1** and **2** are summarized in Table 1. ^{13}C and ^{1}H NMR data of **1** and **2** are summarized in Tables 2 and 3, respectively. The molecular masses of **1** and **2** were determined by high-resolution electrospray ionization fourier transform ion cyclotron resonance (ESI–FR–ICR) mass spectrometry, which gave a monoisotopic signal at 432.21697 a.m.u. for **1** and a mass of 595.24699 a.m.u. for **2**, corresponding to $[C_{27}H_{30}NO_4]^+$ (theoretical: 432.21693 a.m.u. for $[M+H]^+$, Δ=0.09 p.p.m.) for **1** and $[C_{32}H_{39}N_2O_7S]^+$ (theoretical: 595.24725 a.m.u., Δ=0.44 p.p.m.) for **2**.

The detailed analyses of COSY (correlated spectroscopy), heteronuclear single quantum coherence (HSQC) and heteronuclear multiple bond coherence (HMBC) NMR spectra enabled the assignment of all proton and carbon NMR signals as shown in Figures 3 and 4. The ^{1}H, ^{13}C and HSQC NMR data of **1** revealed the presence of 21 sp^2-hybridized carbons and one aliphatic methine carbon, two

Table 1 Physico-chemical properties of 1 and 2

	1	*2*
Appearance	Orange powder	Pale-yellow powder
FT–ICR–MS	432.21697 measured $(M+H)^+$	595.24699 measured $(M+H)^+$
	432.21693 theoretical	595.24725 theoretical
	Δ=0.09 p.p.m.	Δ=0.44 p.p.m.
Molecular formula	$C_{27}H_{29}NO_4$	$C_{32}H_{38}N_2O_7S$
UV λmax (MeOH)	295, 410	295, 330 (sh)

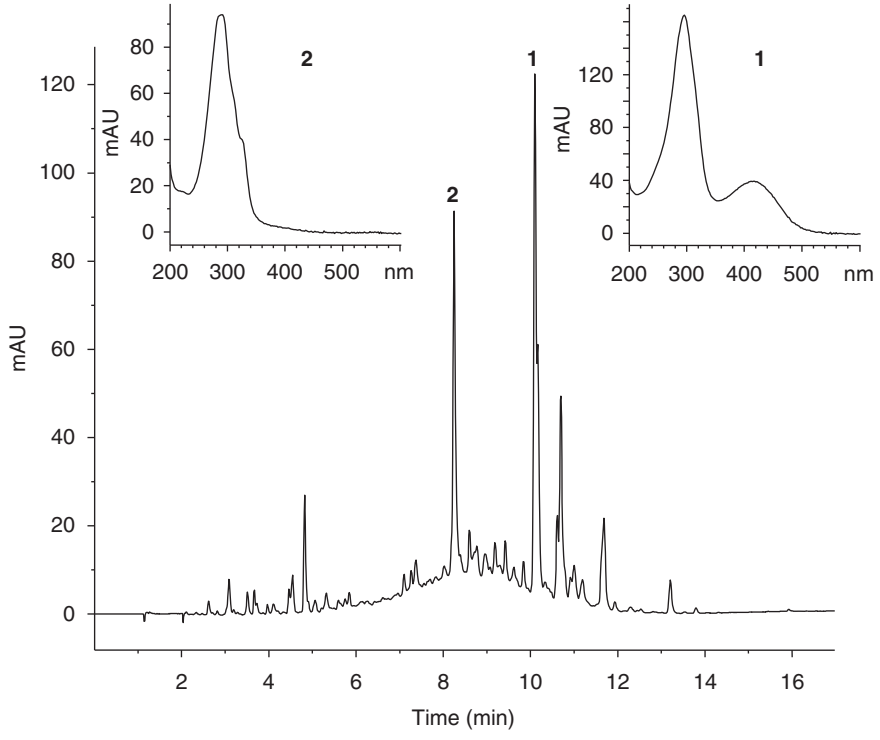

Figure 2 HPLC analysis of a culture filtrate extract from *Streptomyces* sp. GB 4-2 at a cultivation time of 96 h, monitored at 280 nm; insets: UV-visible spectra of **1** and **2** at retention times of 8.2 min (**2**) and 10.1 min (**1**).

Table 2 NMR assignment of 1 in DMSO-d6

	δ (^{1}H) [p.p.m.] J in Hz	δ (^{13}C) [p.p.m.]
1	—	164.4
2	5.08 (d, 11.4)	122.5
3	6.22 (t, 11.8)	132.5
4	7.21 (t, 11.7)	124.2
5	6.10 (dd, 10.1, 14.6)	133.8
6	6.00 (m)	121.3
7	6.00 (m)	143.9
8	—	43.4
9	2.42 (d, 5.53)	49.2
10	—	202.7[a]
11	—	154.3[a]
12	—	138.6
13	—	191.8
14	7.24 (m)	129.2
15	7.07 (dd, 11.2, 15.2)	142.4
16	6.56 (dd, 11.1, 14.7)	129.8
17	7.22 (m)	138.5
18	6.20 (t, 10.9)	127.7
19	6.34 (t, 10.2)	134.2
20	6.65 (m)	127.2
21	6.61 (m)	132.2
22	6.06 (t, 9.9)	129.3
23	5.14 (t, 10.2)	136.3
24	2.68 (m)	33.5
25	3.37; 2.65	43.8
26-NH	7.54 (d, 10.2)	—
1′	1.58 (s)	28.6
2′-OH	11.2 (s, br)	—
3′	0.96 (d, 6.34)	17.8

[a]Deduced by HMBC.

Table 3 NMR assignment of 2 in DMSO-d6

	δ (^{1}H) [p.p.m.] J in Hz	δ (^{13}C) [p.p.m.]
1	—	165.8
2	5.57 (d, 10.1)	122.8
3	6.66 (t, 15.6)	131.1
4	6.66 (t, 15.6)	123.3
5	5.86 (t, 11.7)	133.9
6	6.42 (m)	121.8
7	5.64 (d, 15.2)	143.2
8	—	41.3
9	2.33; 2.53 (d, 19.6)	48.1
10	—	204.5[a]
11	—	156.3[a]
12	—	138.1
13	—	196.5
14	2.49 (m)	45.5
	3.48 (dd, 12.1; 14.8)	45.5
15	3.79 (dt, 11.2, 2.96)	43.9
16	5.24 (dd, 10.4; 14.8)	132.7
17	6.35 (dd, 11.4; 14.5)	127.9
18	5.82 (t, 11.1)	127.6
19	5.92 (t, 10.2)	130.1
20	6.44 (m)	127.6
21	6.44 (m)	129.5
22	6.05 (t, 10.5)	129.3
23	5.11 (t, 10.5)	136.3
24	3.09 (m)	31.6
25	2.76 (m)	31.3
	3.15 (d, 2.57)	31.3
26-NH	7.79 (t, 8.84)	—
1′	1.45 (s)	25.0
2′-OH	11.5 (s, br)	—
3′	0.92 (d, 6.48)	17.9
1″	2.74 (m)	31.3
	2.63 (dd, 8.57;13.5)	31.3
2″	4.33 (m)	51.6
3″	—	172.2
4″-NH	8.26 (d, 8.0)	—
5″	—	169.4
6″	1.85 (s)	22.1

[a]Deduced by HMBC.

methylene carbons, two methyl carbons and one aliphatic quarternary carbon. For compound **2**, the ^{1}H, ^{13}C and HSQC NMR data revealed the presence of 23 sp^2-hybridized carbons, two aliphatic methine carbons, three methylene carbons, three methyl carbons and one aliphatic quarternary carbon. The COSY spectra revealed two spin systems for **1** (H-2–H-7, H-14–H-26–H-3′) and three spin systems for **2** (in addition to H-1″–H-3″). By means of HMBC correlations, the systems could be connected through correlations of the amide proton H-26 and C-1. The cyclic pentenone structure could be assigned by the correlations from H-1′ to C-7, C-8, C-9, C-12 and the correlations from H-9 to C-1′, C-7, C-8, C-10 and C-12. The regiochemistry of the cyclopeptenone was settled by the assignment of $^{2/3}J$ couplings, particularly from H-1′ to the ring carbons C-8, C-9 and C-12. Alternative structural solutions afforded unusual ^4J couplings that have not been observed in the other parts of the molecule and therefore have been excluded. In addition, ^{13}C-NMR chemical shifts are in persuasive accordance to examples from the literature, that is, an α-hydroxy-carbonyl moiety compared with a β-hydroxy-carbonyl moiety.[11,12] By means of COSY and HMBC correlations, the complete carbon chain of **1** could be unambiguously established with the exception of one single correlation connecting C-12 and C-13. Additional HMBC experiments (^4J) with elongated mixing times as well as constant time inverse-detected gradient accordion rescaled-HMBC experiments (J=3–12 Hz and J=3–8 Hz) for long-range ^{1}H–^{13}C NMR correlations did not yield any conclusive correlations.[13] Hence, this connection was indirectly inferred by the ^{13}C-chemical shift of C-12 (138.6 p.p.m.), characteristic of an alkene

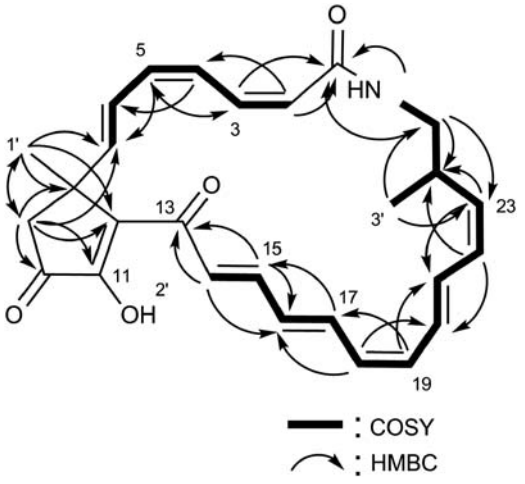

Figure 3 ^{1}H–^{1}H-COSY, HSQC and HMBC correlations observed in **1**.

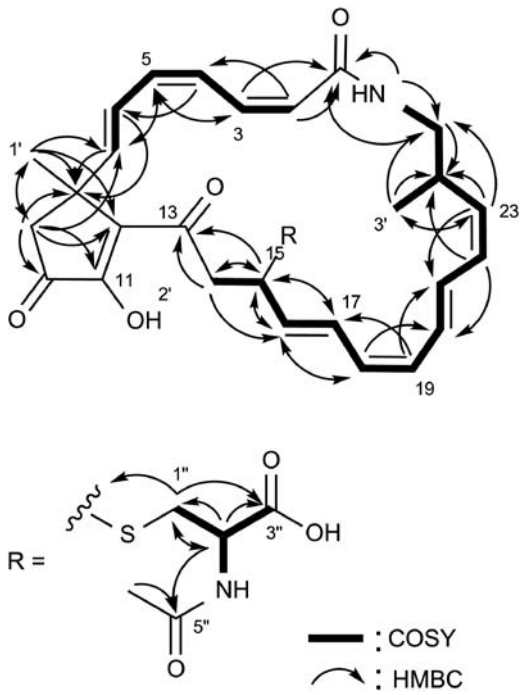

Figure 4 ^{1}H–^{1}H-COSY, HSQC and HMBC correlations observed in **2**.

in a vicinal position to carbonyl C-13. Finally, to obtain coupling constants for overlapping proton signals of **1**, selective 1D total correlation spectroscopy experiments were taken from all olefinic protons with mixing time ranging from 70 to 270 ms. These data suggest double bond configurations as shown in Figure 1.

Amino acid analysis of the total acidic hydrolysate of derivative **1** revealed the absence of amino acids in contrast to derivative **2** for which L-cysteine was found. Taking the amino acid analysis and the results from the FT–ICR–MS together, we conclude that **2** is the *N*-acetyl-L-cysteine adduct of **1**. The linkage to the macrocycle is formed by a thioether to the carbon skeleton, which was further verified by NMR data. The regiochemistry of the *N*-acetyl-L-cysteine adduct of **2** was deduced from the HMBC experiment, as the β-methylene proton H-1″ of cysteine showed a correlation with C-15 of the polyketide backbone. The addition of *N*-acetyl-cysteine to C-15 interrupts the large conjugated π-system of **1**, which is supported by a significant alteration of the UV spectrum of **2** compared with **1**.

Biological activity

1 showed antibacterial activity against the Gram-positive bacteria, *Bacillus subtilis*, *Staphylococcus aureus, S. epidermidis* and *S. lentus* and Gram-negative *Xanthomonas campestris* and also a weak antifungal activity against *Saccharomyces cerevisiae*, *Candida glabrata* and *Botrytis cinerea*. **2** did not show any antimicrobial activity. The minimal inhibitory concentrations of **1** are given in Table 4.

1 showed a remarkable cytostatic activity against various human tumor cell lines (Table 5), whereas **2** showed no growth inhibitory activity up to a concentration of 10 $\mu g\,ml^{-1}$.

Enzyme inhibition tests showed an inhibitory activity of **1** against human recombinant protein tyrosine phosphatase 1B (PTP1B) with an IC_{50} value of 10.1 μM. As a reference, the PTP1B inhibitor RK-682 isolated from *Streptomyces* sp.[14] gave an IC_{50} value of 101.1 μM under the same test conditions.

Table 4 Minimal inhibition concentration of piceamycin (1) against Gram-positive bacteria

Organism	*MIC [$\mu g\,ml^{-1}$]*	*MIC [μM]*
Bacillus subtilis DSM 10	0.43	1.00
Bacillus subtilis DSM 347	0.31	0.72
Staphylococcus aureus DSM 20231	0.14	0.33
Staphylococcus lentus DSM 6672	0.45	1.05
Staphylococcus epidermidis DSM 20044	0.11	0.25

Table 5 Growth inhibitory activity of piceamycin (1) ($\mu g\,ml^{-1}$) against selected human tumor cell lines

Cell line	*GI_{50}*	*TGI*
AGS	0.80	3.4
HepG2	0.30	1.5
MCF 7	0.28	0.7

GI_{50}: 50% growth inhibition; TGI: 100% growth inhibition.

DISCUSSION

A comparison of the 23-membered piceamycin (**1**) with other macrocyclic polyketide compounds revealed a structural relationship to hitachimycin, a 19-membered macrolactam antibiotic with antiprotozoal properties isolated from the culture broth of *Streptomyces scabrisporus*.[15] Hitachimycin was found to be identical with the antitumor antibiotic, stubomycin.[16] The structural differences of **1** and hitachimycin are a methyl group at position 8 replacing a hydrogen atom and a methyl group at position 24 replacing a phenyl ring of hitachimycin. Also, the carbonyl group at C-10 in **1** is replaced by a methoxy group in hitachimycin. Similarly, hitachimycin shows antibacterial and cytostatic activities similar to **1**.

The apparent structural difference between **1** and **2** is the *N*-acetylcysteine moiety covalently attached to the polyketide backbone of **1**. Concomitantly, adduct formation seems to be the reason for the complete absence of the biological activity of adduct **2**. Mechanistically, this finding points to a Michael addition of the nucleophilic thiol group of *N*-acetylcysteine to C-15 of the Michael system (C-13–C-15) as shown in Figure 4. Other cysteine adducts have not been found thus clearly devising C-15 as the most electrophilic position of **1**. Micro-derivatization experiments monitored by HPLC-MS showed that **1** reacts with L-cysteine to give a molecular mass of a cysteine adduct under standard conditions. According to these data, we suggest that the above-mentioned Michael system is the reason for the antibacterial and cytotoxic effects displayed by **1**.

N-acetylcysteine adducts have been reported earlier, although to our knowledge no adduct with a macrocyclic polyketide has been described. Gilpin *et al.*[17] reported on the antibacterial activity of the phenazine antibiotic, SB 212021, which was completely absent in the *N*-acetylcysteine derivative, SB 212305.

Besides the remarkable antibacterial and cytostatic activities, **1** also showed high activity against human recombinant protein tyrosine phosphatase 1B (IC_{50}=10 μM). Small molecule PTP1B inhibitors are of high interest, because of their possible therapeutic application for treatment of diabetes, obesity and cancer.[18]

EXPERIMENTAL SECTION

Producing organism and taxonomy

Strain GB 4-2 was isolated from the mycorrhizosphere of a Norway spruce stand in Schönbuch forest near Tübingen (Germany) on a succinate–malate–citrate–humic acid–agar. The strain was examined for morphological and chemotaxonomic properties known to be of value in streptomycete systematics.[8,9]

Fermentation and isolation

Batch fermentations of strain GB 4-2 were carried out in a 10-l stirred tank fermentor (NB 10; New Brunswick Scientific, Edison, NJ, USA) in a complex medium that consisted of (per liter tap water) oatmeal (Holo Hafergold, Neuform, Germany) 20 g, and trace element solution 5 ml, which was composed of (per liter deionized water) $CaCl_2 \times 2H_2O$ 3 g, iron(III) citrate 1 g, $MnSO_4 \times 1H_2O$ 200 mg, $ZnCl_2$ 100 mg, $CuSO_4 \times 5H_2O$ 25 mg, $Na_2B_4O_7 \times 10H_2O$ 20 mg, $CoCl_2 \times 6H_2O$ 4 mg and $Na_2MoO_4 \times 2H_2O$ 10 mg; the pH was adjusted to 7.3 (5 M HCl) before sterilization. The fermentor was inoculated with 5% by volume of a shake flask culture grown in a seed medium at 27 °C in 500 ml-Erlenmeyer flasks with a single baffle for 72 h in a rotary shaker at 120 r.p.m. The seed medium consisted of glucose 10 g, glycerol 10 g, oatmeal 5 g, soybean meal (Schoenenberger, Magstadt, Germany) 10 g, yeast extract (Ohly Kat, Deutsche Hefewerke, Hamburg, Germany) 5 g, Bacto casamino acids 5 g and $CaCO_3$ 1 g in 1 l tap water. The fermentation was carried out for 4 days with an aeration rate of 0.5 volume air/volume/min and agitation at 250 r.p.m.

For isolation of **1**, the fermentation broth was separated by centrifugation into culture filtrate and mycelium. The culture filtrate (8 l) was adjusted to pH 4 (5 M HCl) and extracted three times with EtOAc. The organic extracts were combined and concentrated *in vacuo* to dryness. The crude product was dissolved in CH_2Cl_2 and added to a diol-modified silica gel column (45×2.6 cm, LiChroprep Diol; Merck, Darmstadt, Germany). The separation was accomplished by a step gradient from CH_2Cl_2 to 5% MeOH. Fractions containing **1** were combined and concentrated *in vacuo* to a small volume, which was purified by Sephadex LH-20 chromatography (column 90×2.5 cm) in the dark using MeOH as the eluent. To obtain pure **1**, the raw product was subjected to a preparative RP-HPLC column (Reprosil-Pur Basic C18, 10 µm, 25×2.0 cm; Maisch, Ammerbuch, Germany) with MeCN–0.1% HCOOH (52:48) at a flow rate of 20 ml min^{-1}.

For isolation of **2**, Hyphlo Super-cel (2%) was added to the fermentation broth, which was separated by multiple sheet filtration into culture filtrate and mycelium. The culture filtrate (8 l) was applied to an Amberlite XAD-16 column (resin volume 800 ml). The resin was washed with 3.2 l H_2O and H_2O–MeOH (8:2), and **2** was eluted with 2.4 l H_2O–MeOH (2:8), concentrated *in vacuo* to an aqueous residue, adjusted to pH 4 and re-extracted three times with EtOAc (each 300 ml). The organic extracts were combined, dissolved in a small volume of MeOH and purified by subsequent chromatography on Sephadex LH-20 and Toyopearl HW-40 (each column 90×2.5 cm) using MeOH as the eluent. To obtain pure **2,** the fractions were separated by preparative RP-HPLC (Nucleosil-100 C-18, 10 µm, 25×1.6 cm; Maisch) with MeCN–0.1% HCOOH using linear gradient elution from 30 to 60% MeCN over 20 min at a flow rate of 20 ml min^{-1}.

HPLC-diode array analyses

The chromatographic system consisted of an HP 1090M liquid chromatograph equipped with a diode-array detector and an HP Kayak XM 600 ChemStation (Agilent Technologies, Waldbronn, Germany). Multiple wavelength monitoring was performed at 210, 230, 260, 280, 310, 360, 435 and 500 nm, and UV-visible spectra were measured from 200 to 600 nm. A 10-ml aliquot of the fermentation broth was centrifuged, and the supernatant was adjusted to pH 4 and extracted with the same volume of EtOAc. After centrifugation, the organic layer was concentrated to dryness *in vacuo* and resuspended in 1 ml MeOH. The corresponding mycelium pellet was extracted with 10 ml MeOH, concentrated to dryness and resuspended in 1 ml MeOH. 10 µl aliquots of the samples were injected onto an HPLC column (125×4.6 mm) fitted with a guard column (20×4.6 mm) filled with 5-µm Nucleosil-100 C-18 (Maisch). The samples were analyzed by linear gradient elution using 0.1% *ortho*-phosphoric acid as solvent A and MeCN as solvent B at a flow rate of 2 ml min^{-1}. The gradient was from 0 to 100% for solvent B in 15 min with a 2-min hold at 100% for solvent B.

Biological activity

The antimicrobial activity spectrum of **1** and **2** was tested in an agar plate diffusion assay and in a microtiter plate assay against *Bacillus subtilis* DSM 347, *Staphylococcus aureus* DSM 20131, *Escherichia coli* K12, *Xanthomonas campestris* DSM 2405, *Saccharomyces cerevisiae* ATCC 9010, *Candida glabrata* DSM 6425 and *Botrytis cinerea* Tü 157 in a concentration of 0.1–1 mg ml^{-1}.

The minimal inhibitory concentration of **1** was tested in a microtiter plate assay using *Bacillus subtilis* DSM 10, *Staphylococcus lentus* DSM 6672, *Staphylococcus epidermidis* DSM 20044 and *Staphylococcus aureus* DSM 20231. The test strains were grown in 96-well microtiter plates with standard concentrations of **1** and incubated for 18–24 h at 27 °C.

The inhibitory activities of **1** and **2** on the growth of tumor cells were tested according to NCI guidelines[19] using human cell lines from gastric adenocarcinoma, breast carcinoma (MCF 7) and hepatocellular carcinoma (HepG2). Cells were grown in 96-well microtiter plates in RPMI-1640 with 10% fetal calf serum in a humidified atmosphere of 5% CO_2 in air. **1** and **2** (0.1–10 µl ml^{-1}) were added to the cells after incubation for 24 h. Stock solutions were prepared in DMSO; the final DMSO concentration of the cultures was 0.1%. The cells were fixed and the cell protein analyzed with sulforhodamine B after 48 h incubation.

The inhibitory activity of **1** against human recombinant PTP1B was tested using the Biomol Green PTP1B tyrosine phosphatase drug discovery kit (cat. no. AK822-0001, Biomol, Hamburg, Germany). The PTP1B concentration in the assay was 150 U per well. Optical density was measured at 620 nm using the microtiter plate reader, Infinite M200 (Tecan, Crailsheim, Germany). As a reference for inhibition of PTP1B, RK-682 (cat. no. 557322-200UG, Calbiochem, Darmstadt, Germany) was used.

Structure elucidation

ESI-MS spectra were obtained on a QTRAP 2000 LC-MS/MS spectrometer (Applied Biosystems, Darmstadt, Germany). High-resolution ESI–FT–ICR mass spectra were recorded on an APEX II FT–ICR mass spectrometer (4.7 T; Bruker-Daltonics, Bremen, Germany), and NMR spectra were recorded on a DRX 500 spectrometer (Bruker, Karlsruhe, Germany) at 500 and 125 MHz for ^{1}H and ^{13}C, respectively. The chemical shifts are given in p.p.m. referred to DMSO-d_6 as 2.50 p.p.m. (^{1}H) and 39.51 (^{13}C).

The micro-derivatization experiment was carried out in an HPLC vial with a 20-fold excess of L-cysteine in MeCN at 25 °C and measured after 72 h on a QTRAP 2000 LC-MS/MS spectrometer (Applied Biosystems).

The composition and configuration of the amino acids of **1** and **2** were determined after hydrolysis in 6 M HCl at 110 °C for 24 h. The dry hydrolysate was derivatized to the *N*-(*O*-)TFA/ethyl esters and analyzed by chiral GC-MS on a 20 m×0.25 mm Lipodex E/PS255 (30:70) capillary column.

ACKNOWLEDGEMENTS

Financial support from the Deutsche Forschungsgemeinschaft (Graduate College 685 'Infection Biology'; DS, JR), the European Commission (project ACTINOGEN, 6th framework, Grant LSHM-CT-2004-005224; RDS), and Bayer Schering Pharma AG (Berlin, Germany) is gratefully acknowledged. We thank Dr Thomas Paululat, Universität Siegen, for helpful discussions and for performing the CIGAR-NMR experiments, and Ms Gaby Biegert, Universität Tübingen, for isolation of streptomycetes strains from rhizospheric soils.

1 Hohmann, C. *et al*. Albidopyrone, a new α-pyrone-containing metabolite from marine-derived *Streptomyces* sp. NTK 227. *J. Antibiot.* **62,** 75–79 (2009).
2 Garbaye, J. Biological interactions in the mycorrhizosphere. *Experientia* **47,** 370–375 (1991).
3 Whipps, J. M. Microbial interactions and biocontrol in the rhizosphere. *J. Exp. Bot.* **52,** 487–511 (2001).
4 Tarkka, M. T. & Hampp, R. Secondary metabolites of soil streptomycetes in biotic interactions. In *Secondary Metabolites in Biotic Interactions in Soil* (ed Karlosvski, P.) pp 107–126 (Springer, Berlin, 2008).

5 Riedlinger, J. *et al.* Auxofuran, a novel metabolite that stimulates the growth of fly agaric, is produced by the mycorrhiza helper bacterium *Streptomyces* AcH 505. *Appl. Environ. Microbiol.* **72,** 3550–3557 (2006).
6 Keller, S., Schneider, K. & Süssmuth, R. D. Structure elucidation of auxofuran, a metabolite involved in stimulating growth of fly acaric, produced by the mycorrhiza helper bacterium *Streptomyces* AcH 505. *J. Antibiot.* **59,** 801–803 (2006).
7 Lehr, N.-A., Schrey, S. D., Hampp, R. & Tarkka, M. T. Root inoculation with a forest soil streptomycete leads to locally and systemically increased resistance against phytopathogens in Norway spruce. *New Phytol.* **177,** 965–976 (2008).
8 Williams, S. T., Goodfellow, M. & Alderson, G. Genus *Streptomyces* Waksman and Henrici 1943, 339^{AL}. In *Bergey's Manual of Systematic Bacteriology* (eds Williams, S.T. *et al*) Vol. 4, pp 2452–3492 (Williams & Wilkins, Baltimore, 1989).
9 Manfio, G. P., Zakrzewska-Czerwinska, J., Atalan, E. & Goodfellow, M. Towards minimal standards for the description of *Streptomyces* species. *Biotekhnologiya* **8,** 228–237 (1995).
10 Fiedler, H.-P. Biosynthetic capacities of actinomycetes. 1. Screening for novel secondary metabolites by HPLC and UV-visible absorbance spectral libraries. *Nat. Prod. Lett.* **2,** 119–128 (1993).
11 Hatsui, T., Nojima, C. & Takeshita, H. Structure elucidation of the pyrolysates formed by 'retro-benzylic acid rearrangement' of the proto-photocycloadducts of methy 2,4-dioxopentanoate-olefins. *Bull. Chem. Soc. Jpn.* **62,** 2932–2938 (1989).
12 Bolvig, S., Duus, F. & Hansen, E. Tautomerism of enolic triacetylmethane, 2-acyl-1,3-cycloalkanediones, 5-acyl meldrum's acid and 5-acyl-1,3-dimethylbarbituric acids studied by means of deuterium isotope effects on ^{13}C chemical shifts. *Magn. Reson. Chem.* **36,** 315–324 (1998).
13 Hadden, C. E., Martin, G. E. & Krishnamurthy, V. V. Constant time inverse-detection gradient accordion rescaled heteronuclear multiple bond correlation spectroscopy: CIGAR-HMBC. *Magn. Reson. Chem.* **38,** 143–147 (2000).
14 Hamaguchi, T., Sudo, T. & Osada, H. RK-682, a potent inhibitor of tyrosine phosphatase, arrested the mammalian cell cycle progression at G1 phase. *FEBS Lett.* **372,** 54–58 (1995).
15 Ômura, S., Nakagawa, A., Shibata, K. & Sano, H. The structure of hitachimycin, a novel macrocyclic lactam involving β-phenylalanine. *Tetrahedron Lett.* **23,** 4713–4716 (1982).
16 Umezawa, I. *et al.* A new antitumor antibiotic, stubomycin. *J. Antibiot.* **34,** 259–265 (1981).
17 Gilpin, M. L., Fulston, M., Payne, D., Cramp, R. & Hood, I. Isolation and structure determination of two novel phenazines from a *Streptomyces* with inhibitory activity against metallo-enzymes, including metallo-β-lactamase. *J. Antibiot.* **48,** 1081–1085 (1995).
18 Van Huijsduijnen, R. H., Bombrun, A. & Swinnen, D. Selecting protein tyrosine phosphatases as drug targets. *Drug Discovery Today* **7,** 1013–1019 (2002).
19 Grever, M. R., Shepartz, S. A. & Chabner, B. A. The National Cancer Institute: cancer drug discovery and development program. *Semin. Oncol.* **19,** 622–638 (1992).

The Journal of Antibiotics (2009) 62, 519–526

www.nature.com/ja

ORIGINAL ARTICLE

Salinisporamycin, a novel metabolite from *Salinispora arenicora*

Satoru Matsuda[1], Kyoko Adachi[1], Yoshihide Matsuo[1], Manabu Nukina[2] and Yoshikazu Shizuri[3]

A new rifamycin antibiotic, salinisporamycin (1), has been isolated from a culture of a marine actinomycete. The producing organism was identified as *Salinispora arenicora* on the basis of the 16S rRNA sequence. High-resolution FAB-MS established the molecular formula of 1 as $C_{33}H_{43}NO_9$. The planar structure of 1 was elucidated by NMR spectral analysis including COSY, heteronuclear single quantum coherence and heteronuclear multiple bond correlation. The relative stereochemistry of 1 was determined on the basis of rotating frame nuclear Overhauser effect spectroscopy. In addition, the solvatochromic behavior of 1 was investigated by measuring the UV spectra. This compound inhibited the growth of A549 cells, the human lung adenocarcinoma cell line, with an IC_{50} value of 3 μg ml^{-1}, and also showed antimicrobial activity.
The Journal of Antibiotics (2009) **62,** 519–526; doi:10.1038/ja.2009.75; published online 7 August 2009

Keywords: antimicrobial; cytotoxic; rifamycin antibiotic; salinisporamycin; *Salinispora arenicora*; YM23-082

INTRODUCTION

It is thought that the exploration of novel natural products in the marine environment is valuable in view of the diversity of marine microbial and metabolic products.[1] Novel marine natural products have been reported on a continuous basis.[2] Therefore, it can be expected that the LC-MS (HPLC/PDA-ESI-MS) system with simulated data of many antibiotics and others may have an important role for identification of many classes of novel marine natural products.[3,4]

Salinispora sp. was identified as the first seawater-requiring marine actinomycete.[1,5] This bacterium includes the potent proteasome inhibitor salinosporamide A, which is under investigation in a phase 1 clinical trial for the treatment of cancer.[1,6,7] The analysis of the *Salinispora tropica* genome revealed the presence of a polyketide synthase system and nonribosomal peptide synthases, with a large percentage of its genome (~10%) devoted to secondary metabolite biosynthesis, which is greater than the *Streptomyces* genome sequence.[1,7]

In this study, we investigated bioactive products from *Salinispora* sp. Results of this screening showed that YM23-082 extracts had strong antitumor and antimicrobial activities among 17 species of *Salinispora*. Therefore, bioactive products were isolated from YM23-082 extracts using LC-MS methods. The results showed hat saliniketals A (**2**)[8,9] and rifamycin S (**3**)[10] were isolated from YM23-082 extracts. In salinisporamycin (**1**), it was expected that the ansa chain partial structure could be assigned as saliniketals[8,9] and connected to the naphthoquinone ring system. **1** and **2** show structural resemblance to the construct of rifamycin antibiotics. Therefore, **1** and **2** would be biosynthetically related products of rifamycin antibiotics. Also, **1** showed moderate cytotoxic activity against A549 and antimicrobial activities. Their structures are shown in Figure 1.

In our study, we elucidated the taxonomy, physicochemical properties, structure and biological activity of salinisporamycin (**1**) from *Salinispora arenicora* YM23-082.

RESULTS AND DISCUSSION

Identification of taxonomy

The strain YM23-082 was isolated from marine sediment collected in the Yap State in the Federated States of Micronesia, N: 9°31′11.0″, E: 138°10′26.7″ and grew at room temperature on a marine agar 2206 (BD Difco, Tokyo, Japan) plate. The culture YM23-082 showed colonies and an orange pigment was produced frequently.[5] The 16S rRNA sequencing of this strain revealed high sequence identity with *S. arenicola* CNH643 (AY040619.2) (100.0%).[5] This strain included **2**, **3**, staurosporine and K-252C[6] (data not shown). On account of this characteristic, the strain YM23-082 was tentatively identified as a member of the *S. arenicora* CNH643.

Physicochemical properties

The physicochemical properties of **1** are summarized in Table 1. **1** was isolated as an amorphous compound ($[\alpha]_D^{24}$ +36.0, *c* 0.7, MeOH). It was soluble in DMSO, MeOH, Me_2CO and $CHCl_3$, poorly soluble in water, and insoluble in n-Hex. **1** was identified as having an R_F value at 0.84 ($CHCl_3$:MeOH=4:1). Analysis of LC-MS spectral data on positive and negative ions revealed the molecular mass to be 597. The molecular formula of **1** was established as $C_{33}H_{43}NO_9$

[1]Bioorganic Chemistry Group, Marine Biotechnology Institute Co. Ltd., Kamaishi, Iwate, Japan; [2]The United Graduate School of Agricultural Sciences, Iwate University (Yamagata University), Tsuruoka, Yamagata, Japan and [3]MBI chair 'Marine Biosciences', Kamaishi Research Laboratory, Kitasato University, Kamaishi, Iwate, Japan
Correspondence: S Matsuda, Bioorganic Chemistry Group, Marine Biotechnology Institute Co. Ltd. 3-75-1 Heita, Kamaishi, Iwate 026-0001, Japan.
E-mail: s-matsuda@amail.plala.or.jp
Received 17 May 2009; revised 9 July 2009; accepted 13 July 2009; published online 7 August 2009

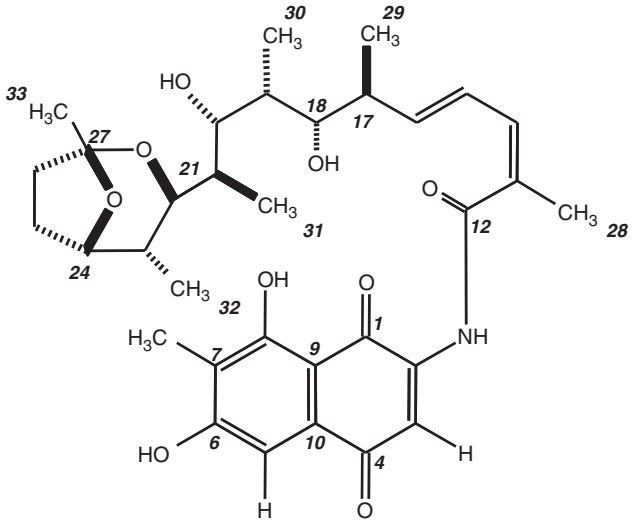

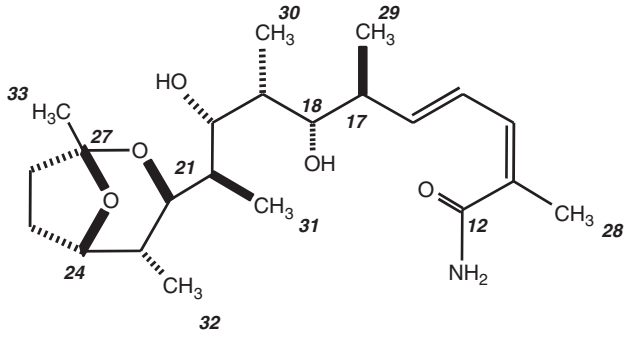

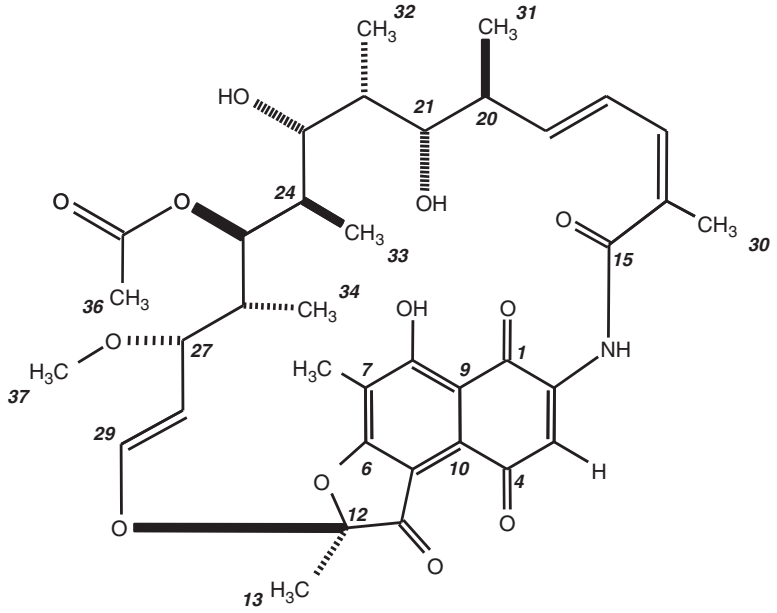

Figure 1 Structures of salinisporamycin (**1**), saliniketal A (**2**) and rifamycin S (**3**).

by high-resolution FAB-MS data ($[M+H]^+$: found, *m/z* 598.3027, calcd for $C_{33}H_{44}NO_9$, *m/z* 598.3011). In addition, the exchangeable protons of **1** were established by hydrogen–deuterium (H–D) exchange mass spectrometry (ESI-IT-MS, profile mode). The H–D exchange signals were found at *m/z* 625.47 $[M+Na]^+$ (calcd for $C_{33}H_{38}D_5NNaO_9$, *m/z* 625.32) with a dimer ion at *m/z* 1227.13 $[2M+Na]^+$, indicating the presence of the intermolecular exchange of 5 hydrogen atoms (data not shown). The UV spectrum of **1** was nearly identical with that of **3** in solvent MeOH. Also, the UV spectrum of **1** showed a short wavelength at 595 nm in the solvent DMSO. The absorption at 595 nm was possibly due to the presence of conjugated double bonds between the naphthoquinone chromophore and the α-, β-, γ- and δ-unsaturated system. However, the imide-amide tautomeric form of **1** could not be distinguished from the NMR spectral data.

Structural elucidation

^1H and ^{13}C NMR spectral data for **1** are summarized in Table 2. All one-bond ^1H-^{13}C connections were confirmed by heteronuclear single quantum coherence (HSQC) correlations. Two methylene signals at δ_c 24.1 (C-25) and 35.4 (C-26) were observed in the DEPT spectrum and HSQC correlations. Also, other carbon signal types were assigned by the DEPT spectrum and HSQC correlations.

The ansa chain partial structure of **1** was confirmed by COSY and heteronuclear multiple bond correlations (HMBCs) in solvent CD_3OD. These results showed a structural resemblance to the ansa chain of rifamycin antibiotics.[10] These assignments are summarized in Figure 2.

The α-, β-, γ- and δ-unsaturated system signals at δ_H 6.46 (1H, br d, 11.3, H-14), 6.79 (1H, dd, 15.0, 10.9, H-15), 6.03 (1H, dd, 15.0, 8.3, H-16), 2.07 (3H, d, 1.1, CH_3-28) and a quaternary sp^2 carbon

Table 1 Physicochemical properties of 1

Appearance	Amorphous
Molecular formula	$C_{33}H_{43}NO_9$
LC-ESI-MS (*m/z*)	598 $[M+H]^+$
	596 $[M-H]^-$
High-resolution FAB-MS (m/z)	
Found	598.3027 $[M+H]^+$
Calcd	598.3011 $[M+H]^+$
$[\alpha]_D$	+36.0 (*c* 0.7, MeOH)
TLC (R_F value)	$CHCl_3$:MeOH (4:1)
(SiO_2, Merck F_{254})	R_F 0.84
UV λ_{max} nm (log ε)	225 (4.66), 272 (4.52), 319 (4.26), 408 (3.83)
in MeOH	
UV λ_{max} nm (log ε)	281 (4.58), 307 (4.49), 320 (4.49), 358 (4.27),
in DMSO	432 (3.73), 595 (3.69)
IR ν_{max} (KBr) cm^{-1}	3399, 2926, 1600, 1496, 1458, 1387, 1327,
	1098, 974

signal at δ_C 129.7 (C-13) were mainly confirmed by $^3J_{HH}$ coupling constants of olefinic protons and HMBC correlations. The $^4J_{HH}$ coupling constant of proton signals at CH_3-28 and H-14 was determined by COSY correlation. In addition, the configuration of C-15/C-16 was assigned as *E* on the basis of the $^3J_{HH}$ coupling constant of H-15/H-16 at 15.0 Hz. This result was supported by the fact that H-14 and CH_3-28 were determined by rotating frame nuclear Overhauser effect spectroscopy (ROESY) correlations (data not shown). Also, the amide bond signals at δ_H 9.14 (1H, br s, 2-NH) and δ_C 167.1 (C-12) were determined by HMBC correlations in solvent DMSO-d_6 (Table 2). This result was supported by assignment of the amide bond as a primary amide on the basis of the molecular formula.

In contrast, for determination of the terminal ansa chain partial structure of **1**, the tetrahydrofuran ring signals at δ_H 4.20 (1H, br dd, 6.8, 3.8, H-24) and the ketal functional group at δ_C 106.6 (C-27) were confirmed by HMBC correlations. Those results were supported by the finding that the IR spectrum showed characteristic absorption bands at 1098 cm^{-1}, indicating the presence of ether bonds in the molecule.

The two exchangeable proton signals at δ_H 4.57 (1H, m, 18-OH) and 4.64 (1H, m, 20-OH) were mainly determined by COSY correlations in solvent DMSO-d_6. In support of these results, exchangeable proton signals were observed in the pre-saturation spectrum in solvent DMSO-d_6, decreasing the integral intensity of the peak area. Also, the IR spectrum showed characteristic absorption bands at 3399 cm^{-1} (3431 cm^{-1} of **3**), indicating the presence of a hydroxyl group in the molecule. Consequently, these results showed a structural resemblance to the saliniketals.[8,9]

In the detailed analysis, the chemical shifts in the ansa chain of **1** were compared with values in the literature reported for saliniketal A[8] (Table 2). The chemical shifts revealed that **1** was nearly identical with the spectra of saliniketal A. In addition, the chiral centers of C-17/C-18, C-18/C-19, C-19/C-20, C-20/C-21, C-21/C-22 and C-22/C-23 were mainly determined by the $^3J_{HH}$ coupling constants, COSY and ROESY correlations (Figure 3, Table 2). These results revealed that $^3J_{HH}$ coupling constants of **1** were almost identical with the literature values reported for saliniketal A[8] and the recorded NMR spectra of **2**. The COSY correlation in the ansa chain partial structure signals at δ_H 3.62 (1H, m, 7.5, H-18) and 1.71 (1H, m, H-19) were not observed in solvent DMSO-d_6, because the torsion angle between H-18/H-19 is close to 90°[11] (Figure 3).

The bicyclic ring structure signals at δ_H 1.93 (1H, m, H-25a), 2.02 (1H, m, H-26a) and 3.94 (1H, br d, 10.5, 1.5, H-22) were determined by ROESY correlations (Figure 4). This result was supported by stereochemical assignments in a bicyclic ring structure that a diaxial arrangement signals at δ_H 3.82 (1H, br d, 10.5, 0.9, H-22) and 1.84 (1H, br dq, 10.5, 6.8, 3.8, H-23), and was confirmed by a large coupling constant at 10.5 Hz (Figures 3 and 4). Consequently, the ansa chain of **1** was established to be the same as saliniketal.[8,9]

The naphthoquinone ring system of **1** was mainly confirmed by the ^{13}C NMR spectral data and HMBC correlations (Figure 2, Table 3). With the help of a detailed analysis, the quaternary carbon signal at δ_C 164.5 (C-6) and other carbon signals were nearly identical with values reported in the literature for 31-homorifamycin W.[12] The two quaternary carbon signals at δ_c 181.3 (br, C-1) and 172.0 (br, C-8) gave broad peak signals possibly due to tautomerization (Table 3). These results were supported by the finding that the IR and UV spectra showed characteristic absorption bands at 1496 cm^{-1} (1465 cm^{-1} of **3**) and wavelengths at 319 and 408 nm (315 and 410 nm of **3**), indicating the presence of a chromophoric system in the naphthoquinone form.[10,12] In addition, the IR spectrum showed a characteristic absorption band at 1600 cm^{-1} (1606 cm^{-1} of **3**), indicating the presence of a naphthoquinone carbonyl group linked in the intramolecular hydrogen bond.[12]

The naphthoquinone ring system of **1** was established by the ^{13}C NMR spectral data and HMBC correlations in solvent DMSO-d_6 (Table 3, Figure 5). With the help of a detailed analysis, the naphthoquinone ring system of **1** had chemical shifts comparable to the literature values reported for rifamycin Z.[13] This result revealed that the ^{13}C NMR signals at δ_C 170.3 (C-1, diff. (−11.5 p.p.m.)) and δ_C 180.4 (br, C-6, diff. (+20.4 p.p.m.)) could not be distinguished from the spectra of rifamycin Z. Therefore, the quaternary carbon signal at C-6 was assigned as a carbonyl carbon on the basis of its chemical shift. Intriguingly, the two quaternary carbon signals at δ_c 180.4 (br, C-6) and 162.1 (br, C-8) gave broad peak signals possibly due to tautomerization. The enolic proton signal at δ_H 12.55 (1H, br s, 8-OH) was confirmed by HMBC correlations in solvent DMSO-d_6. These results were supported from the assignment of ^1H-^{13}C connections made by HSQC correlations in solvent DMSO-d_6. Consequently, these results showed the isomerization of the naphthoquinone ring system of **1** by different solvents. However, the enolic proton signal (1-OH) was not determined by the ^1H NMR spectral data (Table 3). Finally, the amide bond between the ansa chain and the naphthoquinone ring system signals at δ_H 9.14 (1H, br s, 2-NH) and δ_C 111.7 (C-3) were determined by HMBC correlations in solvent DMSO-d_6. These results were supported by the finding by H–D exchange mass spectrometry that showed the characteristic intermolecular exchange of five hydrogen atoms.

Biological activity

Compound **1** showed moderate cytotoxic activity against A549 cells with an IC_{50} value of 3 μg ml^{-1}. Compound **3** did not show cytotoxic activity against A549 cells at 200 μg ml^{-1}.[10,12,14] Among all rifamycin antibiotics, **1** showed cytotoxic activity.[14]

The antimicrobial activity of **1** was tested against six microorganisms by paper disk methods. This compound showed moderate activity against two microorganisms (Table 4). The antimicrobial activity of **1** was shown to be weaker than that of **3**. The sensitivity of bacteria to **1** seems to be inhibited by the presence of hydroxyl groups (1, 8, 18, 20-OH) (Figures 1 and 5). An earlier study found that the high sensitivity of bacteria to **3** was promoted by four hydrogen bond interactions between four free hydroxyl groups (1, 8,

Table 2 750 MHz ^{1}H and 125 MHz ^{13}C NMR data on 1, 2 and 3

	DMSO-d_6										*CD_3OD*					
	1				***2***			***3***			***1***			***Saliniketal a***[a]		
Position	δ_C	δ_H	*Multi, J (Hz)*	*HMBC*	δ_H	*Multi, J (Hz)*	*Position*	δ_H	*Multi, J (Hz)*	*Position*	δ_C	δ_H	*Multi, J (Hz)*	δ_C	δ_H	*Multi, J (Hz)*
1	170.3									1	181.3 (br)					
2	143.1									2	143.2					
2-NH		9.14	(br s)	C-1, C-3, C-12	7.21	(br s)	15-NH	9.41	(br s)							
					7.03	(br s)										
3	111.7	7.18	(s)	C-1, C-2, C-10			3	7.29	(s)	3	116.4	7.55	(s)			
4	186.7									4	187.9					
5	117.7	6.32	(s)	C-4, C-7, C-9						5	112.7	6.96	(s)			
6	180.4 (br)[b]									6	164.5					
7	112.2									7	117.8					
8	162.1 (br)									8	172.0					
8-OH		12.55	(br s)	C-7, C-8, C-9												
9	100.6									9	106.6					
10	131.1									10	132.5					
11	7.9	1.75	(s)	C-6, C-7, C-8			13	1.61	(s)	11	8.2	2.06	(s)			
12	167.1									12	170.1			175.1		
13	127.1									13	129.7			131.4		
14	137.7	6.43	(br d, 11.3)	C-12, C-16, C-28	6.02	(br d, 11.3)	17	6.20	(dd, 10.5, 1.5)	14	138.6	6.46	(br d, 11.3)	134.1	6.17	(br d, 11.1, 1.2)
15	125.3	6.78	(dd, 15.0, 12.0)	C-17	6.57	(dd, 15.0, 11.3)	18	6.12	(dd, 15.8, 10.5)	15	127.6	6.79	(dd, 15.0, 10.9)	128.3	6.60	(dd, 15.3, 11.1)
16	145.7	6.07	(dd, 15.0, 7.5)	C-14, C-29	5.76	(dd, 15.0, 8.3)	19	5.88	(dd, 15.8, 7.5)	16	146.0	6.03	(dd, 15.0, 8.3)	142.0	5.78	(dd, 15.3, 8.4)
17	40.4	2.31	(m, 8.3, 7.5, 6.8)	C-15, C-16, C-18, C-29	2.22	(m, 7.5)	20	2.10	(m)	17	42.4	2.43	(m, 8.3, 7.5)	42.3	2.35	(m, 9.3, 8.4, 6.8)
18	73.3	3.62	(m, 7.5)		3.57	(m, 9.0)	21	3.57	(m)	18	75.8	3.78	(dd, 9.8, 1.9)	75.8	3.71	(dd, 9.3, 1.8)
18-OH		4.57	(m)		4.52	(br s)	21-OH	4.38	(m)							
19	34.3	1.71	(m)	C-20	1.73	(m)	22	1.61	(m)	19	36.4	1.83	(m, 6.8, 4.5, 1.9)	35.7	1.88	(m, 7.4, 4.9, 1.8)
20	75.6	3.33[c]	(m, 8.3, 3.8, 3.0)		3.33[c]	(m)	23	ND[d]		20	78.4	3.50	(dd, 8.3, 4.5)	78.2	3.52	(dd, 8.3, 4.9)
20-OH		4.64	(m)	C-19, C-20, C-21	4.67	(br s)	23-OH	4.38	(m)							
21	35.7	1.69	(m, 0.9)	C-31	1.69	(m, 6.8)	24	1.48	(m)	21	37.1	1.82	(br dq, 8.3, 6.8, 1.5)	37.1	1.84	(br dq, 8.3, 7.2, 1.4)
22	72.8	3.82	(br d, 10.5, 0.9)	C-20, C-21, C-31	3.83	(br d, 10.5)	25	5.01	(m)	22	75.2	3.94	(br d, 10.5, 1.5)	74.9	3.97	(br d, 10.8, 1.4)
23	33.4	1.84	(br dq, 10.5, 6.8, 3.8)		1.85	(m, 3.8)	26	1.32	(m)	23	35.3	1.97	(br dq, 10.5, 6.8, 3.8)	35.2	2.00	(br dq, 10.8, 7.3, 3.4)
24	79.1	4.14	(br dd, 6.8, 3.8)		4.15	(br dd, 6.8, 3.8)	27	ND[d]		24	81.8	4.20	(br dd, 6.8, 3.8)	81.6	4.23	(br dd, 6.3, 3.4)
25a	23.6	1.81	(m)		1.83	(m)	28	5.09	(br dd, 9.0)	25a	24.1	1.93	(m)	24.9	1.90	(m)
25b		1.77	(m)		1.76	(m)	29	6.11	(d, 12.8)	25b		1.88	(m)		1.94	(m)
26a	33.9	1.92	(m)		1.92	(m)				26a	35.4	2.02	(m)	35.1	2.05	(m)
26b		1.69	(m)		1.71	(m)				26b		1.80	(m)		1.80	(m)
27	104.2									27	106.6			106.4		
28	20.1	2.03	(br s)	C-12, C-13, C-14	1.86	(br s)	30	2.01	(br s)	28	20.7	2.07	(d, 1.1)	20.9	1.94	(d, 1.2)
29	16.2	0.90	(d, 6.8)	C-16, C-17, C-18	0.87	(d, 7.5)	31	0.84	(d, 7.5)	29	17.1	0.99	(d, 6.8)	17.1	0.96	(d, 6.8)

Table 2 Continued

	DMSO-d_6										*CD_3OD*					
	1				***2***			***3***			***1***			***Saliniketal a***[a]		
Position	δ_C	δ_H	*Multi, J (Hz)*	*HMBC*	δ_H	*Multi, J (Hz)*	*Position*	δ_H	*Multi, J (Hz)*	*Position*	δ_C	δ_H	*Multi, J (Hz)*	δ_C	δ_H	*Multi, J (Hz)*
30	11.1	0.91	(d, 6.8)	C-19, C-20	0.92	(d, 6.8)	32	0.86	(d, 6.8)	30	11.3	1.00	(d, 6.8)	11.1	1.02	(d, 7.3)
31	9.8	0.76	(d, 6.8)	C-20, C-21, C-22	0.75	(d, 6.8)	33	0.56	(d, 6.8)	31	10.5	0.88	(d, 6.8)	10.2	0.89	(d, 7.2)
32	12.4	0.64	(d, 6.8)	C-22, C-23, C-24	0.65	(d, 6.8)	34	0.15	(d, 6.8)	32	13.0	0.71	(d, 6.8)	12.3	0.76	(d, 7.3)
33	24.0	1.31	(s)	C-26, C-27	1.31	(s)				33	24.4	1.39	(s)	24.2	1.39	(s)
							36	1.92	(s)							
							37	2.97	(s)							
							14	1.96	(s)							

[a]Data adapted from Williams *et al.*[8]
[b]Broad peak signal.
[c]^{1}H NMR observed at 40 °C.
[d]Overrapped H_2O.

21, 23-OH) and DNA-dependent RNA polymerase.[14] Compound **2** was also found to show no significant antimicrobial activity.[8]

METHODS

Spectroscopic measurements

Optical rotations were obtained on a Horiba SEPA-300 digital polarimeter (Horiba, Kyoto, Japan). The UV spectrum pattern was measured on a Beckman DU 640 spectrometer (Beckman Coulter, Tokyo, Japan) and the IR spectrum was measured with a Jasco FT/IR-430 instrument (Jasco, Tokyo, Japan). The ^{1}H and all 2D NMR spectra (COSY (gradient-selected ^{1}H–^{1}H COSY), HSQC (gradient-selected HSQC), HMBC (gradient-selected HMBC), and ROESY) were recorded with a Varian Unity INOVA 750 instrument (Varian, Tokyo, Japan) at 750 MHz. The ^{13}C NMR spectrum was recorded on a Varian Unity INOVA 500 instrument at 125 MHz. Chemical shifts were referenced to the solvent peaks of δ_H 3.31 and δ_C 49.15 for CD_3OD and δ_H 2.49 and δ_C 39.5 for DMSO-d_6. High-resolution FAB-MS data were obtained on a Jeol JMS 700 spectrometer. LC-MS spectra were measured with a Thermo Fisher Scientific K.K. LCQ-Advantage instrument (Thermo Fisher Scientific K.K., Yokohama, Japan).

Taxonomy

The 16S rRNA gene has been identified using degenerate PCR and sequencing methods.[15] The 16S rRNA gene sequence was compared with bacterial sequence data stored in the DDBJ database by using the BLAST algorithm.[16]

Fermentation

The medium consisted of Bacto peptone (BD Difco) 5 g, yeast extract 1 g, iron (III) citrate 0.1 g, distilled water 250 ml and sea water 750 ml (pH 7.6). A 1.0 l Erlenmeyer flask containing 500 ml of medium was incubated first with a stock culture of YM23-082 and then on a rotary shaker at 30 °C for 3 days. The 5 ml samples of the seed culture were then placed in 1.0 l Erlenmeyer flasks containing 500 ml of a production medium consisting of Pharmamedia (Traders protein) 20 g, yeast extract 1 g, iron (III) citrate 0.1 g, distilled water 250 ml and sea water 750 ml (pH 7.6). Fermentation took place on a rotary shaker at 30 °C for 7 days.

LC-MS methods

All samples were analyzed by HPLC/PDA with a linear gradient from 10 to 100% CH_3CN at intervals of 1 min. The LC-MS was conducted on an Inertsil ODS-2 column (GL Sciences, Tokyo, Japan) (1.5 mm i.d. ×250 mm). The HPLC fractions were eluted at a rate of 0.1 ml min^{-1} with solvent A consisting of 0.1% formic acid/solvent B consisting of 0.1% formic acid in CH_3CN (80:20) for 5 min, followed by a linear gradient from solvent A to B for 45 min, solvent B alone for 60 min and then back to the initial solvents. The column oven temperature was set at 40 °C. The PDA (photodiode array detector) was monitored at 220–800 nm. Ionization of ESI was optimized by human angiotensin II (Sigma, Tokyo, Japan). The total ion chromatogram was alternately monitored at positive and negative ions in the mass range of *m/z* 150.0–2000.0. The capillary temperature was set at 220 °C, spray voltage was optimized to 5.2 kV and the sheath nitrogen gas flow was set at 28 arbitrary units (arb). The LC-MS spectral data were compared with those in the in-house database, NCBI database (http://pubchem.ncbi.nlm.nih.gov/) and literature values for *Salinispora* sp. metabolites.[1,6,7,17]

Extraction and isolation

The YM23-082 fermentation broth (10.0 l) was centrifuged and the mycelium extracted with MeOH, and the supernatant was then extracted with 2 times EtOAc. The combined extract was passed through filter paper (Advantec Co. Ltd., Ehime, Japan) and evaporated. Then, the extract was partitioned between EtOAc and saturated NaCl. After that, the EtOAc layer was dried with anhydrous Na_2SO_4 and evaporated. Furthermore, the EtOAc layer was partitioned between n-Hex and 90% water MeOH. The anti-A549 active 90% water MeOH layer was evaporated and chromatographed on a silica gel column with $CHCl_3$, MeOH and water. The anti-A549 eluates, $CHCl_3$/MeOH (98:2), $CHCl_3$/MeOH (97:3), $CHCl_3$/MeOH (96:4) and $CHCl_3$/MeOH (95:5), were subjected to LC-MS methods.

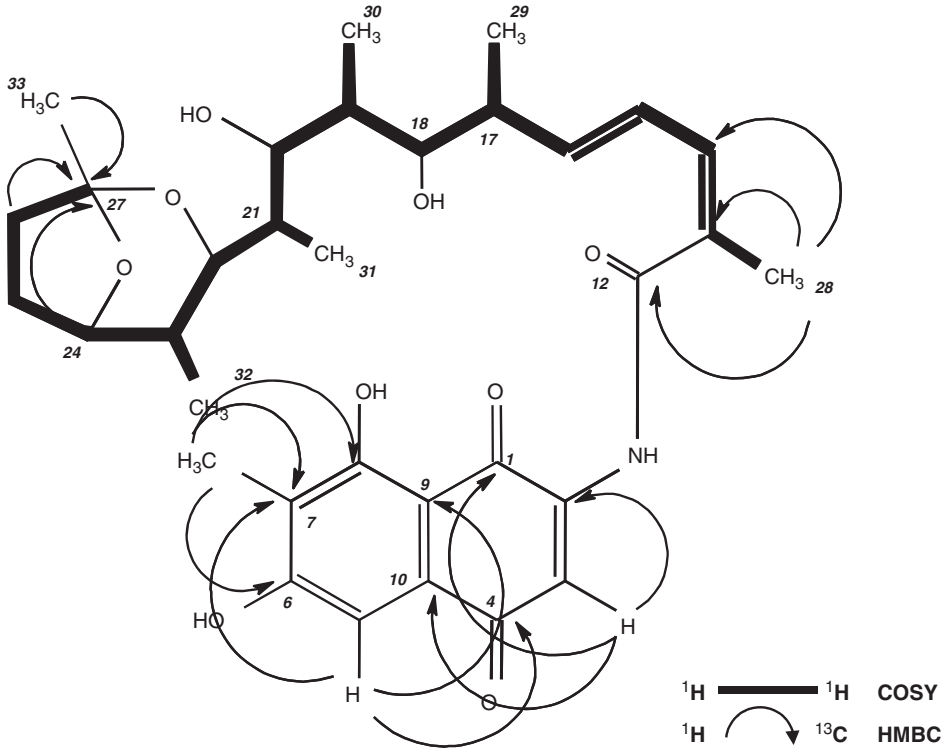

Figure 2 2D NMR spectral data in solvent CD_3OD.

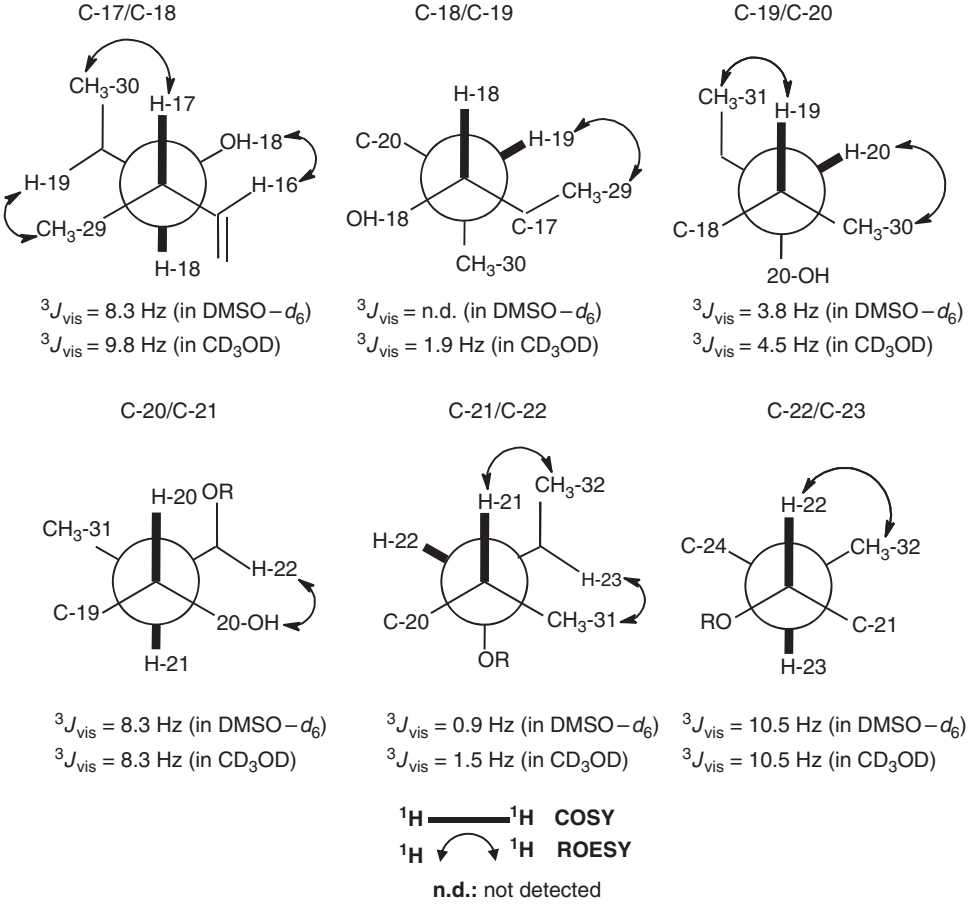

Figure 3 Data on ROESY correlations, and coupling constants and partial structures of **1**.

Salinisporamycin (1)

The UV spectrum pattern of **1** was nearly identical with the spectrum of rifamycin antibiotics.[10] However, the MW was not the same in this experiment as in the databases mentioned above. Therefore, the silica gel chromatographed eluates were separated by HPLC (Inertsil ODS-2 column, 4.6 mm i.d. ×250 mm) with a linear gradient from 10 to 100% CH_3CN to afford **1** (0.6 mg). Compound **1** LC-MS: RT, 38.4 min; PDA, 240, 270, 326, 409 nm; MS, *m/z* 598 $[M+H]^+$, *m/z* 596 $[M-H]^-$.

Saliniketal A (2)

The silica gel chromatographed eluates were separated by HPLC (Inertsil ODS-2 column, 4.6 mm i.d. ×250 mm) with isocratic elution of 30% CH_3CN to afford **2**[8,9] (2.6 mg). Compound **2** LC-MS: RT, 25.1 min; PDA, 252 nm; MS, *m/z* 396 $[M+H]^+$, n.d. $[M-H]^-$; 750 MHz, DMSO-d_6: Table 2. The chemical shifts revealed that **2** was identical with the values reported in the literature for saliniketal A.[8]

Rifamycin S (3)

The silica gel chromatographed eluates were separated by HPLC (Inertsil ODS-2 column, 4.6 mm i.d. ×250 mm) with a linear gradient from 20 to 100% CH_3CN to afford **3**[10] (4.6 mg). Compound **3** LC-MS: RT; 37.5 min, PDA; 239, 276, 334, 409 nm, MS; *m/z* 696 $[M+H]^+$, *m/z* 694 $[M-H]^-$; TLC: R_F value at 0.87 ($CHCl_3$:MeOH=4:1); UV λ_{max} nm (log ε) in MeOH: 228 (4.86), 271 (4.71), 315 (4.43), 410 (3.93); IR ν_{max} (KBr) cm^{-1}: 3431, 2926, 2854, 1710, 1606, 1465, 1415, 1384, 1354, 1259, 1164, 1074, 976; 750 MHz, DMSO-d_6:

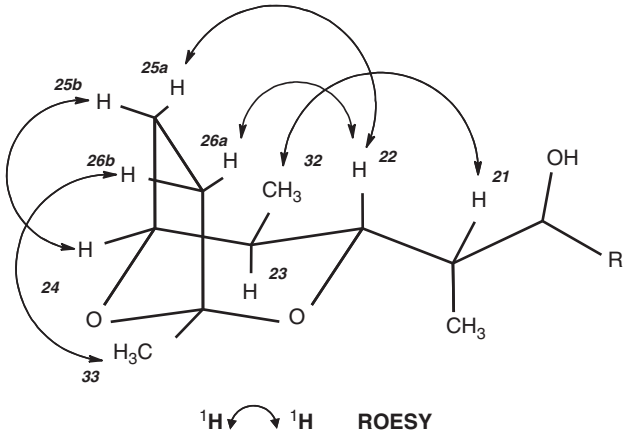

Figure 4 ROESY correlations and partial structure of **1**.

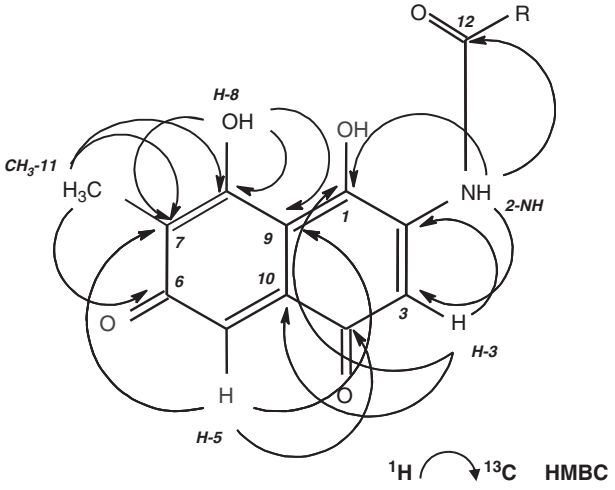

Figure 5 Heteronuclear multiple bond correlations and naphthoquinone ring system of **1** in solvent DMSO-d_6.

Table 3 750 MHz ^1H and 125 MHz ^{13}C NMR data of naphthoquinone ring system of 1, 31-homo rifamycin W and rifamycin Z

	CD_3OD					*DMSO-d_6*				
	1		***31-Homo rifamycin W***[a]			***1***		***Rifamycin Z***[b]		
Position	δ_C	δ_H	δ_C	δ_H	*Diff. (p.p.m.)*[c]	δ_C	δ_H	δ_C	δ_H[d]	*Diff. (p.p.m.)*
1	181.3 (br)[e]		182.3		−1.0	170.3		181.8		−11.5
1-OH		—		—			ND		—	
2	143.2		142.7		0.5	143.1		140.4		2.7
2-NH		—		—			9.14		8.90 (ND)	
3	116.4	7.55	117.6	7.52	−1.2	111.7	7.18	114.2	7.30 (7.70)	−2.5
4	187.9		187.3		0.6	186.7		184.0		2.7
5[f]	112.7	6.96	127.1	—	—	117.7	6.32	123.5	—	—
6	164.5		164.2		0.3	180.4 (br)		160.0		20.4
6-OH		—	—				—		10.50 (7.70)	
7	117.8		118.7		−0.9	112.2		117.6		−5.4
8	172.0 (br)		166.5		5.5	162.1 (br)		162.1		0.0
8-OH		—		—			12.55		12.70 (9.40)	
9	106.6		106.7		−0.1	100.6		106.5		−5.9
10	132.5		129.7		2.8	131.1		127.7		3.4
11	8.2	2.06	8.5	2.12	−0.3	7.9	1.75	8.7	2.15 (1.62)	−0.8
12	170.1		172.0		−1.9	167.1		171.6		−4.5

Abbreviation: ND, not detected.
[a]Data adapted from Wang *et al.*[12]
[b]Data adapted from Cricchio *et al.*[13]
[c]Diff. (p.p.m.)=obs. [δ_C]−ref. [δ_C].
[d]In solvent DMSO-d_6/acetone-d_6 (7:3) (Pyridine-d_5).
[e]Broad peak signal.
[f]C-6 of rifamycin Z and 31-homo rifamycin W were assigned as diagnostic of quaternary carbon signal.

Table 4 Antimicrobial activity properties of 1, 2 and 3

Taxin	*Strain*	***1***	***2***	***3***
Firmicutes	*Staphylococcus aureus* IFO 12732	0.46	37	0.0056
Firmicutes	*Bacillus subtilis* IFO 3134	4.1	111	1.4
Bacteroidetes	*Cytophaga marinoflava* IFO 14170	>200	>200	12.3
Gammaproteobacteria	*Escherichia coli* IFO 3301	>200	>200	>200
Gammaproteobacteria	*Pseudomonas aeruginosa* IF03446	>200	>200	>200
Yeast	*Candida albicans* IFO 1060	>200	>200	>200

Antimicrobial activity (MIC, $\mu g\,ml^{-1}$).

Table 2. **3** was established by 2D NMR, and the chemical shifts showed that **3** was nearly identical with the values reported in the literature for proansamycin B,[10] 8-deoxy-rifamycin[18] and 31-homorifamycin W.[12]

Cytotoxic and antibacterial activity

A549 cells were cultured in Dulbecco's modified Eagle's medium containing 10% fetal bovine serum. The cells were seeded in a flat-bottomed 96-well microplate (4000 cells per 200 µl per well), and then cultured for 14 h at 37 °C in a CO_2 incubator (5% CO_2-air). Serially diluted **1** was added to each well, and the cells were further cultured for 48 h. The number of cells was counted by Alamar Blue assay.[19] The MIC of **1**, **2** and **3** were analyzed by paper disk methods.[20]

ACKNOWLEDGEMENTS

We thank Professor Ryuichi Sakai of the Faculty Department at Kitasato University for the high-resolution FAB-MS measurements. We are also grateful for the technical assistance of Ms Kumiko Kawahata, Ms Thie Ohshima and Ms Tomoe Sasaki. This work was performed as part of the project entitled 'Construction of a Genetic Resource Library of Unidentified Microorganisms' supported by the New Energy and Industrial Technology Development Organization (NEDO).

1 Bull, A. T. & Stach, J. E. M. Marine actinobacteria: new opportunities for natural product search and discovery. *Trends Microbiol.* **15,** 491–499 (2007).
2 Blunt, J. W. *et al.* Marine natural products. *Nat. Prod. Rep.* **25,** 35–94 (2008).
3 Smyth, W. F. & Rodriguez, V. Recent studies of the electrospray ionization behaviour of selected drugs and their application in capillary electrophoresis–mass spectrometry and liquid chromatography-mass spectrometry. *J. Chromatogr. A* **1159,** 159–174 (2007).
4 Corcia, A. D. & Nazzari, M. Liquid chromatographic–mass spectrometric methods for analyzing antibiotic and antibacterial agents in animal food products. *J. Chromatogr. A* **974,** 53–89 (2002).
5 Maldonado, L. A. *et al. Salinispora arenicola* gen. nov., sp. nov. and *Salinispora tropica* sp. nov., obligate marine actinomycetes belonging to the family *Micromonosporaceae*. *Int. J. Syst. Evol. Microbiol.* **55,** 1759–1766 (2005).
6 Jensen, P. R., Williams, P. G., Oh, D. C., Zeigler, L. & Fenical, W. Species-specific secondary metabolite production in marine actinomycetes of the genus *Salinisporara*. *Appl. Environ. Microbiol.* **73,** 1146–1152 (2007).
7 Udwary, D. W. *et al.* Genome sequencing reveals complex secondary metabolome in the marine actinomycete *Salinispora tropica*. *Proc. Natl Acad. Sci. USA* **104,** 10376–10381 (2007).
8 Williams, P. G. *et al.* Saliniketals A and B, Bicyclic Polyketides from the Marine Actinomycete *Salinispora arenicola*. *J. Nat. Prod.* **70,** 83–88 (2007).
9 Paterson, I., Razzak, M. & Anderson, E. A. Total synthesis of (–)-Saliniketals A and B. *Org. Lett.* **10,** 3295–3298 (2008).
10 Stratmann, A. *et al.* New insights into Rifamycin B biosynthesis: isolation of Proansamycin B and 34a-Deoxy-rifamycin W as early macrocyclic intermediates indicating two separated biosynthetic pathways. *J. Antibiot.* **55,** 396–406 (2002).
11 Hoch, J. C., Dobson, C. M. & Karplus, M. Vicinal coupling constants and protein dynamics. *Biochemistry* **24,** 3831–3841 (1985).
12 Wang, N. J., Han, B. L., Yamashita, N. & Sato, M. 31-homorifamycin W, a novel metabolite from *Amycolatopsis mediterranei*. *J. Antibiot.* **47,** 613–615 (1994).
13 Cricchio, R. *et al.* Rifamycin Z, a novel ansamycin from a mutant of *Nocardia Mediterranea*. *J. Antibiot.* **34,** 1257–1260 (1981).
14 Floss, H. G. & Yu, T. W. Rifamycin–mode of action, resistance, and biosynthesis. *Chem. Rev.* **105,** 621–632 (2005).
15 Hayakawa, Y. *et al.* Piericidins C_7 and C_8, new cytotoxic antibiotics produced by a marine *Streptomyces* sp. *J. Antibiot.* **60,** 196–200 (2007).
16 Altsuchul, S. F., Gish, W., Miller, W., Myers, E. W. & Lipman, D. J. Basic local alignment search tool. *J. Mol. Biol.* **215,** 403–410 (1990).
17 Hewavitharana, A. K., Shaw, P. N., Kim, T. K. & Fuerst, J. A. Screening of rifamycin producing marine sponge bacteria by LC–MS–MS. *J. Chromatogr. B* **852,** 362–366 (2007).
18 Ghisalaba, O, Traxer, P, Fuhrer, H & Richer, W. J Early intermediates in the biosynthesis of Ansamycins III and identification of further 8-deoxyansamycins of the rifamycin type. *J. Antibot.* **33,** 847–856 (1980).
19 Matsuo, Y. *et al.* Urukthapelstatin A, a novel cytotoxic substance from marine--derived *Mechercharimyces asporophorigenens* YM11-542 I. fermentation, isolation and biological activities. *J. Antibiot.* **60,** 251–255 (2007).
20 Jang, J. H., Kanoh, K., Adachi, K. & Shizuri, Y. New dihydrobenzofuran derivative, Awajanoran, from marine-derived *Acremonium* sp. AWA16-1. *J. Antibiot.* **59,** 428–431 (2006).

The Journal of Antibiotics (2009) 62, 527–529

www.nature.com/ja

NOTE

Two new members of mycophenolic acid family from *Penicillium brevicompactum* Dierckx

Xinhua Lu[1,2], Zhihui Zheng[2], Hua Zhang[2], Changhong Huo[1], Yuesheng Dong[2], Ying Ma[2], Xiao Ren[2], Aibing Ke[2], Jiangong He[2], Yucheng Gu[1,3] and Qingwen Shi[1]

The Journal of Antibiotics (2009) **62,** 527–529; doi:10.1038/ja.2009.54; published online 3 July 2009

Keywords: IMPDH inhibitor; mycophenolic acid; mycophenolic derivatives

Inosine-5′-monophosphate dehydrogenase (IMPDH; EC 1.1.1.205) is an essential rate-limiting enzyme in the purine metabolic pathway, catalyzing NAD-dependent oxidation of inosine-5′-monophosphate (IMP) to xanthosine-5′-monophosphate (XMP) of the *de novo* synthesis of guanine nucleotides.[1] The activity of IMPDH is correlated with the growth of cells, and IMPDH has become one of the important targets of antiviral, antimicrobial, anti-cancer and immunosuppressive therapy drugs.[2] Several classes of IMPDH inhibitors are now in clinical use or are under development.[3–7] However, some of them suffer from a certain degree of toxicity and/or susceptibility to metabolic inactivation.[8]

In the program of searching for IMPDH inhibitors, the culture broth of a fungal strain *Penicillium brevicompactum* F01-1358 showed a strong inhibitory activity against IMPDH. Bioassay-guided fractionation of the crude extract of F01-1358 resulted in the isolation of two new mycophenolic compounds, F01-1358A (**2**) and B (**3**) (Figure 1), as well as mycophenolic acid (MPA) (**1**). In this study, we report the fermentation, isolation, structure elucidation and preliminary IMPDH inhibitory activity of compounds **2** and **3**.

Fungus F01-1358 was isolated from a soil sample collected in the Jiangjin district of Chongqing, China. The strain was identified as *P. brevicompactum* Dierckx by morphological and cultural characteristics, and was deposited in the China General Microbiological Culture Collection (accession number: CGMCC No. 2038).

The strain F01-1358 was cultivated at 27 °C on a rotary shaker at 220 r.p.m. in the medium consisting of 1.0% starch, 2.0% glucose, 0.8% malt extracts, 0.4% yeast extracts, 0.3% bean powder, 0.13% NaCl and 0.15% $CaCO_3$ (pH 7.0 before sterilization). The 5-day-old whole broth (5.0 l) was adjusted to pH of 3.0–3.5 by 2.0 N HCl and centrifuged at 3000 r.p.m. for 15 min. The mycelia were extracted with 75% acetone. After the insoluble mycelia were removed by centrifugation, the acetone was evaporated under normal pressure, the remaining aqueous solution was extracted with ethyl acetate and the organic layer was dried over Na_2SO_4 and concentrated under reduced pressure to yield a brown residue (8.0 g). The residue was subjected to a silica gel flash column chromatography and eluted with gradient of chloroform–methanol from 100:1 to 10:1. The fractions showing an inhibitory activity against IMPDH were collected and concentrated to yield a pale yellow solid. A white crystal (4.8 g, compound **1**) was obtained by recrystallization in isopropanol. Further purification of the mother solution was carried out on a preparative reverse phase (RP)-HPLC (detection: UV at 250 nm; column: Phenomenex (Torrance, CA, USA) C_{18}, 10 μm, 21.2×250 mm; mobile phase: 70% CH_3CN–water with 0.1% acetic acid; flow rate: 16.0 ml min^{-1}) and yielded **2** (23.0 mg) and a fraction (16.0 mg) containing compound **3**. Pure compound **3** (4.0 mg) was obtained by another run of preparative RP-HPLC with a mobile phase of 65% CH_3CN–water with 0.1% acetic acid.

Compound **1**, a white crystal with UV λ_{max} (MeOH) 249 and 304 nm, was identified as MPA (**1**) (Figure 1) by the analysis of its spectral data (electrospray ionization (ESI)-MS, ^{1}H- and ^{13}C-NMR) and by comparing them with that reported in the literature.[9]

F01-1358A (**2**) was obtained as a white crystalline powder with a molecular formula $C_{20}H_{26}O_6$ (high resolution fast atom bombardment mass spectra (HRFABMS) *m/z* 363.1808, $M+H^+$, calcd for 363.1808, Δ0.0 mmu error). The IR (KBr) spectrum suggested that **2** had a hydroxyl group (3423 cm^{-1}), two carbonyl groups (1734 and 1705 cm^{-1}) and an isolated alkenyl group (1622 cm^{-1}). The ^{1}H-NMR spectrum of **2** showed signals for a secondary aliphatic methyl group at δ 0.98 (3H, d, J=6.5 Hz), two aromatic methyl groups at δ 2.05 (3H, s) and δ 1.67 (3H, s), an aromatic methoxyl group at δ 3.67 (3H, s), as well as a singlet at δ 5.14 (2H) corresponding to an aliphatic methylene with an oxygen atom attached. ^{13}C-NMR and DEPT spectra confirmed the presence of 20 carbons, containing 4 primary, 5 secondary, 2 tertiary including an olefinic carbon, 7 aromatic

[1]School of Pharmaceutical Sciences, Hebei Medical University, Shijiazhuang, Hebei, PR China; [2]New Drug Research and Development Center, North China Pharmaceutical Group Corporation, National Microbial Medicine Engineering and Research Center, Shijiazhuang, PR China and [3]Syngenta, Jealott's Hill International Research Centre, Bracknell, Berkshire, UK
Correspondence: Professor Q Shi, School of Pharmaceutical Sciences, Hebei Medical University, 361 Zhongshan East Road, Shijiazhuang, Hebei 050017, PR China.
E-mail: shiqingwen@hebmu.edu.cn
Received 21 April 2009; revised 29 May 2009; accepted 2 June 2009; published online 3 July 2009

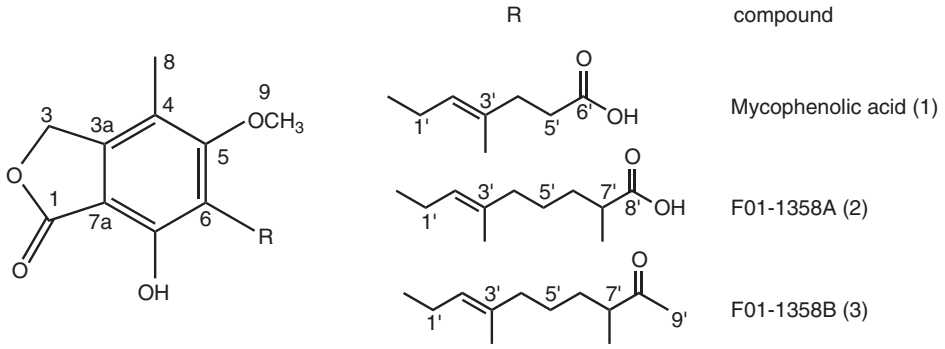

Figure 1 Structures of mycophenolic acid (**1**), F01-1358A (**2**) and F01-1358B (**3**).

Table 1 ^{1}H (500 MHz) and ^{13}C (125 MHz) NMR spectral data of 1, 2 and 3 in MeOH-d_4

	Mycophenolic acid (1)		*F01-1358A (2)*			*F01-1358B (3)*		
Position	*δ_H (mult, J in Hz)*	*δ_C*	*δ_H (mult, J in Hz)*	*COSY*	*HMBC (H to C)*	*δ_C (multi)*	*δ_H (mult, J in Hz)*	*δ_C (multi)*
1		172.9				173.8 (s)		174.1 (s)
3	5.20 (2H, s)	70.0	5.14 (2H, s)		1, 4, 7a, 3a	70.8 (t)	5.16 (2H, s)	70.6 (t)
3a		144.0				146.5 (s)		146.6 (s)
4		116.7				117.8 (s)		116.7 (s)
5		163.6				164.8 (s)		164.8 (s)
6		122.0				123.9 (s)		124.2 (s)
7		153.6				154.7 (s)		156.5 (s)
7a		106.3				107.6 (s)		107.8 (s)
8	2.15 (3H, s)	11.5	2.05 (3H, s)		4, 5, 3a	11.4 (q)	2.08 (3H, s)	11.3 (q)
9	3.76 (3H, s)	61.0	3.67 (3H, s)		5	61.5 (q)	3.70 (3H, s)	61.4 (q)
1′	3.39 (2H, d, *J*=7.0)	22.5	3.29 (2H, d, *J*=7.0)	2′	2′, 3′, 7, 5	23.6 (t)	3.30 (2H, d, *J*=7.0)	23.6 (t)
2′	5.25 (1H, t, *J*=7.0)	122.9	5.10 (1H, t, *J*=7.0)	1′	3′-CH_3, 1′, 4′	124.0 (d)	5.14 (1H, t, *J*=7.0)	124.4 (d)
3′		133.8				136.0 (s)		135.6 (s)
3′-CH_3	1.81(3H, s)	16.1	1.67 (3H, s)		4′, 2′, 3′	16.1 (q)	1.71 (3H, s)	16.1 (q)
4′	2.31 (2H, t, *J*=7.5)	34.2	1.88 (2H, t, *J*=7.0)	5′	3′-CH_3, 5′, 6′, 2′, 3′	40.5 (t)	1.91 (2H, t, *J*=7.0)	40.5 (t)
5′	2.44 (2H, t, *J*=7.5)	32.7	1.31 (2H, m)	6′-Ha, 4′	6′, 3′, 4′	26.5 (t)	1.29 (2H, m)	26.2 (t)
6′		179.1	Ha 1.45 (1H, m)	6′-Hb, 5′, 7′	7′-CH_3, 4′, 5′, 8′	34.4 (t)	Ha 1.50 (1H, m)	33.3 (t)
			Hb 1.22 (1H, m)	6′-Ha, 7′	7′-CH_3, 4′, 5′, 8′		Hb 1.20 (1H, m)	
7′			2.26 (1H, m)	7′-CH_3, 6′-Ha, 6′-Hb	7′-CH_3, 6′, 5′, 8′	40.6 (d)	2.47 (1H, m)	47.9 (d)
7′-CH_3			0.98 (3H, d, *J*=6.5)	7′	6′, 7′, 8′	17.7 (q)	0.96 (3H, d, *J*=7.0)	16.4 (q)
8′						181.0 (s)		215.8 (s)
9′							2.01 (3H, s)	22.0 (q)

Abbreviations: COSY, correlated spectroscopy; NMR, nuclear magnetic resonance.

quaternary carbons and 2 carbonyl carbons at δ 173.8 and δ 181.0. The protons of **2** connected to their respective carbons (Table 1) were assigned unambiguously through the heteronuclear multiple quantum coherence (HMQC) spectrum. The ^{1}H-, ^{13}C- and 2D-NMR data of **2** suggested the presence of a phthalan-1-one system with a long aliphatic chain, and indicated that **2** should be a mycophenolic derivative.[10] This partial structure of phthalan-1-one was established by spectral data in comparison with those of MPA (**1**) and supported by its heteronuclear multiple bond coherence (HMBC) correlations from H-3 to C-1, 4, 7a, 3a, CH_3-8 to C-4, C-5, C-3a and CH_3-9 to C-5. This result was further supported by the UV absorption at 250 and 304 nm, which was very similar to that of MPA (**1**). The COSY spectrum suggested other two substructures from C-1′ to C-2′ and from C-4′ to C-7′-CH_3. The HMBC correlations observed from CH_3-7′ to C-8′, C-7′, 6′ positioned the carbonyl group at C-8′ (δ 181.0). Cross-peaks from CH_3-3′ to C-4′, C-3′, C-2′ and from H-2′ to 3′-CH_3, C-1′, C-4′ in the HMBC experiment connected the two subunits through C-3′ and finally determined the aliphatic chain. The connection between the phthalan-1-one and the aliphatic chain was established by HMBC correlations from H-1′ to C-2′, 3′, 7, 5. Therefore, the structure of F01-1358A (**2**) (Figure 1) was identified as (6*E*)-8- (1,3-dihydro-4-hydroxy-6-methoxy-7-methyl-3-oxa-5-isobenzofuranyl)-2,6-dimethyl-6-octenoic acid.

F01-1358B (**3**) was obtained as a white crystalline solid using UV (MeOH) at λ_{max} 250 and 304 nm. Its HRFABMS yielded a peak at *m/z* 361.2007 (calcd for 361.2015, $M+H^+$, Δ0.8 mmu error), suggesting that compound **3** has a molecular formula $C_{21}H_{28}O_5$. The IR (KBr) spectrum suggested the presence of a hydroxyl group (3422 cm^{-1}), two carbonyl groups (1734 and 1717 cm^{-1}) and an isolated alkenyl group (1617 cm^{-1}). The UV, IR and NMR spectra of **3** showed considerable similarities to those of **2**, indicating **3** belonged to the mycophenolic derivative. With the structure of **2** established, the

structural elucidation of **3** was relatively straightforward. Further comparison of NMR data found that the ketone group signal at δ 215.8 replaced the peak at δ 181.0 (carboxylic carbonyl group) and one more methyl group (δ 2.01 (3H, s), δ 22.0 (q)] was present in **3**. The HMBC correlations of H-9′ to C-8′ and C-7′ indicated that an acetyl group in **3** replaced the carboxylic acid group in **2** and connected to C-7′. The significant chemical shift change of C-7′ in the two compounds (δ 40.6 in **2** to 47.9 in **3**) further supported the above-stated conclusion. This result was also supported by the IR spectrum at 1717 cm^{-1} instead of 1705 cm^{-1}. Therefore, the structure of F01-1358B (**3**) was characterized as 6-[(2*E*)-3, 7-dimethyl-8-oxa-2-nonen-1-yl]-7-hydroxy-5-methoxy-4-methyl-1 (3H)-isobenzofuranone (Figure 1). All the ^{1}H- and ^{13}C-NMR signals of **3** were assigned unambiguously on the basis of ^{1}H-^{1}H COSY, HMQC and HMBC spectroscopic data analysis (Table 1).

The activity of IMPDH was evaluated using the method reported by Magasanik *et al.*[11] The recombinant human type II IMPDH was prepared in our laboratory. The enzyme activity assay was carried out in a 96-well microtiter plate by monitoring the absorbance at 340 nm due to the formation of NADH. Compounds **1**, **2** and **3** were dissolved in DMSO and serially triple-diluted before being added to the initial assay mixture for pre-incubation with the enzyme at a final concentration of no more than 2% (v/v). As a result, compounds **1**, **2** and **3** inhibited IMPDH at the IC_{50} of 15.8, 13.2 and 35.6 μM, respectively, which indicated that the activity of compound **3** was significantly lower than that of **1** and **2**. This result suggested that the carboxylic acid group that does not exist in the structure of **3** may be essential for the inhibitory activity to IMPDH.

Mycophenolic acid, discovered in 1896, attracted a lot of interest because of its variety of biological activities, such as anticancer,[12,13] antivirus,[14] peroxisome proliferator activated receptor-γ agonism[15] and on account of one of its derivatives mycophenolate mofetil has been developed as an immunosuppressant.[3] Our findings provide two chemical entities of MPA family and their preliminary inhibitory activity to IMPDH. Further bioactivity evaluation for better understanding of their properties need to be investigated.

ADDENDUM IN PROOF

Compound **2** appears to be identical to homo-MPA reported as an impurity during the fermentation of MPA by E Gulyas *et al.* in the US Patent Application US 2008/254520.[16]

ACKNOWLEDGEMENTS

The Syngenta Postgraduate Studentship awarded to Xinhua Lu (2008-Hebei Medical University-Syngenta-2) is appreciated. We thank the colleagues from the New Drug Research and Development Center, North China Pharmaceutical Group Ltd for their kindly assistance especially Mr Dong Guo and Mrs Shiqing Zhu for NMR and MS measurements and Mr Yeying Li, Mrs Xiaolan Cui and Ying Shi for the fungus identification and fermentation.

1 Jackson, R. C., Weber, G. & Morris, H. P. IMP dehydrogenase, an enzyme linked with proliferation and malignancy. *Nature* **256,** 331–333 (1975).
2 Shu, Q. N. & Nair, V. Inosine monophosphate dehydrogenase (IMPDH) as a target in drug discovery. *Med. Res. Rev.* **28,** 219–232 (2008).
3 Hood, K. A. & Zarembski, D. G. Mycophenolate mofetil: a unique immuno-suppressive agent. *Am. J. Health Syst. Pharm.* **54,** 285–294 (1997).
4 Ishikawa, H. Mizoribine and mycophenolate mofetil. *Curr. Med. Chem.* **6,** 575–597 (1999).
5 Jain, J. *et al.* Characterization of pharmacological efficacy of VX-148, a new, potent immunosuppressive inosine 5′-monophosphate dehydrogenase inhibitor. *J. Pharmacol. Exp. Ther.* **302,** 1272–1277 (2002).
6 Floryk, D. & Thompson, T. C. Antiproliferative effects of AVN944, a novel inosine 5-monophosphate dehydrogenase inhibitor, in prostate cancer cells. *Int. J. Cancer* **123,** 2294–2302 (2008).
7 Arai, M. *et al.* Halicyclamine A, a marine spongean alkaloid as a lead for anti-tuberculosis agent. *Bioorg. Med. Chem.* **16,** 6732–6769 (2008).
8 Franklin, T. J., Jacobs, V., Bruneau, P. & Ple, P. Glucuronidation by human colorectal adenocarcinoma cells as a mechanism of resistance to mycophenolic acid. *Adv. Enz. Regul.* **35,** 91–100 (1995).
9 Jones, C. E., Taylor, P. J., McEwan, A. G. & Hanson, G. R. Spectroscopic characterization of copper (II) binding to the immunosuppressive drug mycophenolic acid. *J. Am. Chem. Soc.* **128,** 9378–9386 (2006).
10 Habib, E. *et al.* Mycophenolic derivatives from *Eupenicilliumparvum*. *J. Nat. Prod.* **71,** 1915–1918 (2008).
11 Magasanik, B., Moyed, H. S. & Gehring, L. B. Enzymes essential for the biosynthesis of nucleic acid guanine; inosine 5′-phosphate dehydrogenase of Aerobacter aerogenes. *J. Biol. Chem.* **226,** 339–350 (1957).
12 Domhan, S. *et al.* Molecular mechanisms of the antiangiogenic and antitumor effects of mycophenolic acid. *Mol. Cancer Ther.* **7,** 1656–1668 (2008).
13 Batovska, D. I. *et al.* Hydroxamic acid derivatives of mycophenolic acid inhibit histone deacetylase at the cellular level. *Biosci. Biotechnol. Biochem.* **72,** 2623–2631 (2008).
14 Hideaki, U. *et al.* Mycophenolic acid inhibits syncytium formation accompanied by reduction of gp120 expression. *J. Antibiot.* **58,** 514–518 (2005).
15 Ubukata, M. *et al.* Mycophenolic acid as a latent agonist of PPARgamma. *Bioorg. Med. Chem. Lett.* **17,** 4767–4770 (2007).
16 Gulyas, E. *et al.* Method for producing impurity level in mycophenolic acid fermentation. *US 20080254520* Oct. **16,** (2008).

The Journal of Antibiotics (2009) 62, 531–532

www.nature.com/ja

NOTE

Dechlororoseophilin: a new cytotoxic metabolite from *Streptomyces griseoviridis*

Yoichi Hayakawa, Shun-ya Nagatsuka and Takashi Kawasaki

The Journal of Antibiotics (2009) **62,** 531–532; doi:10.1038/ja.2009.59; published online 17 July 2009

Keywords: cytotoxic metabolite; dechlororoseophilin; roseophilin; *Streptomyces griseoviridis*

Roseophilin,[1] a cytotoxic pigment produced by *Streptomyces griseoviridis* 2464-S5, has a unique structure containing two pyrrole and one furan rings as shown in Figure 1. The strain also produces a structurally related tripyrrole antibiotic, prodigiosin R1.[2] Recently, we identified the *rph* gene cluster for prodigiosin biosynthesis in *S. griseoviridis*.[3] The *rph* cluster, however, does not contain genes characteristic of roseophilin biosynthesis, although roseophilin is considered to be biosynthesized partially with the same pathway as prodigiosin R1. We attempted to search the biosynthetic intermediates of roseophilin for further biosynthetic study. Color-guided fractionation of the culture extract resulted in the isolation of a new metabolite, dechlororoseophilin (**1**, Figure 1). We report herein the fermentation, isolation, structure elucidation and biological activity of **1**.

The producing organism was cultivated in 500-ml Erlenmeyer flasks containing 100 ml of a medium consisting of glycerol 4.0%, soybean meal 1.5%, molasses 1% and calcium carbonate 0.4% (pH 6.8) on a rotary shaker at 27 °C for 5 days. The fermentation broth (2.0 l) was centrifuged and the mycelium was extracted with acetone. After evaporation, the aqueous concentrate was extracted with ethyl acetate. The extract was applied to a silica gel column, which was washed with chloroform–methanol (10:1) and eluted with chloroform–methanol–29% ammonia water (200:20:1). The eluted pigment was subjected to reversed-phase HPLC (XBridge C_{18}, Waters Corporation, Milford, MA, USA) using 88% methanol with 0.2% triethylamine. A pigment fraction was concentrated and dissolved in ethyl acetate. After the solution was washed with 0.1 M hydrochloric acid and water, the organic layer was concentrated to dryness to give a red powder of **1** (8.2 mg). The physico-chemical properties of **1** are summarized as follows: m.p. 81–86 °C; high-resolution FAB-MS *m/z* 419.2697 (MH^+, calcd for $C_{27}H_{35}N_2O_2$, 419.2701); UV λ_{max} (ε) 536 nm (142 000) in methanol, 536 nm (143 000) in 0.01 M HCl—methanol, 300 nm (43 400), 485 nm (42 100) in 0.01 M NaOH—methanol; IR (KBr) ν_{max} 3450, 2910, 1590, 1290 cm^{-1}.

The molecular formula of **1** was established as $C_{27}H_{34}N_2O_2$ by high-resolution FAB-MS. ^{13}C and ^1H NMR data for **1** are summarized in Table 1. All one-bond ^1H-^{13}C connectivities were confirmed by the heteronuclear multiple-quantum coherence (HMQC)[4] spectrum. COSY and heteronuclear multiple-bond correlation (HMBC)[5] experiments identified three partial structures as shown in Figure 2. Three aromatic protons (1-H–3-H) were coupled with each other and an exchangeable proton (1-NH) was coupled with 1-H. A pyrrole moiety was constructed by ^1H-^{13}C long-range correlations from 1-H to C-2, C-3 and C-4, from 2-H to C-1 and C-4, and from 3-H to C-1 and C-4. NOESY correlations on 1-H, 2-H and 3-H confirmed the structure of a 2-pyrrolyl group and their assignments. ^1H-^{13}C long-range couplings were observed from 6-H to C-5, C-7 and C-8, and from a methoxy proton (27-H_3) to C-7. A high-field chemical shift for C-6 (δ 94.8) and a low-field chemical shift for C-5 (δ 162.0) showed that a 2,5-disubstituted 3-methoxyfuran moiety consisted of C-5 to C-8 and C-27. A small vicinal coupling (<1 Hz) was observed between 22-H and 23-H in the COSY spectrum. Both the protons displayed long-range correlations to three sp^2 carbons (C-9, C-10 and C-11), indicating that a five-membered ring was composed of C-9, C-10, C-11, C-22 and C-23. Long-range couplings from 24-H to C-11 and from 23-H to C-12 established a sequence of C-24/C-23/C-11/C-12. This substructure was expanded to include the second pyrrole ring due to long-range correlations from 12-H to C-10, C-11 and C-13 and chemical shifts for C-10 to C-13. Proton spin networks from 14-H_2 to 26-H_3 and HMBC data constructed a branched alkyl chain (Figure 2), which was connected to C-13 by a long-range correlation from 14-H (δ 2.83) to C-13. The remaining exchangeable proton (δ 13.46) was assigned to 10-NH in the pyrrolium ion. The partial structures were joined to establish the structure of **1** from NOEs between 3-H and 6-H, between 6-H and 7-OCH_3, and between 7-OCH_3 and 22-H (Figure 2). The absolute stereochemistry of roseophilin has been identified as 22*R*,23*R* by synthetic studies.[6,7] Roseophilin and **1**

Faculty of Pharmaceutical Sciences, Department of Medicinal and Life Science, Tokyo University of Science, Yamazaki, Noda, Chiba, Japan
Correspondence: Professor Y Hayakawa, Faculty of Pharmaceutical Sciences, Tokyo University of Science, 2641 Yamazaki, Noda, Chiba 278-8510, Japan.
E-mail: hykw@rs.noda.tus.ac.jp
Received 30 May 2009; revised 22 June 2009; accepted 24 June 2009; published online 17 July 2009

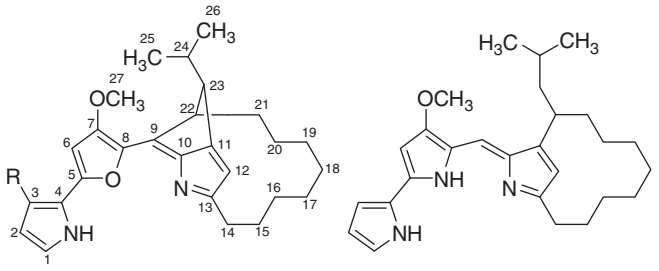

Dechlororoseophilin (**1**) R = H
Roseophilin R = Cl

Prodigiosin R1

Figure 1 Structures of dechlororoseophilin (**1**) and related compounds produced by *Streptomyces griseoviridis* 2464-S5.

Table 1 ^{13}C and ^{1}H NMR data for dechlororoseophilin in $CDCl_3$

No.	δ_C	δ_H (*J*=*Hz*)
1	128.8	7.36 br s
2	112.1	6.32 dd (4.0, 2.5)
3	116.9	6.91 dd (4.0, 1.0)
4	120.5	
5	162.0	
6	94.8	6.43 s
7	166.7	
8	133.5	
9	144.0	
10	135.3	
11	159.0	
12	110.4	6.16 s
13	164.3	
14	28.2	3.52 m, 2.83 ddd (13.5, 6.0, 3.5)
15	28.0	2.07 m, 1.30 m
16	24.9	1.31 m, 1.15 m
17	28.3	0.99 m, 0.42 m
18	27.0	0.88 m, 0.77 m
19	27.5	0.75 m, 0.40 m
20	24.5	0.98 m, 0.90 m
21	34.1	1.99 m, 1.78 m
22	55.0	3.77 dd (4.5, 3.0)
23	51.6	2.69 d (6.5)
24	33.1	1.79 m
25	21.4	1.00 3H d (6.5)
26	19.6	0.78 3H d (6.5)
27	59.9	4.10 3H s
1-NH		13.80 br
10-NH		13.46 br

exhibited similar ^{13}C chemical shifts (± 0.4 p.p.m.)[1] in the alkyl region and were required to have the same relative stereochemistry. Dechlororoseophilin is a candidate intermediate for roseophilin biosynthesis. It is expected that the compound can be used for the identification of a gene involved in the chlorination process.

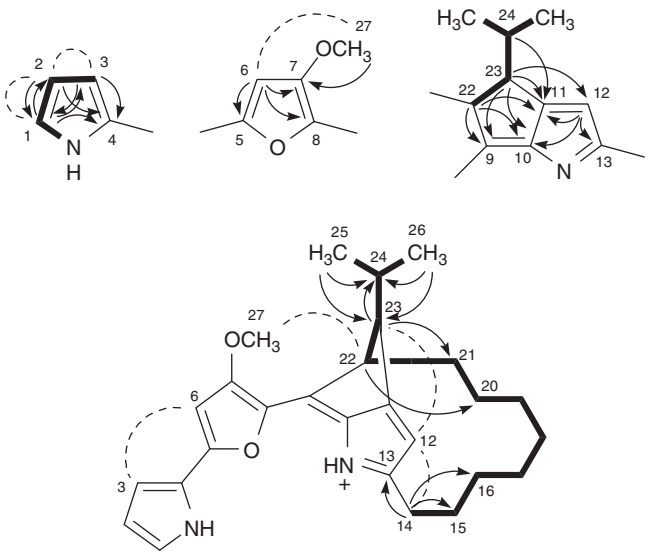

Figure 2 NMR analyses of **1**. Bold lines indicate ^{1}H spin networks, arrows show ^{1}H-^{13}C long-range correlations and dashed curves display NOE correlations.

The cytotoxic activities of **1** and roseophilin were examined by using four tumor cell lines. The cells were plated and incubated for 3 days with various concentrations of samples. After the cells were treated with 0.5 mg ml^{-1} of 3-(4,5-dimethylthiazol-2-yl)-2, 5-diphenyltetrazolium bromide (MTT) for 4 h at 37 °C, cell growth was measured as absorbance at 570 nm. The IC_{50} values for dechlororoseophilin and roseophilin were 2.6 and 1.0 μM against HT-1080 human fibrosarcoma cells, 2.1 and 0.72 μM against C6 rat glioma cells, 2.7 and 2.1 μM against MCF7 human breast cancer cells, and 2.0 and 1.9 μM against T-47D human breast cancer cells, respectively.

ACKNOWLEDGEMENTS

This study was supported in part by a Grant-in-Aid for Scientific Research, The Ministry of Education, Science, Sports and Culture, Japan. We thank F Hasegawa, Tokyo University of Science, for assistance with mass spectrometry.

1 Hayakawa, Y., Kawakami, K., Seto, H. & Furihata, K. Structure of a new antibiotic, roseophilin. *Tetrahedron Lett.* **33,** 2701–2704 (1992).
2 Kawasaki, T., Sakurai, F. & Hayakawa, Y. A prodigiosin from the roseophilin producer *Streptomyces griseoviridis*. *J. Nat. Prod.* **71,** 1265–1267 (2008).
3 Kawasaki, T., Sakurai, F., Nagatsuka, S. & Hayakawa, Y. Prodigiosin biosynthesis gene cluster in the roseophilin producer *Streptomyces griseoviridis*. *J. Antibiot.* **62,** 271–276 (2009).
4 Summers, M. F., Marzilli, L. G. & Bax, A. Complete ^{1}H and ^{13}C assignments of coenzyme B_{12} through the use of new two-dimensional NMR experiments. *J. Am. Chem. Soc.* **108,** 4285–4294 (1986).
5 Bax, A. & Summers, M. F. ^{1}H and ^{13}C assignments from sensitivity enhanced detection of heteronuclear multiple-bond connectivity by multiple quantum NMR. *J. Am. Chem. Soc.* **108,** 2093–2094 (1986).
6 Harrington, P. E. & Tius, M. A. Synthesis and absolute stereochemistry of roseophilin. *J. Am. Chem. Soc.* **123,** 8509–8514 (2001).
7 Boger, D. L. & Hong, J. Asymmetric total synthesis of *ent*-(−)-roseophilin: assignment of absolute configuration. *J. Am. Chem. Soc.* **123,** 8515–8519 (2001).

The Journal of Antibiotics (2009) 62, 533–535

www.nature.com/ja

NOTE

A new benzoxepin metabolite isolated from endophytic fungus *Phomopsis* sp.

Yoshihito Shiono[1], Ayumi Nitto[1], Keiko Shimanuki[1], Takuya Koseki[1], Tetsuya Murayama[1], Tokichi Miyakawa[2], Jun Yoshida[3] and Ken-ichi Kimura[3]

The Journal of Antibiotics (2009) **62,** 533–535; doi:10.1038/ja.2009.65; published online 17 July 2009

Keywords: benzoxepin; benzophomopsin A; Ca^{2+}-signaling; *Phomopsis* sp.

Endophytes live symptomlessly and intracellularly inside host plants. The interaction of endophytes with host plants has, in particular, received considerable attention. Studies carried out in the last two decades have shown that endophytes are rich sources of structurally diverse natural products with interesting biological activities.[1] These studies emphasize that chemical compounds help control the equilibrium between the endophytes and the host plants.

In our previous research on novel bioactive compounds isolated from endophytic fungi, we reported eremoxylarins A and B isolated from endophytic fungus xylariaceous YUA-026 as novel calcineurin inhibitors. These compounds were obtained as potential inhibitors of Ca^{2+}-signaling by the use of a yeast-based screening system for the activity that restores the growth of a Ca^{2+}-sensitive, drug-sensitive strain of *Saccharomyces cerevisiae* (*zds1*Δ *erg3*Δ *pdr1*Δ *pdr3*Δ) on solid medium containing $CaCl_2$.[2,3] Among the microbial compounds similarly screened, we found that benzophomopsin A (**1**) inhibited the Ca^{2+}-signal transduction more strongly than did a known compound, xylarinol A (**2**) (Figure 1). Herein, we report the isolation and structure elucidation of a new benzoxepin derivative **1** together with **2** and their effects on Ca^{2+}-signal transduction.

The producing strain, *Phomopsis* sp. KS-37-2, was isolated from the stem of a cherry tree in Yamagata, Japan.

Phomopsis sp. KS-37-2 was cultivated on sterilized, unpolished rice (20 g/Petri dish×50) at 25 °C for 3 weeks. The moldy, unpolished rice was extracted with MeOH, and the MeOH extract was concentrated. The resulting aqueous concentrate was extracted with *n*-hexane at first, and the water layer was subsequently partitioned with EtOAc. The purification of the EtOAc layer was guided by the intense blue characteristic coloration with vanillin–sulfuric acid solution on TLC plates. The EtOAc residue was purified on a silica gel column using a stepwise gradient of *n*-hexane–EtOAc (100:0–0:100). The 50–60% EtOAc fractions (85.0 mg) were combined and further purified by octa decyl silyl (ODS, Fuji Silysia Chemical Ltd., Aichi, Japan) column chromatography using 80% aqueous MeOH as the eluent to afford fractions 1–15 (100 ml each). Fraction 5 (35.0 mg) was rechromatographed on a silica gel column using $CHCl_3$–MeOH (80:20) as the eluent to yield benzophomopsin A (**1**, 5.5 mg) and xylarinol A (**2**, 11.0 mg).

The metabolite xylarinol A (**2**) was isolated as a white powder. Xylarinol A has recently been isolated from the fruiting bodies of *Xylaria polymorpha* as a radical scavenger.[4] A comparison of our spectroscopic data with the literature values confirmed that **2** was xylarinol A.

The molecular formula of **1** was $C_{12}H_{12}O_3$, which required seven degrees of unsaturation, as revealed by HR–FAB–MS. The IR spectrum of **1** showed absorption bands at 3384, 1584 and 1465 cm^{-1}, which are characteristic of the hydroxyl and aromatic groups. The formation of a monomethoxyl derivative (**1a**) [$C_{13}H_{14}O_3$ (FAB–MS: *m/z* 241 $[M+Na]^+$); δ_H 3.83 (3H, s, OMe)] after treating **1** with trimethylsilyldiazomethane confirmed the presence of a phenolic hydroxyl group. The UV spectrum of **1** revealed the presence of aromatic rings. The ^{13}C NMR and DEPT spectra of **1** showed peaks corresponding to five sp^2 methine (δ 103.5, 114.8, 123.0, 128.0, 131.3), three sp^2 quaternary carbons (δ 126.6, 136.9, 152.3), one sp^3 quaternary carbon (δ 104.1), one sp^3 methylene (δ 56.8), one sp^3 methine (δ 66.9) and one methyl group (δ 16.0). The seven unsaturation equivalents implied by the molecular formula indicated that **1** has three rings.

The ^1H-NMR spectrum showed signals attributable to a vicinal sp^2 spin network [δ 6.82 (1H, d, J=7.6 Hz), 6.89 (1H, d, J=7.6 Hz), 7.09 (1H, t, J=7.6 Hz)] and two protons of a *cis* double bond [δ 5.95 (1H, d, J=12.7 Hz) and 6.82 (1H, d, J=12.7 Hz)]. In addition, the ^1H NMR spectrum revealed signals that were due to an isolated oxymethylene [δ 4.63 (1H, d, J=13.9 Hz), 5.12 (1H, d, J=13.9 Hz)], a doublet methyl group [δ 1.05 (3H, d, J=6.5 Hz)] and an oxymethine

[1]Department of Bioresource Engineering, Faculty of Agriculture, Yamagata University, Tsuruoka, Yamagata, Japan; [2]Department of Molecular Biotechnology, Graduate School of Advanced Sciences of Matter, Hiroshima University, Higashi-Hiroshima, Japan and [3]Laboratory of Chemical Biology, Department of Biological Chemistry and Food Science, The United Graduate School of Agricultural Sciences, Iwate University, Morioka, Iwate, Japan
Correspondence: Dr Y Shiono, Department of Bioresource Engineering, Faculty of Agriculture, Yamagata University, Tsuruoka, Yamagata 997-8555, Japan.
E-mail: yshiono@tds1.tr.yamagata-u.ac.jp
Received 23 April 2009; revised 25 June 2009; accepted 29 June 2009; published online 17 July 2009

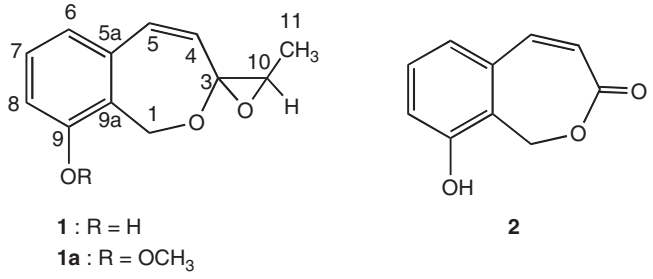

1 : R = H
1a : R = OCH_3

2

Figure 1 Structures of compounds **1** and **2**.

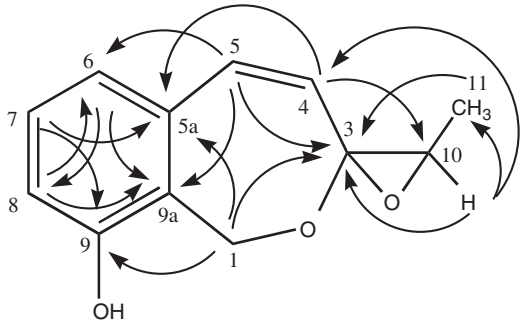

Figure 2 Important HMBC correlations for **1**.

group [δ 4.15 (1H, q, J=6.5 Hz)]. For the connectivity of partial structures, we conducted heteronuclear multiple bond correlation (HMBC) experiments (Figure 2 and Table 1). The aromatic moiety in **1** was confirmed on the basis of HMBC correlations from H-6 and H-8 to C-9a and from H-7 to C-5a and C-9. HMBC correlations from H-1 to C-3, C-5a and C-9, from H-4 to C-10, and from H-5 to C-3, C-6 and C-9a were also observed. These results indicated the presence of a 1,3-dihydro-benzo[*c*]oxepine moiety in **1**. The presence of an epoxy group at C-3 and C-10 was confirmed from the molecular formula, the chemical shifts of the ^1H and ^{13}C NMR signals at these positions, and the large $^1J_{CH}$ values for C-10 ($J_{C-10,H-10}$=153 Hz).[5] The residual OH group was hence thought to be a phenolic OH located at C-9. The relative stereochemistry of **1** was deduced from NOE experiments. An NOE was observed between H-4 and Me-11. From this result, the relative configuration at the position of C-10 was determined, as shown in Figure 1.

Benzophomopsin A (**1**), which possesses benzo-fused oxacycloalkenes moiety, was closely related to heptacyclosordariolone and cladoacetal A that were isolated earlier from cultures of *Sordaria macrospora* and *Cladosporium* sp., respectively.[6,7]

Intracellular Ca^{2+} is thought to have an important function in various biological signaling processes. Ca^{2+} has also been found to affect the progression of the G2/M cell cycle multilaterally in the yeast *S. cerevisiae*.[8] The mutant yeast strain (*zds1*Δ*erg3*Δ*pdr1*Δ *pdr3*Δ) used in this study is unable to grow at high $CaCl_2$ concentrations because of the hyperactivation of the Ca^{2+}-signal pathway. Two parallel pathways of Ca^{2+}-signaling, calcineurin and Mpk1 MAP kinase cascade, coordinately activate Swe1 in response to $CaCl_2$. Swe1, in turn, activates the inhibitory phosphorylation of the Cdc28 cyclin-dependent protein kinase in the G2 phase, resulting in cell cycle arrest in G2/M.[9] Thus, the calcineurin inhibitor, FK506, and the heat-shock protein 90 inhibitor, radicicol, by inhibiting the Ca^{2+}-induced Swe1 activation, promote the growth of the *zds1*Δ strain yeast on Ca^{2+}-agar plate.[9,10] The growth-promoting activities of compounds **1** and **2** were determined semi-quantitatively by similar procedures used for the screening assay.[3] Paper discs containing different amounts of compounds **1** and **2** were placed on a YPD agar plate containing $CaCl_2$ and the cell-growth zones formed around the discs were observed after 3 days of incubation at 28 °C. Compound **1** gave rise to a growth zone at 1.25 μg per disc and it restored the growth inhibition caused by a high Ca^{2+} dose dependently (Figure 3). In contrast, the activity of compound **2** was much weaker, giving rise to only a faint growth zone at 10 μg per disc of this compound. The activity of **1** observed by this assay was apparently similar to those observed with eremoxylarins A and B, which were found to inhibit calcineurin.[3] However, **1** did not inhibit calcineurin even at 100 μM (data not shown). Though YCM1008A is already known as a Ca^{2+}-signaling inhibitor from *Fusarium* sp.,[11] **1** has different structures and producing strain from it. Thus, further studies are required for an in-depth understanding of the inhibitory activity of **1**.

Table 1 ^1H and ^{13}C-NMR data of **1**

No	δ_C	δ_H	*HMBC*
1	56.8 t	4.63 (1H, d, 13.9)	3, 5a, 9
		5.12 (1H, d, 13.9)	3, 5a, 9
3	104.1 s		
4	103.5 d	5.95 (1H, d, 12.7)	5a, 10
5	131.3 d	6.82 (1H, d, 12.7)	3, 6, 9a
5a	136.9 s		
6	123.0 d	6.89 (1H, d, 7.6)	8, 9a
7	128.0 d	7.09 (1H, t, 7.6)	5a, 9
8	114.8 d	6.82 (1H, d, 7.6)	6, 9a
9	152.3 s		
9a	126.6 s		
10	66.9 d	4.15 (1H, q, 6.5)	3, 4, 11
11	16.0 q	1.05 (3H, d, 6.5)	3, 10

^{13}C- (100 MHz) and ^1H- (400 MHz) NMR spectra were taken on JEOL NMR system EX-400 in $CDCl_3$, the solvent peak were used as internal standard (δ_C 77.0, δ_H 7.26), and values in parentheses were coupling constants in Hz.

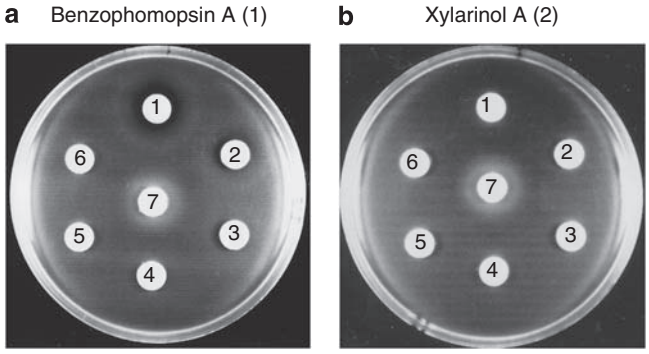

Figure 3 Restored growth activity of **1** (**a**) and **2** (**b**) against the mutant strain of *Saccharomyces cerevisiae* (*zds1*Δ *erg3*Δ *pdr1*Δ *pdr3*Δ) with 0.3 M $CaCl_2$. Assays were carried out as described earlier.[3] 1: 10 μg per disc, 2: 5 μg per disc, 3: 2.5 μg per disc, 4: 1.25 μg per disc, 5: 0.625 μg per disc, 6: 0.31 μg per disc, 7: 0.02 μg per disc (FK506).

PHYSICO-CHEMICAL PROPERTIES

1: White powder amorphous; $[\alpha]_D^{20}$—46° (*c* 0.11, MeOH), UV λ_{max} MeOH nm (ε) 253 (27,000), 261 (sh, 22,000), IR (KBr) ν_{max} cm^{-1} 3384, 1584, 1465, 1014, FAB–MS: *m/z* 205 $(M+H)^+$, HR–FAB–MS *m/z* 205.0872 (calcd for $C_{12}H_{12}O_3$+H, 205.0865), for ^1H and ^{13}C NMR see Table 1.

1a: Yellow oil, ^{1}H-NMR (400 MHz, $CDCl_3$)δ 1.05 (1H, d, J=6.5 Hz, 11-Me), 3.83 (3H, s, 9-OMe), 4.58 (1H, d, J=13.8 Hz, 1-H), 5.18 (1H, d, J=13.8 Hz, 1-H), 5.97 (1H, d, J=12.5 Hz, 4-H), 6.76 (1H, d, J=12.5 Hz, 5-H), 6.82 (1H, d, J=7.6 Hz, 8-H). 6.94 (1H, d, J=7.6 Hz, 6-H), 7.24 (1H, t, J=7.6 Hz, 7-H). FAB–MS: m/z 241 $(M+Na)^+$.

ACKNOWLEDGEMENTS

We thank Ms. Teiko Yamada of the Faculty of Agriculture at Tohoku University for HR–MS measurements.

1 Gunatilaka, A. A. L. Natural products from plant-associated microorganisms: distribution, structural diversity, bioactivity, and implications of their occurrence. *J. Nat. Prod.* **69,** 509–526 (2006).
2 Shiono, Y. & Murayama, T. New eremophilane-type sesquiterpenoids, eremoxylarins A and B from xylariaceous endophytic fungus YUA-026. *Z. Naturforsch.* **60b,** 885–890 (2005).
3 Ogasawara, Y., Yoshida, J., Shiono, Y., Miyakawa,, T. & Kimura, K. New eremophilane sesquiterpenoid compounds, eremoxylarins A and B directly inhibit calcineurin in a manner independent of immunophilin. *J. Antibiot.* **61,** 496–502 (2008).
4 Lee, I. *et al.* Xylarinols A and B, two new 2-benzoxepin derivatives from the fruiting bodies of *Xylaria polymorpha*. *J. Antibiot.* **62,** 163–165 (2009).
5 Someno, T. *et al.* ICM0301s, new angiogenesis inhibitors from *Aspergillus* sp. F-1491. II. Physico-chemical properties and structure elucidation. *J Antibiot.* **57,** 104–109 (2004).
6 Bouillant, M. L., Bernillon, J., Favre-Bonvin, J. & Salin, N. New hexaketides related to sordariol in *Sordaria macrospora*. *Z. Naturforsch.* **44c,** 719–723 (1989).
7 Höller, U., Gloer, J. B. & Wicklow, D. T. Biologically active polyketide metabolites from an undetermined fungicolous hyphomycete resembling *Cladosporium*. *J. Nat. Prod.* **65,** 876–882 (2002).
8 Mizunuma, M., Hirata, D., Miyahara, K., Tsuchiya, E. & Miyakawa, T. Role of calcineurin and Mpk1 in regulating the onset of mitosis in budding yeast. *Nature* **392,** 303–306 (1998).
9 Shitamukai, A., Mizunuma, M., Hirata, D., Takahashi, H. & Miyakawa, T. A positive screening for drugs that specifically inhibit the Ca^{2+}-signaling activity on the basis of the growth promoting effect on a yeast mutant with a peculiar phenotype. *Biosci. Biotechnol. Biochem.* **64,** 1942–1946 (2000).
10 Chanklan, R. *et al.* Inhibition of Ca^{2+}-signal-dependent growth regulation by radicicol in budding yeast. *Biosci. Biotechnol. Biochem.* **72,** 132–138 (2008).
11 Koizumi, F. *et al.* YCM1008A, a novel Ca^{2+}-signaling inhibitor, produced by *Fusarium* sp. YCM1008. *J. Antibiot.* **60,** 455–458 (2007).

The Journal of Antibiotics (2009) 62, 537

www.nature.com/ja

CORRIGENDUM

Salinisporamycin, a novel metabolite from *Salinispora arenicora*

Satoru Matsuda, Kyoko Adachi, Yoshihide Matsuo, Manabu Nukina and Yoshikazu Shizuri

The Journal of Antibiotics (2009) **62,** 537; doi:10.1038/ja.2009.91

Correction to: *The Journal of Antibiotics* (2009) **62**, 519–526; doi:10.1038/ja.2009.75

The authors of the above article noted an error in the publication of this paper (AOP and in this issue) in the spelling of the bacterium *Salinispora arenicora* in the title and throughout the text. The correct spelling of this bacterium is *Salinispora arenicola*.